General Disclaimer

One or more of the Following Statements may affect this Document

- This document has been reproduced from the best copy furnished by the organizational source. It is being released in the interest of making available as much information as possible.

- This document may contain data, which exceeds the sheet parameters. It was furnished in this condition by the organizational source and is the best copy available.

- This document may contain tone-on-tone or color graphs, charts and/or pictures, which have been reproduced in black and white.

- This document is paginated as submitted by the original source.

- Portions of this document are not fully legible due to the historical nature of some of the material. However, it is the best reproduction available from the original submission.

MASSACHUSETTS INSTITUTE OF TECHNOLOGY
CENTER FOR MATERIALS SCIENCE AND ENGINEERING
CAMBRIDGE, MASSACHUSETTS 02139

CHARGE-FLOW STRUCTURES AS POLYMERIC EARLY-WARNING FIRE-ALARM DEVICES

Carl M. Sechen

TECHNICAL REPORT NO. 1

NASA Grant NSG-3061

Sponsored by: NASA/Lewis Research Center
Dr. Richard E. Gluyas, Project Manager

Principal Investigator: Stephen D. Senturia
Associate Professor of Electrical Engineering
Massachusetts Institute of Technology

Grant Period: 5/1/75 - 2/28/77

May, 1977

This Technical Report was submitted by the author in May, 1977 to the Department of Electrical Engineering and Computer Science of the Massachusetts Institute of Technology as his thesis, in partial fulfillment of the requirements for the degree of Master of Science.

CHARGE-FLOW STRUCTURES AS POLYMERIC EARLY-WARNING FIRE ALARM-DEVICES

ABSTRACT

The objective of this thesis was to investigate a new device called the charge-flow transistor (CFT) and its applications for fire detection and gas sensing. A simpler device, the lock-and-key, was first used to determine the utility of various thin-film polymers as possible sensing materials. Two polymers, PFI and PSB, were found to be particularly suitable for fire detection. One polymer, PAPA, was found to be promising as a relative humidity sensor.

The charge-flow capacitor was examined next. This structure is basically a parallel-plate capacitor with a polymer-filled gap in the metallic top electrode. Its behavior was successfully modeled as an RC transmission line, and it demonstrated the basic principle of CFT operation in an easy-to-fabricate device structure.

Finally, the charge-flow transistor was investigated. Prototype devices were fabricated and tested. A model of device performance was developed. Extensive fire tests performed with a PFI-coated CFT indicated very good sensitivity to smouldering fires. It was discovered that the effective threshold voltage of the CFT depended on whether surface or bulk conduction in the thin film was dominant. For the case of PFI, the surface conductivity was substantially larger than the bulk conductivity.

ACKNOWLEDGEMENTS

The author acknowledges the tremendous effort of Professor Stephen D. Senturia who supervised this thesis and provided many theoretical insights throughout the course of this work. The author is deeply indebted to Tony Colozzi whose invaluable suggestions made possible the experimental measurements. Appreciation is gratefully expressed to Debbie Samkoff for preparing the polymer solutions and to Tally Stone for typing the manuscript. Thanks are also extended to technical artist John Mara for his fine work in preparing the figures. Acknowledgement is made of the research assistant support which was made available by the NASA/Lewis Research Center under grant number NSG-3061.

TABLE OF CONTENTS

CHAPTER 1: INTRODUCTION

The objective of this thesis was to examine a new device called the charge-flow transistor (CFT) where the principal application was fire detection. Chapter 1 focuses on the lock-and-key device. This device was primarily used to characterize the various polymers which were the sensing materials. Chapter 2 presents a new device called the charge-flow capacitor. This structure is at the heart of the CFT, which is discussed in Chapter 3. Chapter 4 concludes the thesis with a summary and a look at some future applications of the CFT.

1.1 THE LOCK-AND-KEY DEVICE

Beginning with the work of Byrd and Sheratte [1,2], it was established that the conductivity of certain polymers was a function of the kind and quantity of gases present in their environments. The lock-and-key device shown in Fig. 1 was the first reasonably successful polymeric early-warning fire-alarm device [3,4]. A key feature of the lock-and-key design is that the deposition of the polymer is the final fabrication step. This allows the use of conventional microelectronic device fabrication procedures for the electrodes.

The principle of operation of the lock-and-key device is based on the fact that its interelectrode resistance is proportional to the resistivity of the polymer. The polymers of interest are those that change their electrical resistivity in response to various gases, particularly those produced in a fire environment. The interelectrode resistance is monitored, for example, with the circuit shown in Fig. 2 in which a battery provides a source of voltage and the device current is observed with an

LOCK-AND-KEY DEVICE

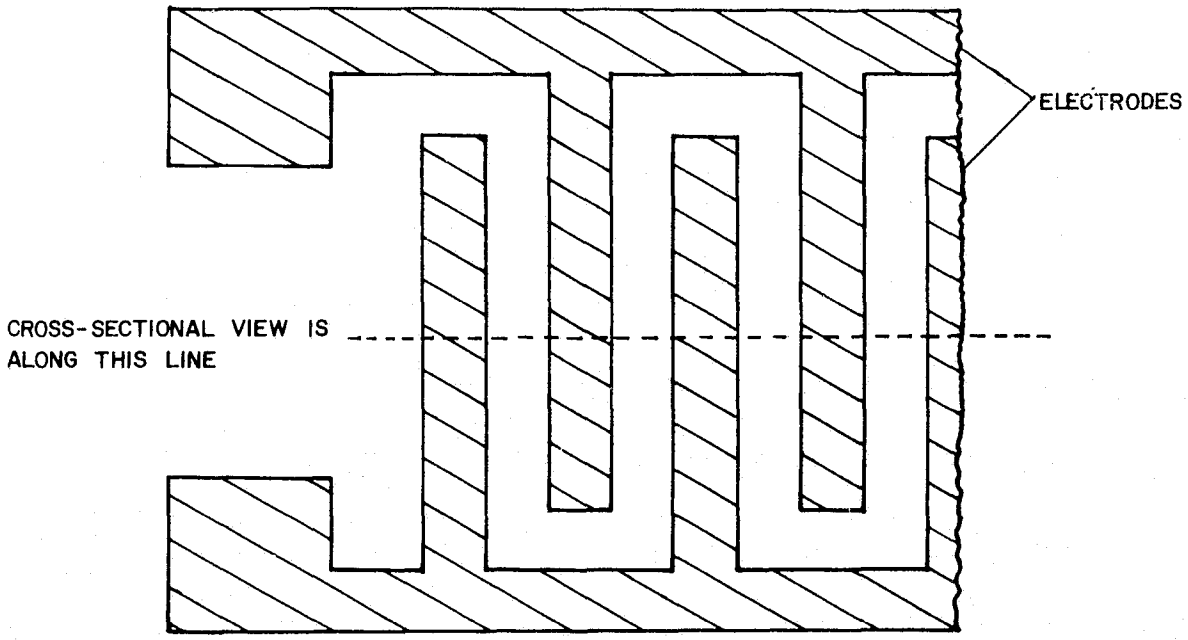

(a) TOP VIEW

(b) CROSS-SECTIONAL VIEW

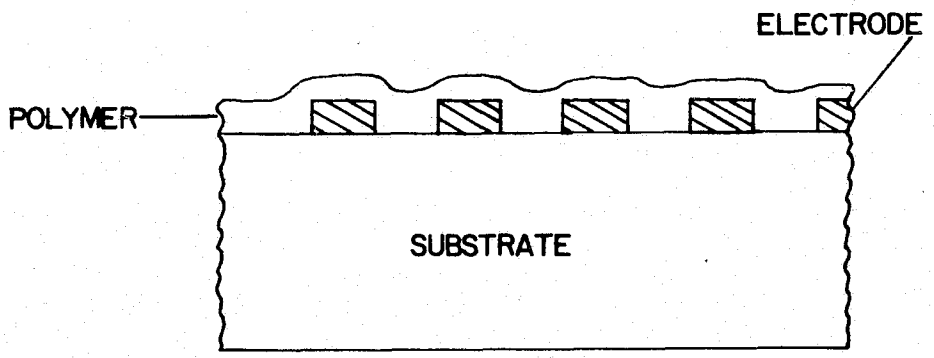

Figure 1

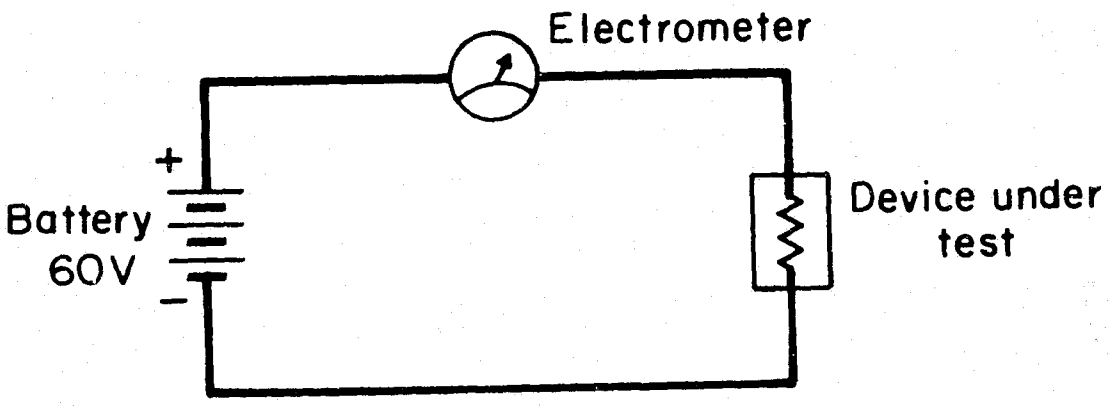

Figure 2

Typical lock-and-key test circuit

electrometer.

The fabrication procedure of the lock-and-key devices used in this program is presented next. Corning #1 glass slides (24 x 40 mm) were used as the insulating substrate (it is important that the resistivity of the substrate be considerably greater than the maximum-encountered polymer resistivity). The first step was the evaporation of aluminum and the definition of the electrode pattern using standard photolithographic techniques. The 42 interelectrode gaps were 150 μm wide and the aluminum thickness was about 1.0 μm. Second, polymer films were deposited by employing a photoresist spinner to evenly distribute a thin layer of a solution of the desired polymer in a volatile solvent. After the solvent has evaporated, a thin film approximately 3000 Å thick [8] of the polymer material remains. Finally, a conductive silver composition was used to attach leads to the bonding pads.

1.2 THE POLYMERS

Lock-and-key devices were made with the polymers PSB, PFI and PAPA (see Table 1 for the key to these abbreviated polymer names). In addition, previously-fabricated devices [4] made with the polymers PAPA, PTMP, PEP, PFPA and PEF were also utilized during the subsequent tests. These polymer films, chosen because of their supposedly good fire responses, had extremely large electrical resistances. The typical range was 10^9 to 10^{13} ohms. This fact is of considerable concern because the surface resistance of an uncoated lock-and-key device (that is, all of the fabrication steps outlined in Section 1.1 were completed except for the polymer-film deposition) is approximately 10^{13} ohms [5]. The relative importance of the substrate component of the overall conduction was ascertained in order to

TABLE 1

	POLYMER NAME	ABBREVIATION
1.	poly (p-aminophenylacetylene)	PAPA
2.	poly (p-formamidophenylacetylene)	PFPA
3.	poly (ethynyl ferrocene)	PEF
4.	poly (ethynyl pyridine)	PEP
5.	polymer from 1,2,3,6 tetramethylpyridazine	PTMP
6.	poly Schiff's base polymer from thiophene-2, 5-dicarboxaldehyde and p-phenylenediamine	PSB
7.	polyimdazole polymer from 1, 4-bis (phenylglyoxyloyl) benzene and ferrocene-1, 1'-dicarboxaldehyde	PFI

properly interpret the lock-and-key device results. The subsequent section, as well as results presented in the next two chapters, will show that the presence of the polymer layer apparently suppresses the surface component of the glass-slide conduction.

1.3 LONG-TERM TESTS

Lock-and-key devices were monitored in normal laboratory ambients over a period of several months. By applying 60 volts across the terminals, a current was continuously maintained. The device current was then correlated with variations in room temperature and relative humidity. Monitoring the resistance of devices in this very high resistivity range by conventional techniques requires large battery voltages, extreme care in the shielding of components against stray pickup, and a highly sensitive and stable current amplifier and meter (electrometer).

Long-term test results on the previously made lock-and-key devices for particular relative humidity and temperature ranges are contained in Table 2. The large decrease in baseline current versus time (the cause of this drift has not been ascertained) for all devices except the one made with PEF is particularly noteworthy. However, as will be seen later, PEF failed to show a fire response. Thus, none of these five polymers would be advantageous as commercial fire detectors. This fact led to the investigation of two additional polymers, namely PFI and PSB. From Table 3 it is observed that devices fabricated with these polymers experienced no baseline current drift. Furthermore, as will be discussed later, these two polymers had very good fire responses.

Table 2 contains a significant result concerning the lock-and-key device coated with PAPA. Note that the device resistance increased to

TABLE 2

LONG-TERM-TEST RESULTS ON THE PREVIOUSLY MADE LOCK-AND-KEY DEVICES

(60 volts applied)

Relative Humidity: 52-55%

Temperature: 20.5 ± 0.5°C

Current in a Device Made From:

weeks later	PAPA (pA)	PTMP (pA)	PEP (pA)	PFPA (pA)	PEF (nA)
0	24.3	820	120	1620	38.5
1	22.0	530	42.8	750	30.0
2	17.0	345	15.5	490	27.5
3	4.1	220	12.0	365	24.0
5	2.2	180	10.1	270	23.0
6	0.95	54	6.0	97	21.0
8	0.85	51	5.55	91	21.5
10	0.53	27	5.3	47	21.5
decrease factor after 10 weeks	46	30	23	34	1.8

TABLE 3

LONG-TERM-TEST RESULTS ON LOCK-AND-KEY DEVICES

(60 volts applied)

Relative Humidity: 52-55%

Temperature: 22.5 $\pm$ 0.5 °C

Current in a Device Made From:

weeks later	PFI (pA)	PSB (pA)
0	5.0	3.9
1	4.8	4.4
5	4.9	4.0
13	5.0	4.1

10^{14} ohms after the ten-week period. This is an order of magnitude greater than the maximum resistance of an uncoated device, corroborating the assertion made in the previous section that the surface component of the substrate conduction is apparently suppressed by the polymer layer.

1.4 GAS TESTS

A vacuum system which can be back filled with small quantities of gases was used to test the lock-and-key devices in the presence of various gases in controlled concentrations. Fig. 3 is a diagram of the gas system. After evacuating the entire system up to the gas isolation valves, an accurately measured pressure of a test gas can be introduced into the bell jar. The lock-and-key device in the bell jar was electrically connected to a voltage source and the electrometer through electrical feedthroughs in the bell-jar base plate and a system of coaxial cables. The bell jar and all signal wires were carefully shielded to minimize noise and electrical pickup problems. A diagram of the electrical interconnections appears in Fig. 4.

The responses of the various polymers to changes in relative humidity was considered first. This is because responses to relative-humidity changes might mask responses due to the presence of combustion products. A lock-and-key device was placed in the chamber, and the chamber was evacuated. Then either dry air or room air (at 25.2°C and 43% relative humidity) was introduced into the chamber, covering the pressure range of 0.5 - 760 mm. The lock-and-key device current versus pressure of air was monitored. The three polymers of greatest interest (PAPA, PSB and PFI) had negligible responses to changes in pressure of dry air. In particular, when the pressure of dry air was increased from 0.50 to 760 mm, the current

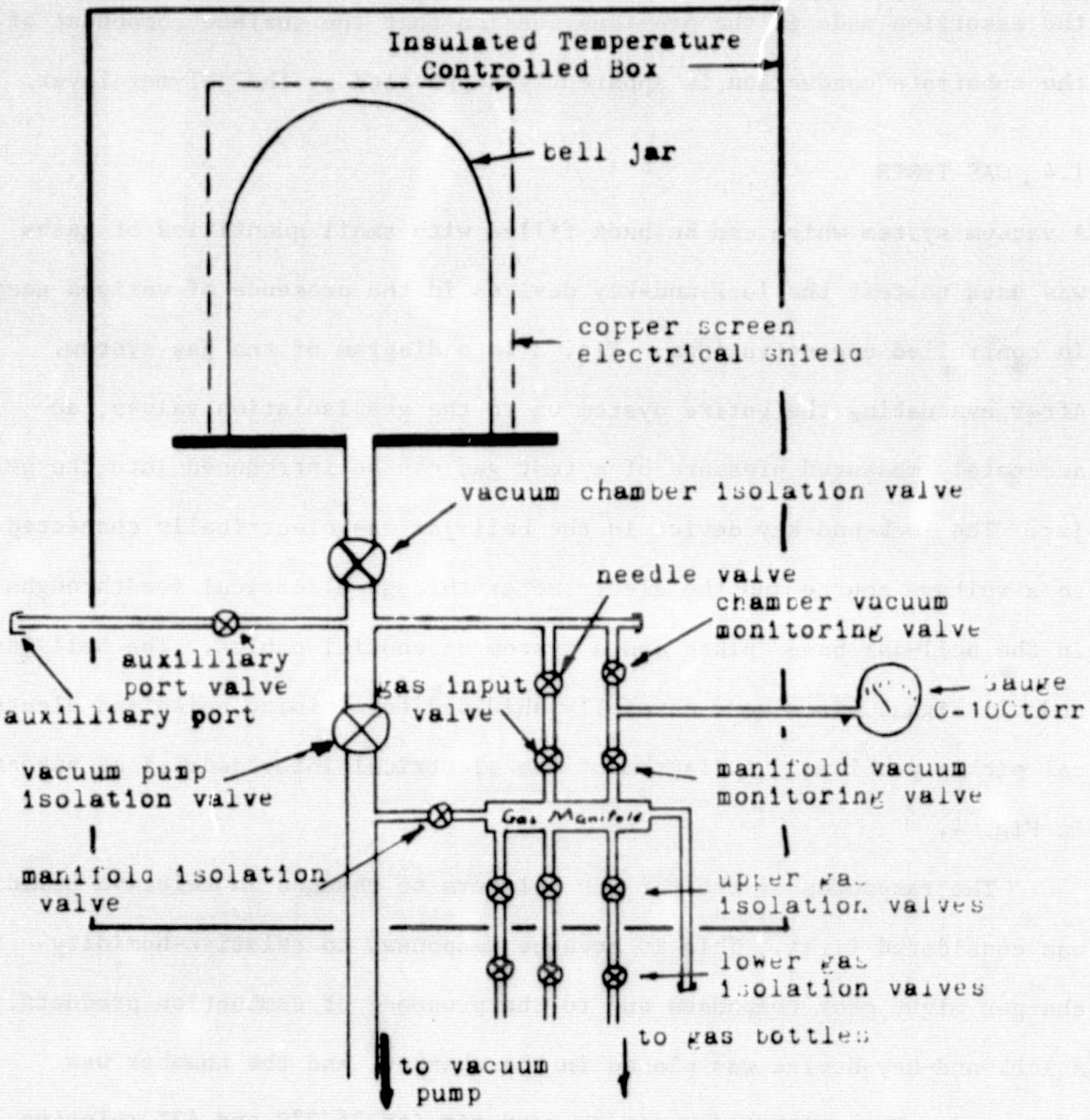

Figure 3

Diagram of the gas response test system [4]

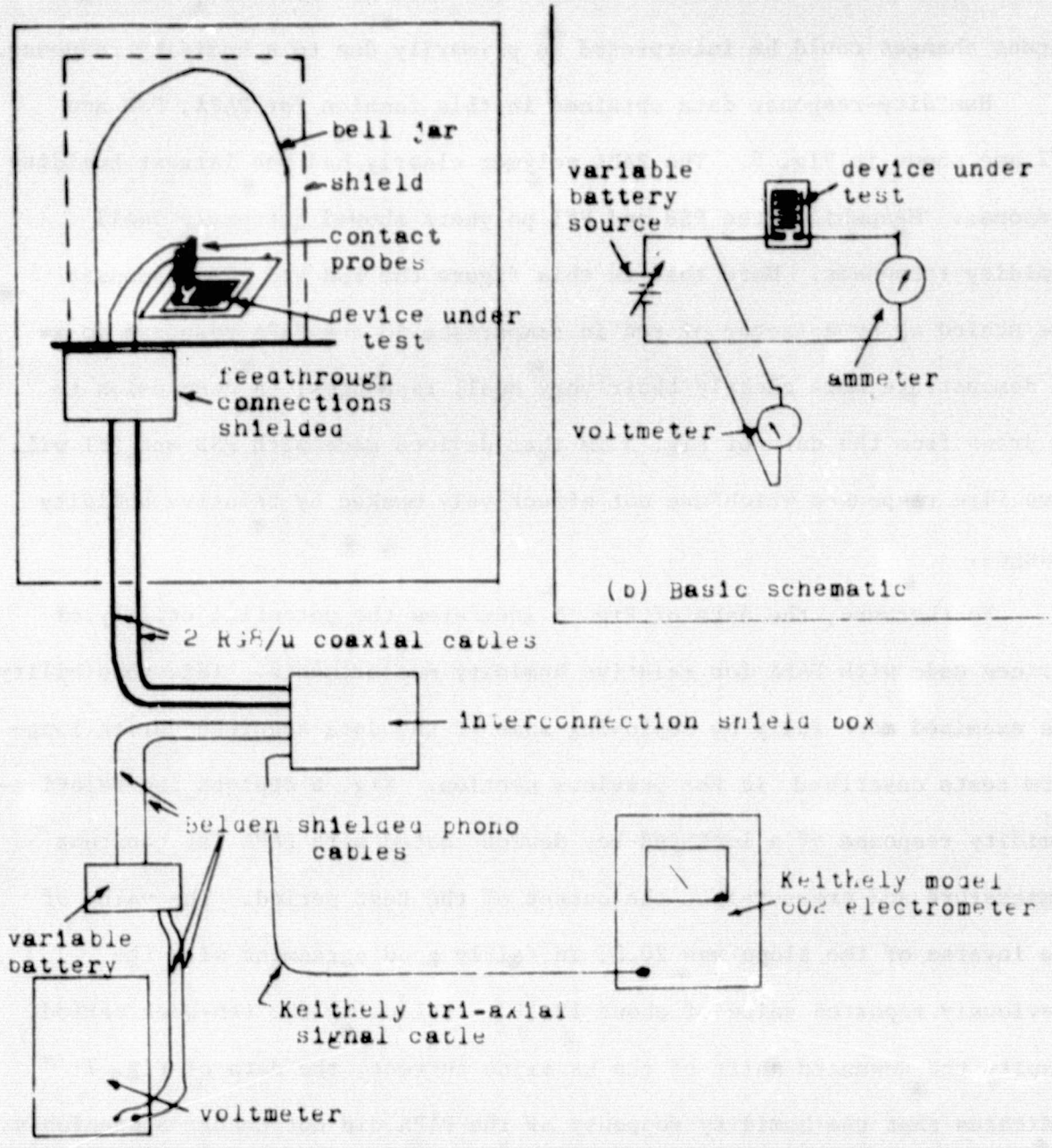

Figure 4

Diagram of the gas response test system [4]

increased by only a factor of 1.05 for PSB and PFI devices and only by a factor of 2.0 for PAPA devices. Thus, when room air was used, any significant changes could be interpreted as primarily due to a humidity response.

Humidity-response data obtained in this fashion for PAPA, PSB and PFI are shown in Fig. 5. The PAPA polymer clearly had the largest humidity response. Meanwhile, the PSB and PFI polymers showed extremely small humidity responses. Note that in this figure the PSB and PFI responses are scaled up by a factor of ten in comparison to the PAPA response so as to demonstrate more clearly their very small responses. A conclusion to be drawn from the data of Fig. 5 is that devices made with PSB and PFI will have fire responses which are not effectively masked by relative humidity changes.

Furthermore, the data of Fig. 5 indicates the potential utility of devices made with PAPA for relative humidity measurements. This possibility was examined more fully by employing some of the data acquired during long-term tests described in the previous section. Fig. 6 depicts the relative-humidity response of a lock-and-key device coated with PAPA (at constant temperature and pressure) at the outset of the test period. The value of the inverse of the slope was 20.8, in fairly good agreement with the previously reported value of about 19 [6]. Following the ten-week period, despite the downward shift of the baseline current, the data of Fig. 7 indicates that the humidity response of the PAPA did not change appreciably. In fact, the inverse slope of 20.5 is extremely close to the outset value. This demonstrates the feasibility of the PAPA polymer for relative-humidity-sensing applications.

The responses of the three polymers to controlled concentrations of

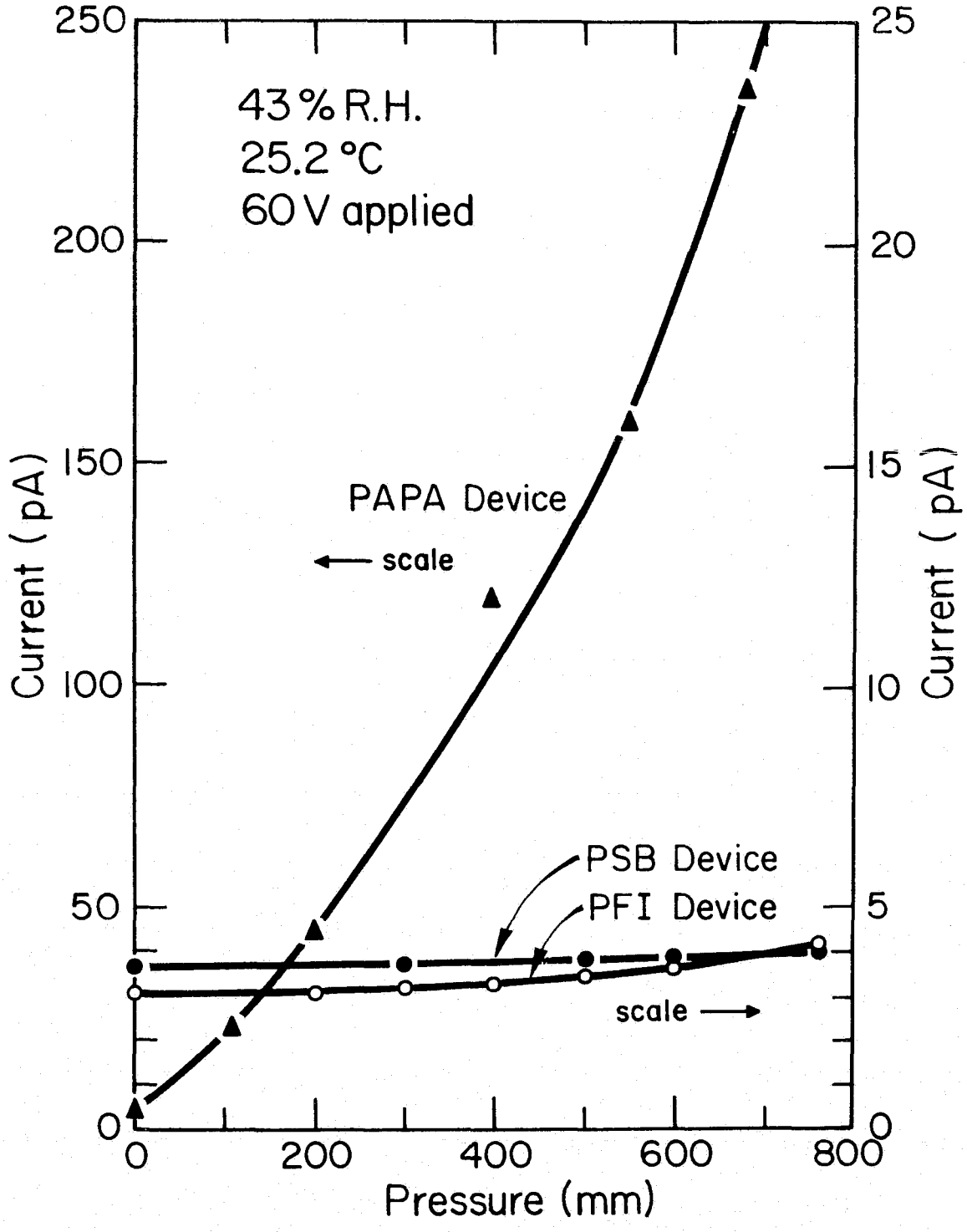

Figure 5

Lock-and-key device current versus pressure of air

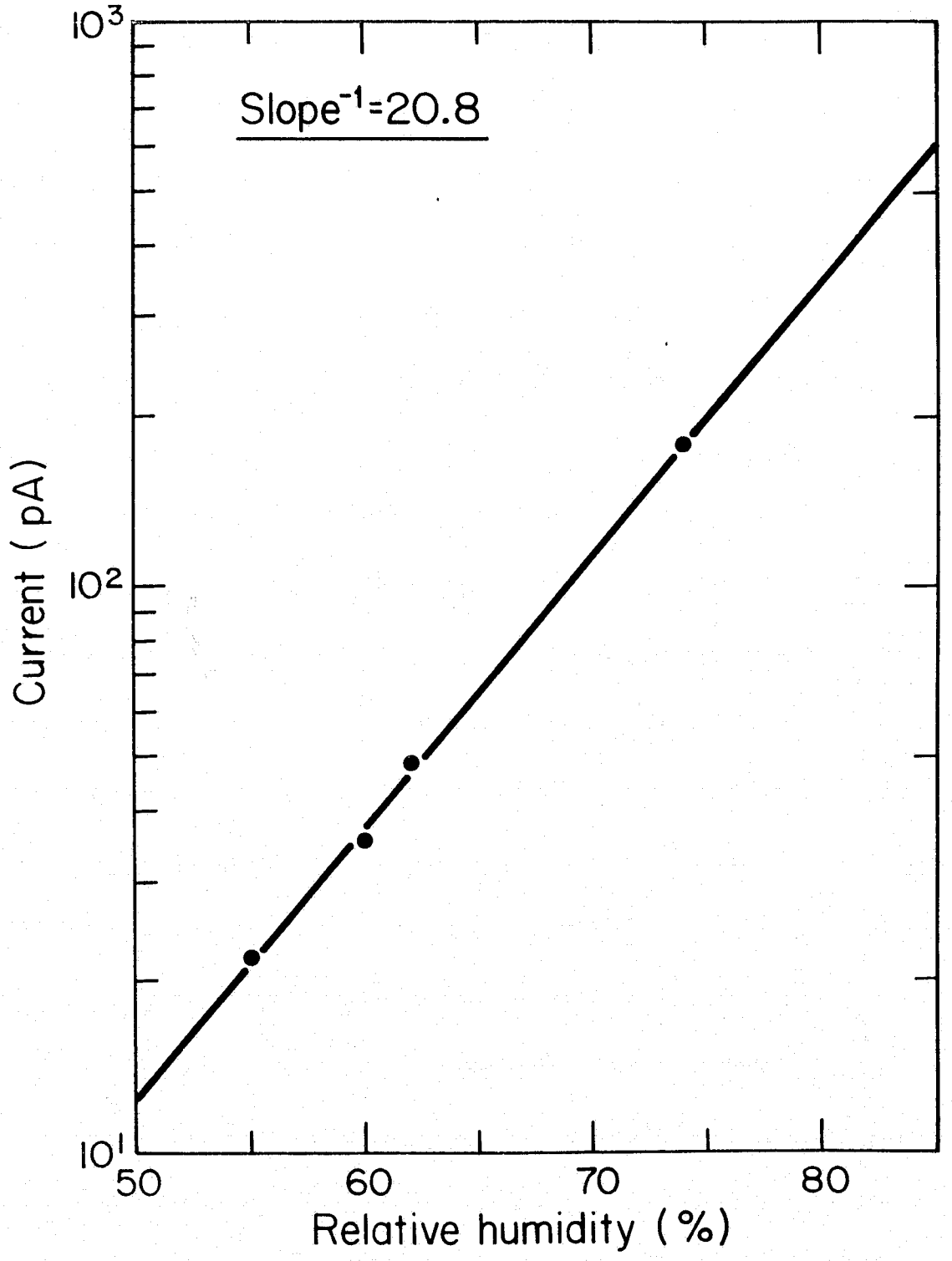

Figure 6

Lock-and-key device coated with PAPA. Current versus relative humidity during first week of long-term tests. Temperature was constant ($20.85 \pm 0.05°C$).

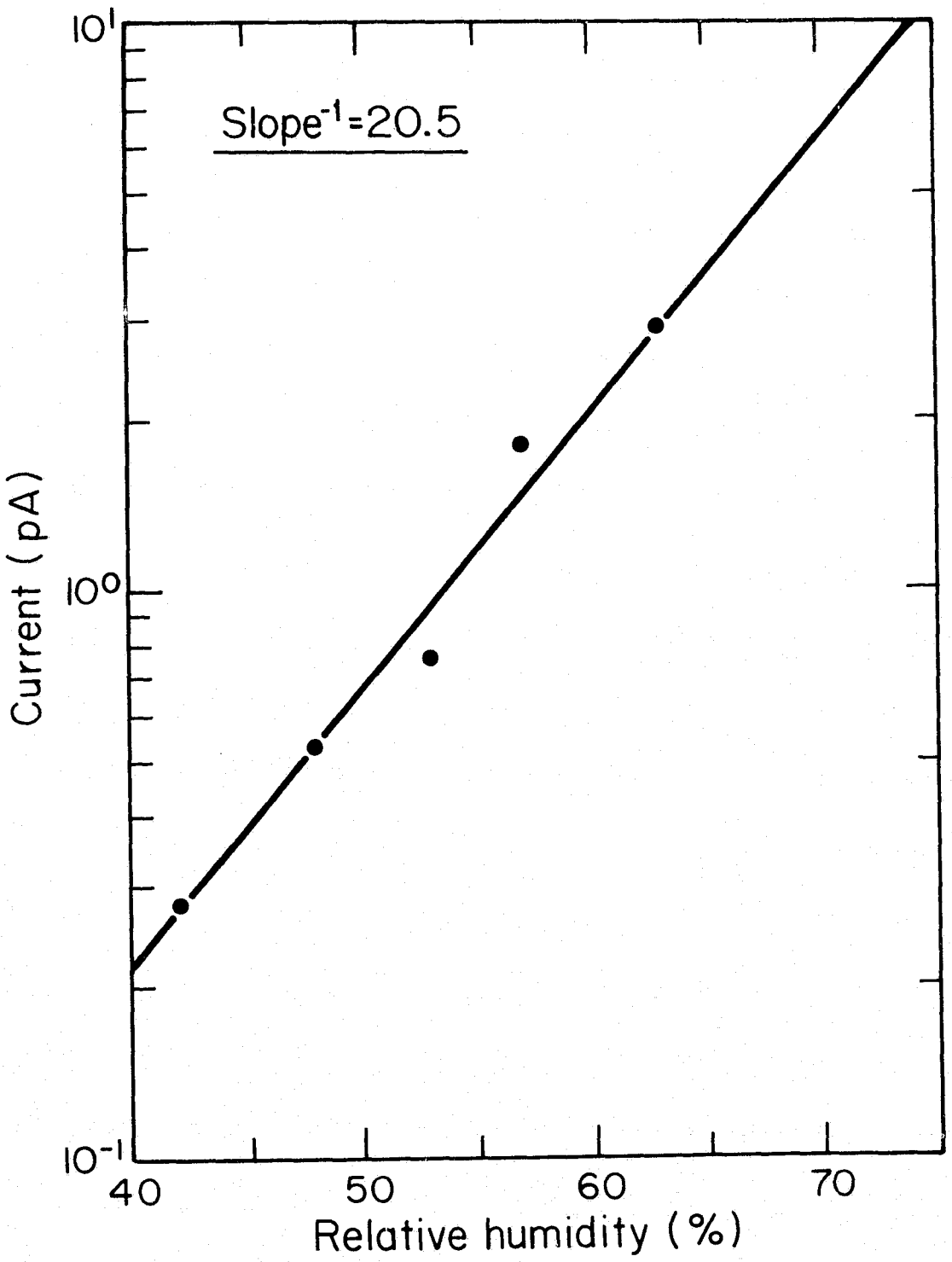

Figure 7

Lock-and-key device coated with PAPA. Current versus relative humidity during final week of long-term tests. Temperature was constant (20.65 $\pm$ 0.05°C).

ambient carbon monoxide was also recorded by means of the gas-test system. The results of these tests revealed the fact that the polymers did not change their conductivities when carbon monoxide was introduced into the testing system. Consequently, the fire responses reported in Sections 1.5, 2.3 and 3.5 are not due to emanations of carbon monoxide during the combustion of the test charges.

1.5 FIRE TESTS

The demonstration of fire responses in these polymers was carried out in a fire-test chamber shown schematically in Fig. 8. A small charge of combustible material (a few milligrams) is placed in the heater coil. The device under test is placed at the other end of the chamber and is electrically connected to the test circuit shown in Fig. 2. Heater current (about 2.5 A), sufficient to cause the charge to smoulder but insufficient to produce active flaming, was used to produce combustion. Air was flowed through the chamber at a sufficient rate to prevent buildup of combustion products in the chamber and also such that small fluctuations in the air-flow rate would have a negligible effect on the response. An air-flow rate of 1740 cc/min was employed, as in previous work [7].

Section 1.4 indicated that only the PSB and PFI polymers were promising as fire detectors. Consequently, extensive fire tests were carried out only for these two polymers. Typical results are illustrated in Figs. 9-13. PSB and PFI lock-and-key devices were tested with five different combustibles. These were acrylic, wool, polyurethane, cotton and PVC wire insulation.

Three general observations were drawn from the lock-and-key device fire tests. First, both the PSB and PFI devices responded very strongly

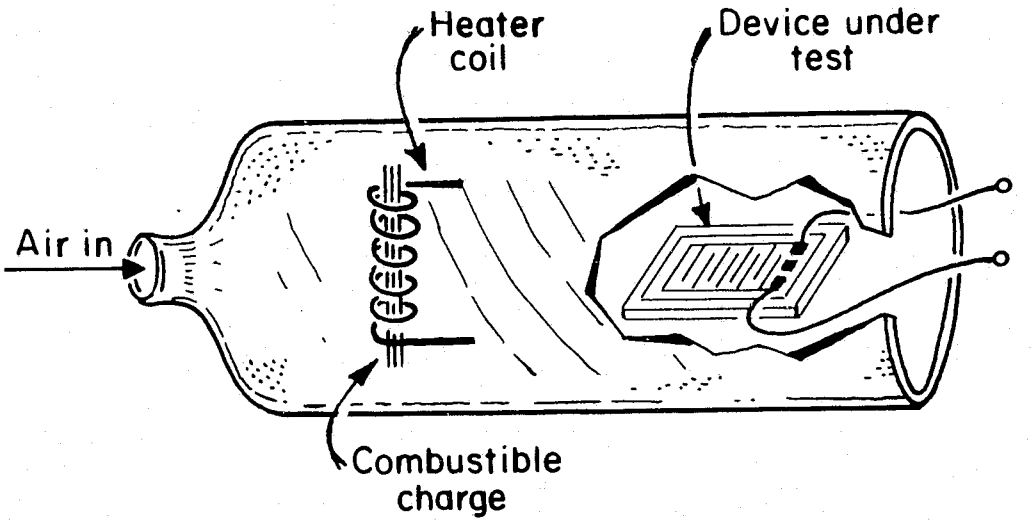

Figure 8

Schematic drawing of fire-test chamber

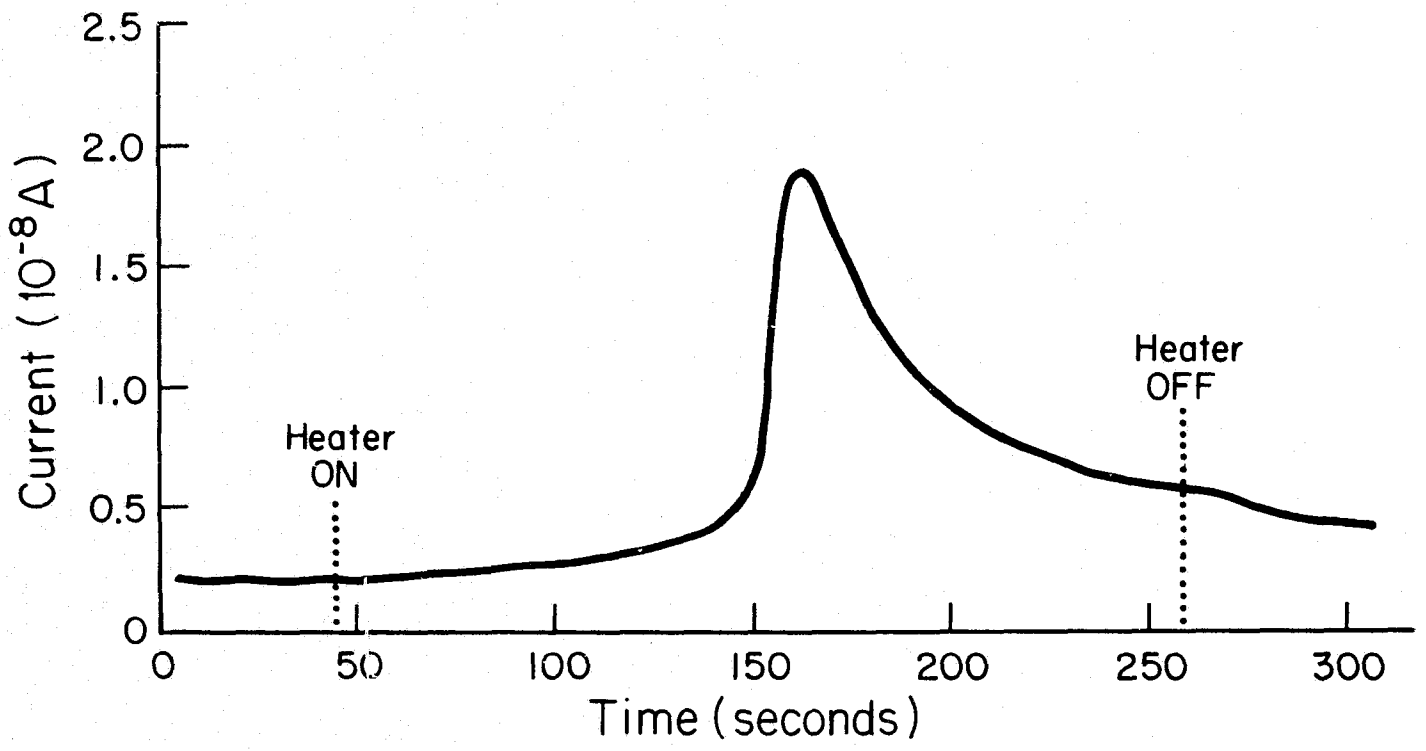

Lock-and-Key PSB with Acrylic

Figure 9

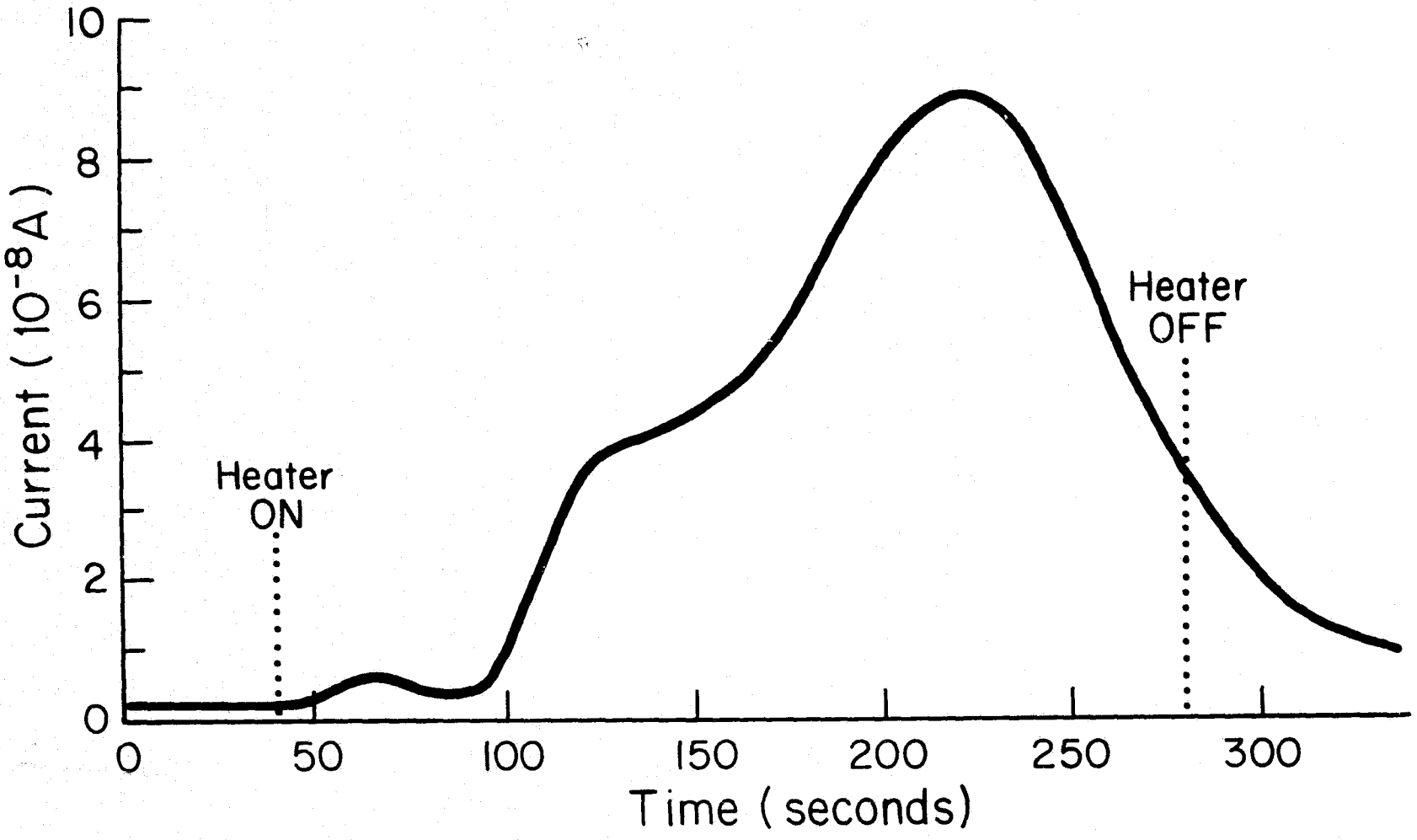

Figure 10

Lock-and-key PSB with wool

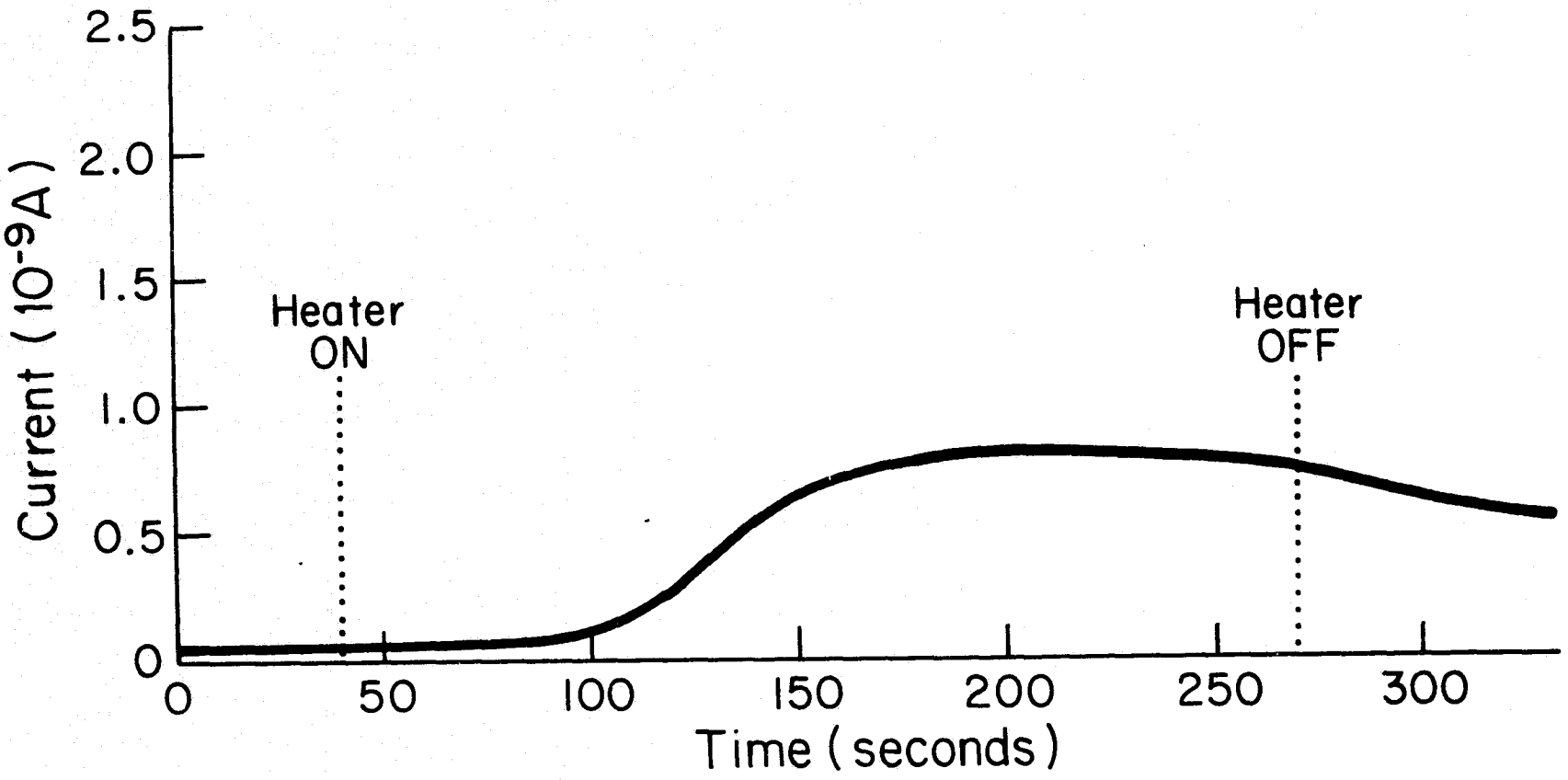

Figure 11

Lock-and-key PSB with polyurethane

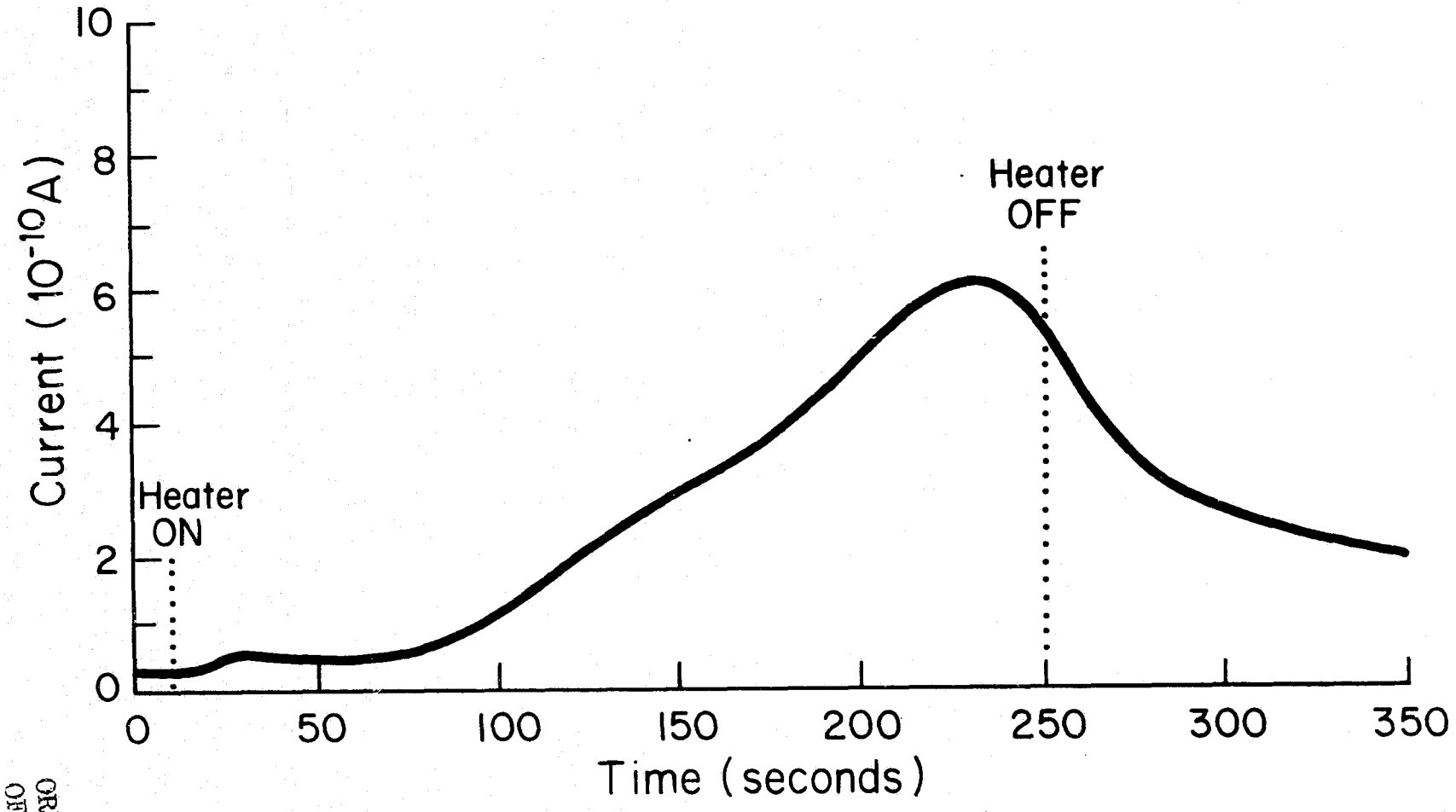

Figure 12

Lock-and-key PSB with cotton

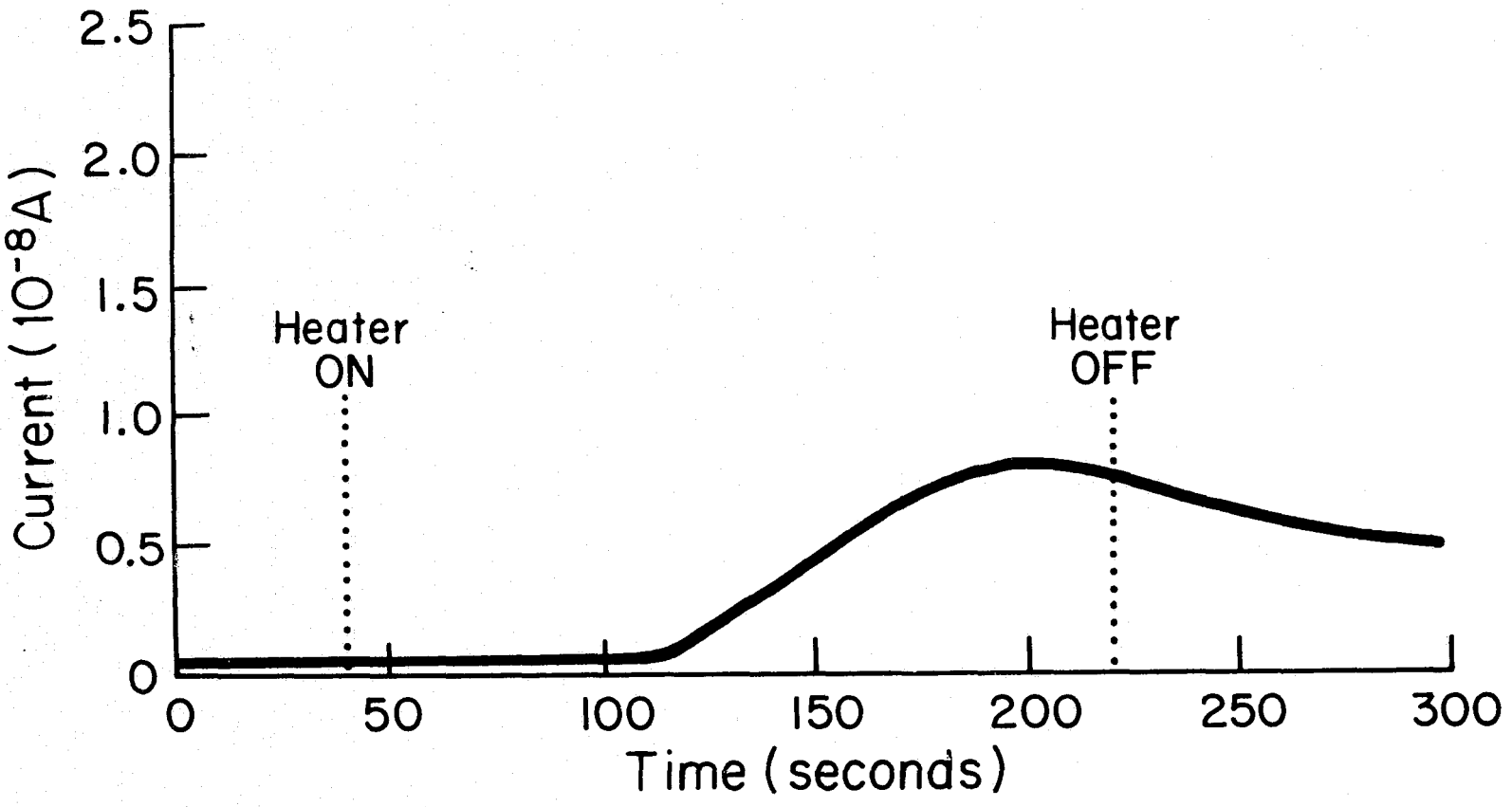

Figure 13

Lock-and-key PFI with PVC

to all five combustibles. Secondly, the PSB devices responded more strongly than the PFI devices for the same amount of combustible material burned. And lastly, the slope of the fire response for a given combustible material was independent of the sensing polymer.

The third observation possesses an important implication. When the heater-coil current is initiated, the temperature of the coil begins to rise. The combustion products for a given material are released at particular temperatures. This then implies that for unchanging external conditions, the combustion products for a particular material are released in a given order and in a given amount of time. Thus, it is concluded that both polymers respond to the same combustion products in an identical fashion. Furthermore, this fact suggests a method of determining what combustion products (to which the polymers respond) are released for a given material and what the actual mode of response is to those combustion products.

Fig. 9 illustrates a PSB lock-and-key device response to an 8.0 mg acrylic charge. The current gain, that is, the peak current divided by the baseline current, is 9.0. Furthermore, the peak occurs about 120 seconds after the heater is turned on. The very sharp increase in device current at 120 seconds after turn-on is a unique characteristic of the acrylic material. The implication is that the acrylic combustion products to which the polymers respond are given off very suddenly once the heater coil reaches a specific temperature.

The response of a PSB lock-and-key device to a 10.1 mg wool charge is shown in Fig. 10. The current gain is 45 and the peak current is observed about 180 seconds after the heater is turned on. Note that wool

yields a characteristic kink in the response roughly 90 seconds after heater turn-on.

Figure 11 depicts the response of a PSB lock-and-key device to the burning of 5.0 mg of polyurethane. The current gain is 14.7 and the maximum current is attained about 160 seconds after heater turn-on. Note the characteristically slow decrease in device current once it reaches its maximum value.

The response of a PSB lock-and-key device to an 8.0 mg cotton charge is illustrated in Fig. 12. The maximum current occurs approximately 220 seconds after heater turn-on and the current gain at this point is 20.5. Cotton fires characteristically produce this relatively long, upward sloping response.

Finally, the response of a PFI lock-and-key device to the combustion of 5.75 mg of PVC wire insulation is shown in Fig. 13. The current gain is 18.0 and the peak current occurs 160 seconds after the heater is turned on. A key feature is the very strong response of PFI and PSB lock-and-key devices to PVC fires. For example, about 7 mg of PVC wire insulation will produce current gains in excess of 10^3.

For the most part, baseline-current recovery times were fairly short. Provided that the device was not exposed to exorbitantly high concentrations of smoke (as in the examples depicted by Figs. 9-13), a recovery time on the order of ten minutes was typical. Moderately high concentrations resulted in significantly longer recovery times (several hours). Furthermore, exceedingly high smoke concentrations appeared to produce some long-term changes in the properties of the polymer. In all probability this was due to the settling of combustion products upon the polymer surface.

By conducting several fire tests in succession, it was found that the lock-and-key devices made with PAPA, PSB and PFI exhibited excellent repeatability. For combustible charges of the same size and for unaltered external conditions, the current gains generated were largely identical. In addition, the magnitude of the fire response was found to be independent of the baseline current.

1.6 DISCUSSION

It has been demonstrated that two polymers, PSB and PFI, possess conductivities which show very little response to relative humidity changes. Furthermore, both polymers responded strongly to all five combustibles, namely, acrylic, wool, polyurethane, cotton and PVC wire insulation. The PSB polymer responds somewhat more strongly than the PFI polymer for the same amount of combustible material burned.

However, the lock-and-key device has a very serious drawback. The baseline currents for the PSB and PFI devices were in the picoampere regime. Such low current levels cannot be detected without sophisticated, expensive instrumentation. The baseline current could be increased somewhat by narrowing the linewidths of the lock-and-key fingers (which were 10 mils wide). By implementing advanced lithographic techniques, this dimension could be reduced by about a factor of 100. However, this would only place the baseline current in the subnanoampere range. This would still require extremely costly current-detection equipment. Thus, it is readily apparent that the lock-and-key device is not practical as a commercial fire-detection device. Nonetheless, the feasibility of polymeric early-warning fire-alarm devices from the polymer standpoint has clearly been demonstrated.

CHAPTER 2: THE CHARGE-FLOW CAPACITOR

2.1 INTRODUCTION

The next task was the examination of device structures which would be more practical. This implies longevity, simplicity, small size, low cost and good sensitivity to fires. The major goal, however, was to obtain easily measurable polymer responses.

The main objective of this thesis was to examine a device structure first proposed by Wishneusky [4] which offers significant improvements over the lock-and-key device. This structure is called the charge-flow transistor (CFT). Initially, however, a somewhat similar, but more basic structure was examined. This structure is called the charge-flow capacitor.

Cross-sectional and top views of the charge-flow capacitor are presented in Fig. 14. Mask layout and reticle fabrication were performed at M.I.T. Lincoln Laboratory, courtesy of Dr. Dan Smythe. Each "finger" was 388 mils long and 4 mils wide, and the spacing between fingers was 4 mils. Fabrication of the structure proceeded as follows. First, Corning #1 glass slides (24 x 40 mm), which were used as the substrate material, were subjected to standard microelectronics-laboratory cleaning procedures. The aluminum evaporator was utilized to deposit the bottom-electrode metal. Definition of the electrode pattern was achieved with standard photolithographic technqiues. Next, an rf sputtering system was utilized to deposit 3000 Å of silicon dioxide over the bottom electrode and the exposed substrate surface. This silicon dioxide layer forms the insulator, which must be of higher resistivity than the polymer. The top electrode was then formed using the same technqiues that were employed for the bottom electrode. The lateral dimensions were identical to those of the bottom

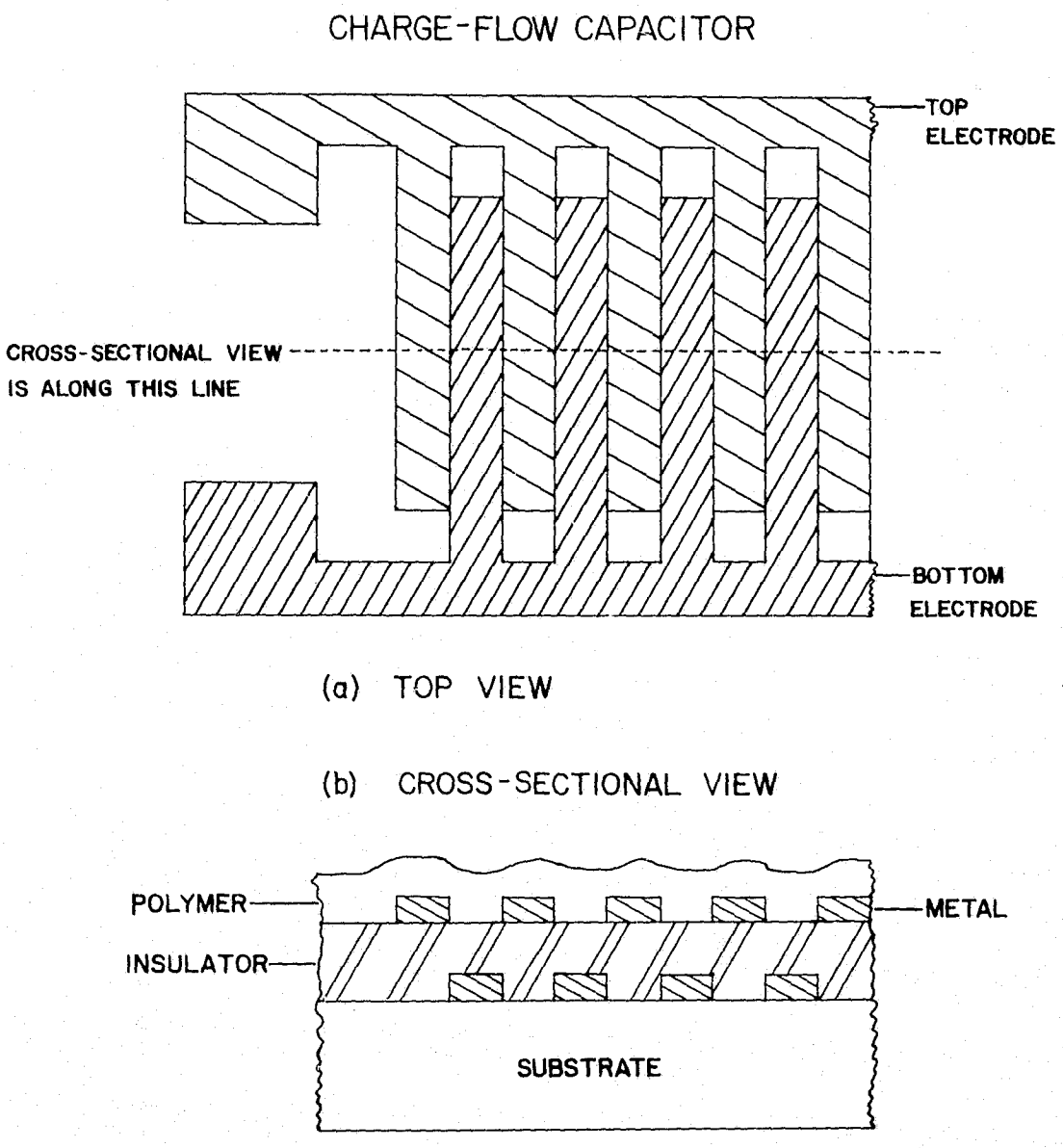
CHARGE-FLOW CAPACITOR
TOP ELECTRODE
CROSS-SECTIONAL VIEW IS ALONG THIS LINE
BOTTOM ELECTRODE
(a) TOP VIEW
(b) CROSS-SECTIONAL VIEW
POLYMER
INSULATOR
METAL
SUBSTRATE

Figure 14

electrode, but the whole structure was shifted so that the fingers did not overlap. Finally, the top electrode and the exposed silicon-dioxide surface were coated with the appropriate polymer. The polymer layer was spun-on by means of a photoresist spinner. The thickness of the polymer layer was about 3000 Å.

The charge-flow capacitor is theoretically analyzed by modeling the polymer-oxide-metal regions in the gaps of the top electrode as RC transmission lines. This analysis closely parallels that for the charge-flow transistor, which is presented in detail in Section 3.3. Only the relavent results will be shown here.

It is desired to demonstrate that the capacitance of the charge-flow capacitor is a function of the polymer resistivity and the frequency of the sinusoidal applied voltage. The transmission line equation,

$$I = -\frac{d_1}{r}\frac{\partial V}{\partial x} \tag{2.1}$$

where d_1 is the polymer-layer thickness and r is the resistivity divided by the length (Z) of the polymer-filled gaps in the top electrode, coupled with equation (3.24) (modified for excitation by a single sinusoid) yields the following:

$$I = V_o \frac{d_1}{Lr}\frac{1+i}{\sqrt{2}}\tanh\left(\frac{W}{2L}\frac{1+i}{\sqrt{2}}\right) \tag{2.2}$$

where V_o is the amplitude of the sinusoid, I is the current entering the polymer-filled gaps, and W is the gap width of the top electrode. L is given by

$$L = \sqrt{\frac{d_1 d_2}{\omega\rho\varepsilon}} \tag{2.3}$$

where d_2 is the oxide-layer thickness, ω is the frequency, ρ is the polymer resistivity and ε is the dielectric constant of the oxide. The admittance of the charge-flow capacitor is easily derived from equation (2.2).

$$Y = \frac{d_1 \alpha}{Wr} (1 + i) \tanh \left(\frac{\alpha}{2} + i \frac{\alpha}{2}\right) \tag{2.4}$$

where

$$\alpha = \frac{W}{\sqrt{2}\, L} \quad . \tag{2.5}$$

Equation (2.4) can be rewritten as

$$Y = \frac{d_1 \alpha}{Wr} (1 + i) \frac{\sinh \alpha + i \sin \alpha}{\cosh \alpha + \cos \alpha} \quad . \tag{2.6}$$

After separating real and imaginary parts,

$$Y = \frac{d_1}{\sqrt{2}\, Lr} \frac{(\sinh \alpha - \sin \alpha) + i (\sinh \alpha + \sin \alpha)}{\cosh \alpha + \cos \alpha} \quad . \tag{2.7}$$

In general, $Y = G + i\omega C$, where ω is the frequency, G is the conductance and C is the capacitance. Thus,

$$G = \frac{d_1}{\sqrt{2}\, Lr} \frac{\sinh \alpha - \sin \alpha}{\cosh \alpha + \cos \alpha} \tag{2.8}$$

$$C = \frac{d_1}{\sqrt{2}\, Lr\omega} \frac{\sinh \alpha + \sin \alpha}{\cosh \alpha + \cos \alpha} \quad . \tag{2.9}$$

If the value of α is significantly larger than unity, equations (2.8) and (2.9) simplify to the following:

$$G = \frac{d_1}{\sqrt{2}\, Lr} \tag{2.10}$$

$$C = \frac{d_1}{\sqrt{2}\ Lr\omega} \quad . \tag{2.11}$$

The necessity of α being significantly greater than unity such that equations (2.10) and (2.11) apply is equivalent to the requirement that

$$\omega\rho > 5 \times 10^7 \quad \Omega\text{-cm/s} \tag{2.12}$$

where equations (2.3) and (2.5) have been employed. In this regime, because of the $\omega^{-1/2}$ dependence of L, the capacitance is proportional to $\omega^{-1/2}$ and the conductance is proportional to $\omega^{1/2}$.

Using a low-frequency capacitance bridge made available by William Westphal, experimental data of capacitance and conductance versus frequency for a charge-flow capacitor coated with PAPA was obtained. This data appears in Figs. 15 and 16. Note that the frequency dependence is in reasonable agreement with that suggested by equations (2.10) and (2.11). The small discrepancy can be attributed to two factors. First, the measurements were made beginning at the highest frequency and were completed at the low-frequency end roughly one hour later. The aging effect of the PAPA polymer (which was described in Section 1.3) was observed to be present here as well, since the capacitance decreased as a function of time at a given frequency. Thus, the capacitances at the low-frequency end are somewhat lower than expected, resulting in a capacitance-versus-frequency slope which is smaller than expected in magnitude. Similarly, the slope of the conductance-versus-frequency plot is somewhat larger than expected.

A second factor contributing to the small discrepancy is that at low

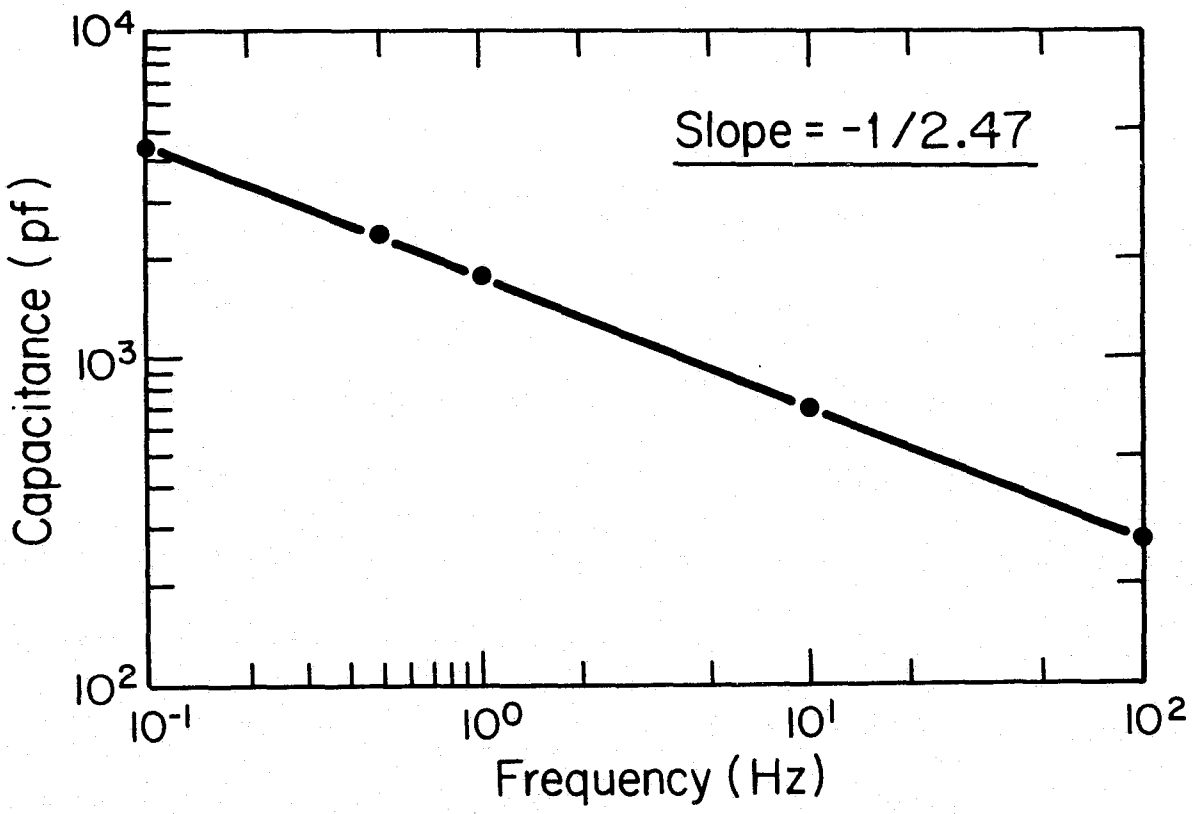

Figure 15

Capacitance of charge-flow capacitor (PAPA) versus frequency

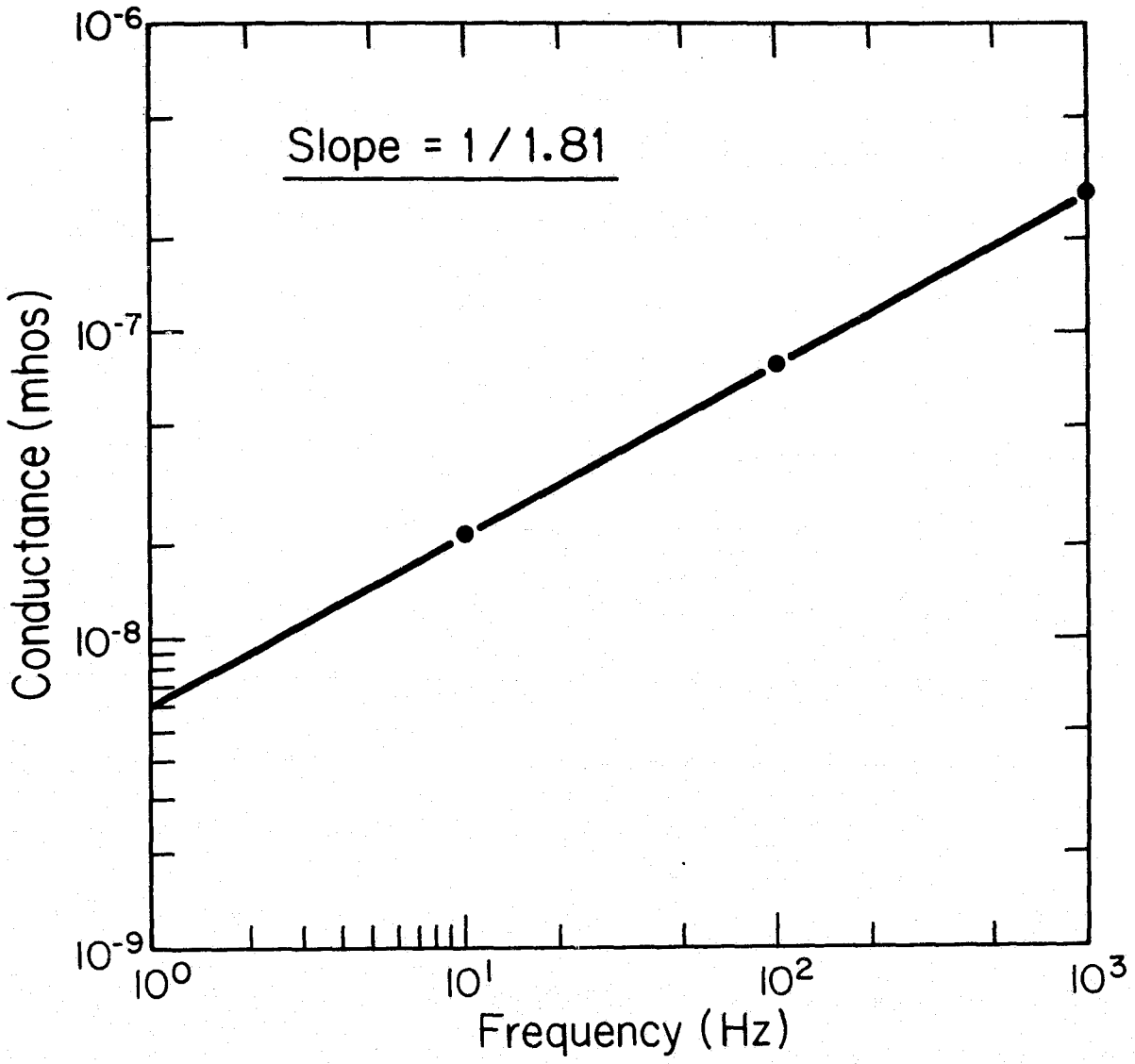

Figure 16

Conductance of charge-flow capacitor (PAPA) versus frequency

frequencies the approximation of $\alpha >> 1$ [governed by equation (2.12)] begins to break down. That is, the values of the bracketed terms in equations (2.8) and (2.9) are somewhat less than unity. This effect reduces the magnitude of the slope of the capacitance-versus-frequency plot and increases the slope of the conductance-versus-frequency plot beyond the theoretical slopes dictated by equations (2.10) and (2.11). This can demonstrated as follows. At $2\pi(80)$ rad/sec, the capacitance is seen to be 300 pf from Fig. 15. Substitution of the data into equations (2.11) and (2.3) yields a resistivity of the PAPA polymer equal to 10^7 ohm-cm. Equation (2.12) then implies that the $\alpha >> 1$ approximation has validity only for $\omega > 2\pi(1)$Hz.

Two observations can now be stated. First, it is clear that the admittance of the charge-flow capacitor given by equation (2.7) is in very good agreement with the experimental results. Second, by operating in the regime where equation (2.12) is satisfied, the resistivity of a thin film may be determined by obtaining conductance or capacitance data versus frequency and then utilizing equations (2.3) and (2.10) or (2.11). This technique is particularly useful in situations where the deposition of the thin film must be the final processing step. That is, thin films which are unable to withstand subsequent processing steps can nevertheless be incorporated into the charge-flow capacitor and resistivity measurements can then be performed.

2.2 CHARACTERISTICS

The properties of the charge-flow capacitor will now be examined from the standpoint of its utility as a fire-detection device. First, a method of

using the device for detection will be described.

Figure 17 illustrates a cross-sectional view of a single top-electrode gap. If a voltage is suddenly applied between the top electrode and the substrate, the capacitor charges in two steps. First, the electrodes themselves charge almost instantaneously to the applied voltage. This situation is depicted in Fig. 17a. Second, the charge gradually flows through the resistive polymer film (Fig. 17b) until, finally, a state is reached where the polymer film is uniformly charged to the electrode voltage (Fig. 17c). The time required for this charging process depends on the resistivity of the polymer. Thus, the rate of charging is a sensitive indicator of the polymer resistivity.

Solely for the purpose of illustrating the idea, the step response is considered to follow a simple exponential. Figure 18 illustrates the current waveforms that would then result from the charging of the charge-flow capacitor for two different values of the polymer resistance. The total charge capacity of the structure does not depend on the resistance of the polymer. Hence, the areas under the current-versus-time waveforms must be equal. This implies that the current equation is of the form

$$I = \frac{Q}{\tau} e^{-t/\tau} \tag{2.13}$$

where τ is an RC product consisting of the resistance R of the polymer and the dc capacitance C of the charge-flow capacitor, and where Q is the total charge which can accumulate in the polymer. Note that Q=CV where V is the amplitude of the suddenly applied dc voltage.

The initial current is clearly a function of the polymer resistance. For two different values of the polymer resistance,there are two different

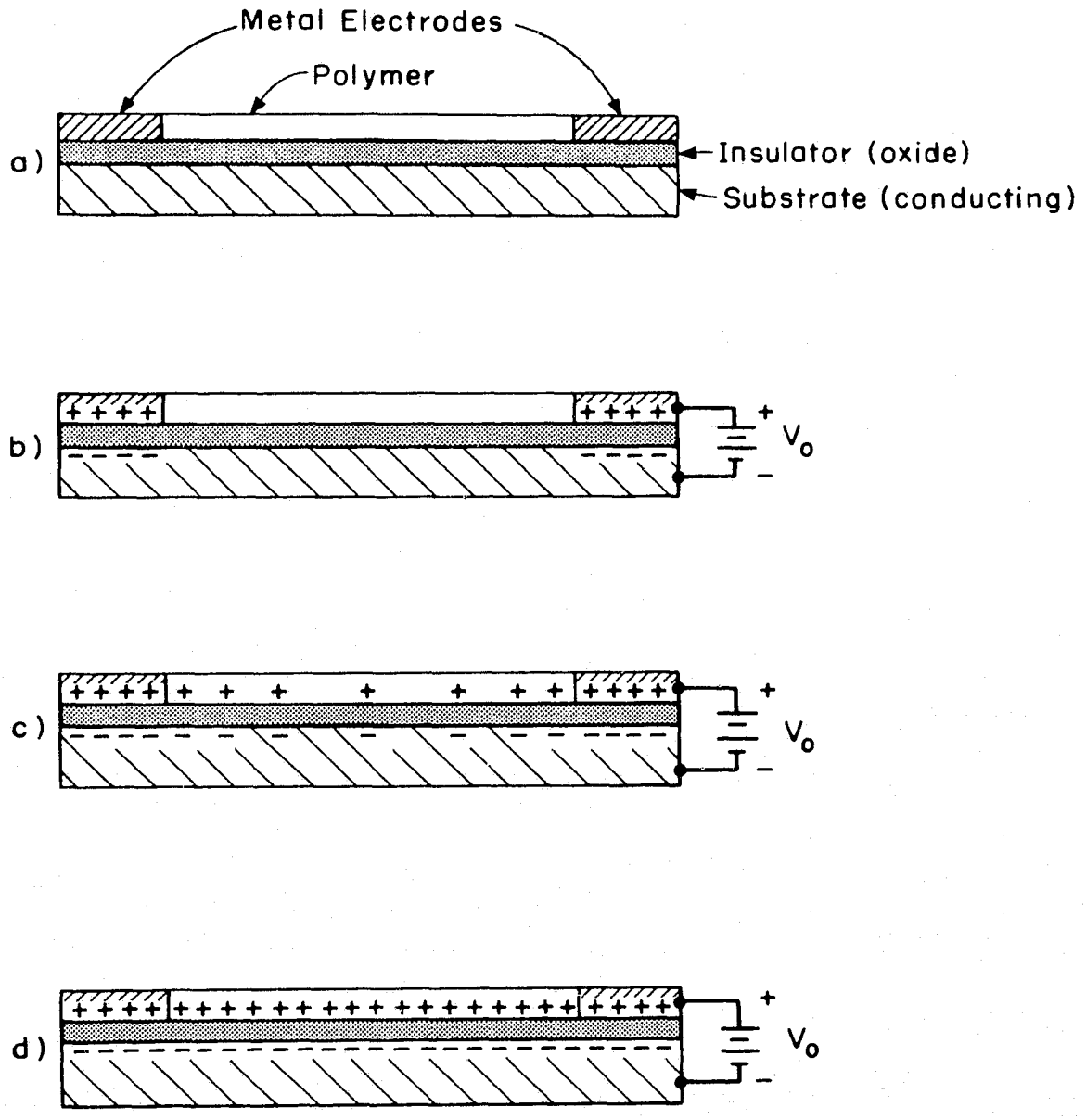

The Charge-Flow Capacitor

Figure 17

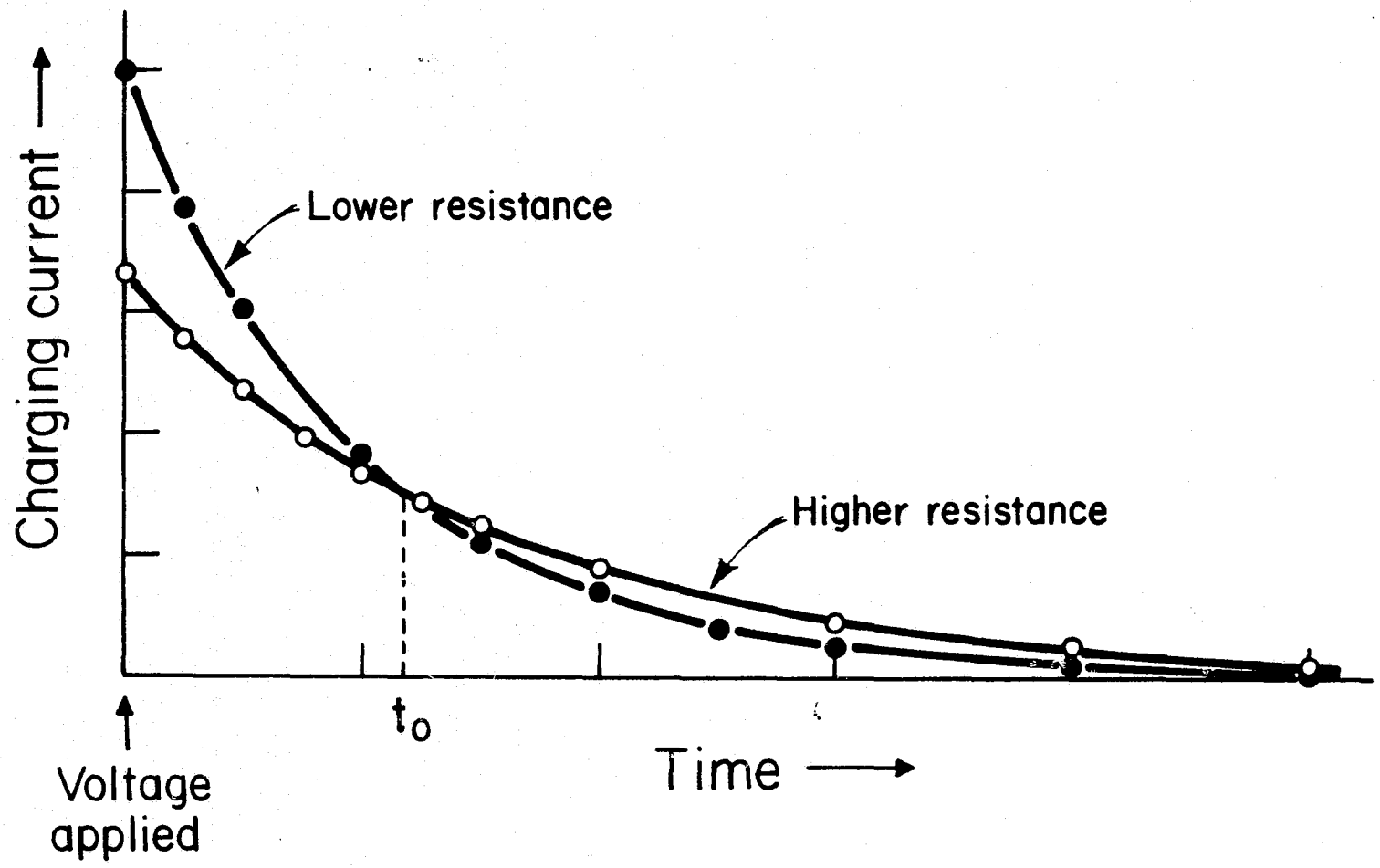

Figure 18

Charging-current waveforms for two different polymer resistances

time constants τ_1 and τ_2. The value of $t = t_o$ where the two waveforms intersect is given by

$$t_o = \frac{\tau_1 \tau_2}{\tau_2 - \tau_1} \ln \frac{\tau_2}{\tau_1} \quad . \tag{2.14}$$

For $0 < t < t_o$, the current is greater for the lower-resistance polymer.

This device could be used to detect changes in polymer resistance by measuring the area under the current-versus-time waveform for a predetermined time (a measurement that is easily accomplished electronically by means of an integrator circuit). The rapidly charging curve will yield a greater area than the slowly charging curve if the area in the range $0 < t < t_o$ is measured. In practice, a voltage would be applied to the device and the area measured up to a preset time. The voltage is subsequently removed for the same time to permit the charge to flow back out of the polymer. This cycle is then repeated. The current waveforms for charging and discharging are symmetric and reproducible unless the polymer resistance changes. Any decrease in polymer resistance produces an increase in the measured area during any charging cycle.

2.3 FIRE TESTS

Employing the identical fire-test apparatus described in Section 1.5, fire tests were performed on the charge-flow capacitors. A symmetrical square-wave voltage was applied as opposed to the dc voltage used for the lock-and-key device measurements. Figure 19 depicts an example of a fire test in which 10.0 mg of polyurethane was burned. The response of the PSB charge-flow capacitor is quite clear. The current spikes shown in Fig. 19 are due to an unavoidable amount of electrode overlap. This limitation is

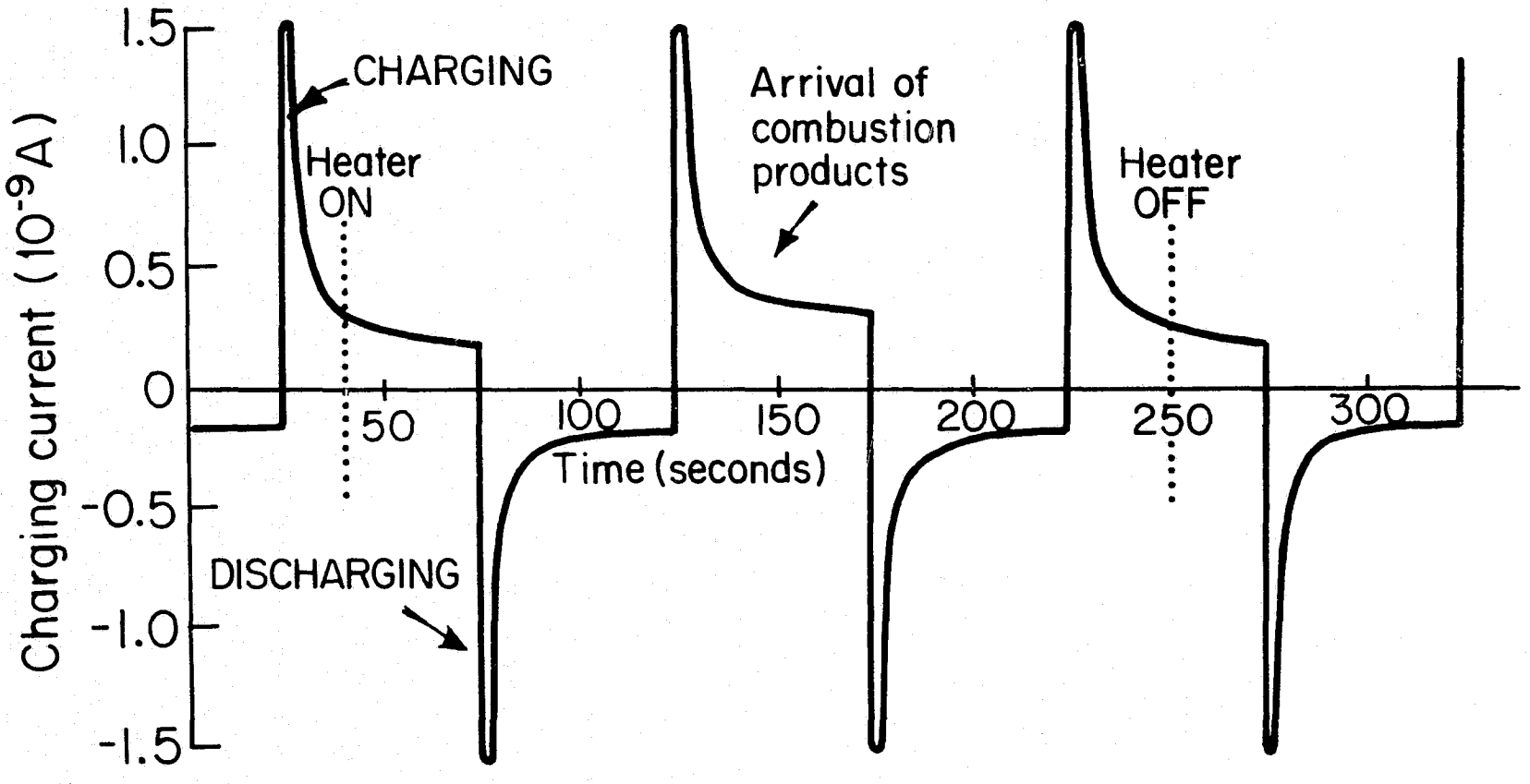

Figure 19

Charge-flow capacitor PSB with polyurethane

imposed by the mask registration tolerance.

Relating the results of Fig. 19 to the theory represented by Fig. 18 is rather straightforward. Observe that the half-period of the waveform in Fig. 19 is 50 seconds. It is deducible that the time t_o in Fig. 18 is, in fact, somewhat greater than 50 seconds for the results shown in Fig. 19. The positive half of the second cycle delineates the case in which the resistance of the polymer is substantially reduced. Consequently, the charging current is increased at the outset. Furthermore, it remains greater than the current represented by the curve prior to the arrival of the combustion products since the half-period of the excitation is less than t_o. Moreover, a conclusion reached is that the square wave switches polarity long before the charge-flow capacitor is fully charged.

Figure 20 portrays a second fire test in which the same PSB charge-flow capacitor was employed. The material burned was 14.0 mg of acrylic. Note that the charging current has a sudden peak about 110 seconds after heater turn-on. In Section 1.5 it was also observed that there was a sudden peak in the PSB lock-and-key device response to an acrylic fire 110 seconds after heater turn-on. Hence, Fig. 20 illustrates the charge-flow principle directly.

2.4 DISCUSSION

The charge-flow capacitor, in contrast to the lock-and-key device, has its capacitance (as opposed to resistance in the latter device) directly influenced by the resistivity of the polymer. This permits the application of an input signal with a finite frequency. It was also discerned that the capacitance of the device is a function of the applied frequency.

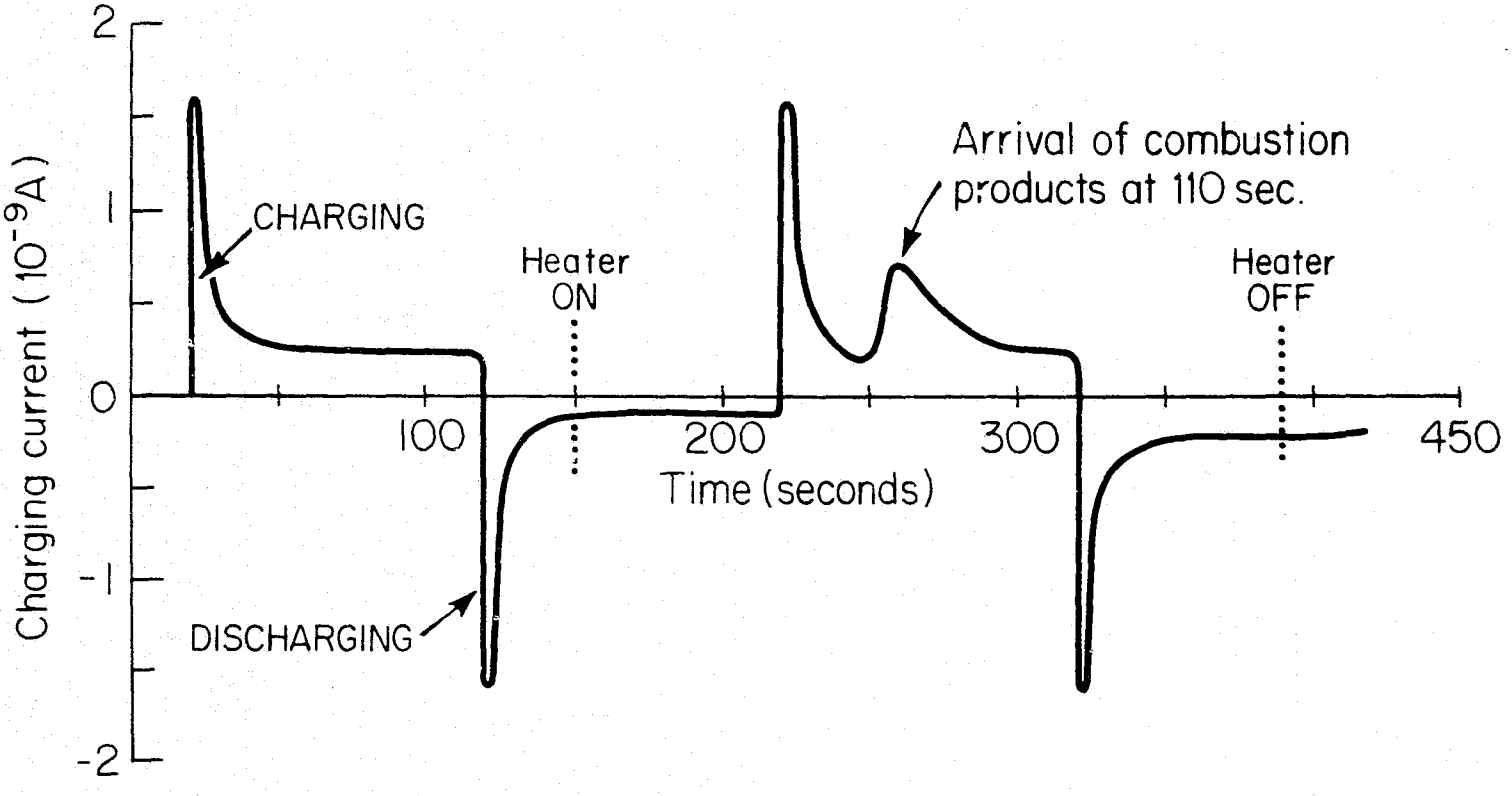

Charge-Flow Capacitor PSB with Acrylic

Figure 20

Furthermore, the polymer resistivity could be monitored by examining the charging-current waveforms. Fire tests were performed and it was observed that the charging-current waveforms vividly indicated the time of arrival of the combustion products.

In Chapter 1 it was noted that the surface conductivity of the uncoated glass or silicon dioxide is somewhat higher than the conductivity of many of the polymers (for example, PSB and PFI). The fact that both the lock-and-key device and the charge-flow capacitor produced a sharp peak in their respective current waveforms 110 seconds after heater turn-on in response to acrylic fires supplies corroborative evidence for the substrate-surface-conduction suppression. That is, the device response was independent of the material which formed the interface below the polymer layer.

While it is clear that the charge-flow capacitor would be effective as a fire-detection device, a glance at Figs. 19 and 20 reveals the fact that the charging-current levels are in the range of hundreds of picoamperes. Once again, as in the case of the lock-and-key device, elaborate detection equipment would be required in conjunction with this device. This fact alone prohibits the utilization of the charge-flow capacitor as a commercial fire-detection device.

However, this device is at the heart of a more useful structure considered in the following chapter, in which the charge-flow capacitor is incorporated into the gate region of an MOS transistor. This not only takes advantage of the efficacy of the charge-flow capacitor as a fire-detection structure, but also utilizes the inherent current amplification of the MOS transistor.

CHAPTER 3: THE CHARGE-FLOW TRANSISTOR

3.1 INTRODUCTION

The charge-flow transistor (CFT) is a new MOS device which was developed primarily for fire-detection applications in which the transverse or sheet resistance of a thin film is monitored [10,11,12]. This new device permits the film resistance to be monitored with voltage and current levels normally used in MOS circuits, and, in addition, offers the following advantages:

1. The CFT is based on MOS technology. The fabrication process is such that all silicon-wafer processing, including metallization and passivation, is completed prior to the depostion of the film. Thus, films that would be unable to survive MOS processing steps can nevertheless be incorporated into the charge-flow transistor.

2. The CFT can be fabricated as part of an MOS integrated circuit. The detection circuitry can thus be integrated with the sensor element, a factor of major importance in ultimately reducing system size and cost.

3. No guarding or shielding of components is required, even for films with very high resistivities.

The microelectronic processing steps utilized in the fabrication of a charge-flow transistor are enumerated in the following section. Subsequent sections outline the theoretical and experimental results. Furthermore, the experimental results are subdivided into two categories: Basic measurements of device properties and the utilization of the device as a fire-detection instrument.

3.2 FABRICATION

The details of the CFT fabrication process are delineated with the aid of

Figs. 21 and 22. Each die consisted of a nine-transistor array. Top views of a die as well as a single charge-flow transistor are shown in Fig. 22. The right-hand column of the array in this figure shows three conventional MOS transistors included for testing and characterization purposes. Beginning with the top of the center column and ending with the bottom of the left-hand column, Fig. 22 shows six charge-flow transistors with gap widths (W) from 0.25 mils to 1.50 mils, in increments of 0.25 mils. Note from Fig. 21 that W is the width of the polymer-filled gap in the gate electrode. The channel length (L) is 2.0 mils and the channel width is 10.0 mils. The bond-pad size is six mils square.

Four masks were required for fabrication of the CFTs. These were: (1) the drain and source diffusion mask, (2) the gate definition mask, (3) the drain-source contact mask and (4) the metallization pattern mask. The layout of these masks and the fabrication of the reticles were performed at M.I.T. Lincoln Laboratory, courtesy of Dr. Dan Smythe.

The fabrication steps are enumerated with reference to Fig. 21. The substrate was an n-type silicon wafer with a resistivity of 13.0 ohm-cm, or equivalently, a net donor concentration of about $3.5 \times 10^{14} cm^{-3}$. The growth of 5000 Å of silicon dioxide on the entire wafer was the first fabrication step. The second step consisted of performing the drain-source diffusion photolithography, followed by the drain-srouce diffusion. This p-type (boron) diffusion was comprised of the utilization of a spin-on dopant (borosilicafilm) and a 1200°C drive-in diffusion of 30 minutes duration. The resultant drain and source diffusions were of depth 2.7 μm and surface concentration $5 \times 10^{18} cm^{-3}$. Furthermore, the impurity profile was of the complementary error function variety due to the nature of spin-

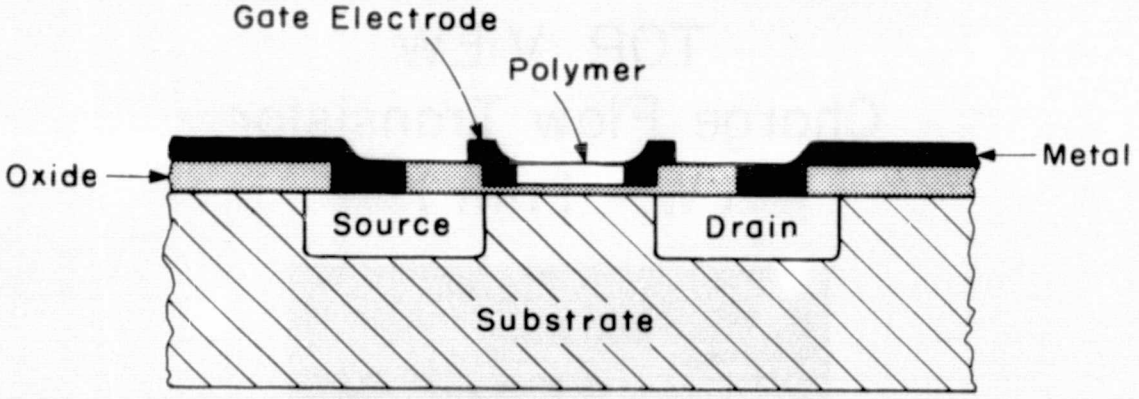

The charge-flow transistor

Figure 21

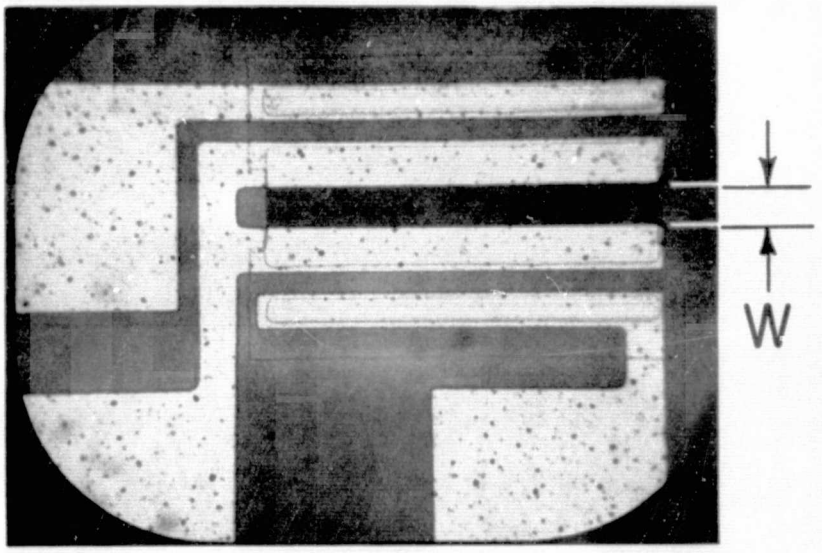

TOP VIEW
Charge Flow Transistor
(W = 1 mil)

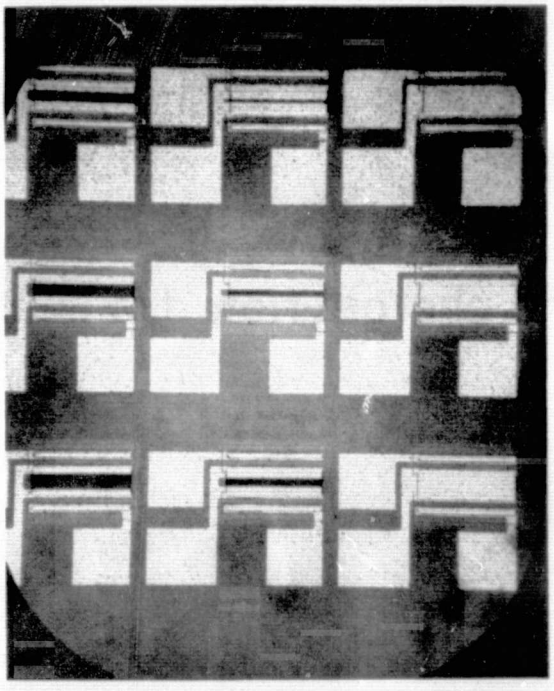

Nine-Transistor Array

Figure 22

on dopants.

The gate photolithography and the gate oxidation steps were conducted next. The 30-minute dry oxidation created a silicon-dioxide layer of thickness 1000 Å over the gate regions. Because this was the last high-temperature fabrication step, final oxide thicknesses were recorded. These were 3100 Å over the drain-source diffusion regions and 6000 Å over the field-oxide regions.

The fourth step consisted of the drain-source contact photolithography and the subsequent aluminum evaporation (with a tungsten-coil evaporator). The resulting aluminum thickness was about 1.0 μm. The fifth step simply consisted of depositing the polymer layer by means of the photoresist spinner. The resultant polymer layer thickness was approximately 3000 Å [8].

Finally, the wafers were scribed and the dice were bonded to eight-pin headers. Because raising the temperature too far above room temperature would permanently damage the polymer layer, the die attachment had to be achieved at room temperature. DUCO cement was selected for this purpose due to its strength, availability and the fact that it can be cured at room temperature. Since this cement is nonconducting, the substrate was necessarily maintained at floating potential.

From Fig. 22 it is seen that each CFT has three bond-pads. By connecting all the sources together, this enabled each header to have three of the nine transistors actively connected to pins. That is, seven of the eight header pins were utilized. Of the three bonded transistors, two were charge-flow transistors and the other was a conventional MOS transistor of identical dimensions.

3.3 THEORETICAL ASPECTS

Recalling Fig. 21, the charge-flow transistor incorporates a charge-flow capacitor into the gate of an enhancement mode MOSFET. Note the polymer-filled gap in the gate electrode. When a gate-to-source voltage larger than the FET threshold voltage is applied, the gate-to-substrate capacitor operates on the same principle as the charge-flow capacitor considered in Chapter 2. During the charging process, the electric field between the polymer and the substrate gradually increases. A complete channel is not formed until the FET threshold voltage is exceeded at all points along the gap. Thus, there is a time delay between the application of the gate-to-source voltage and the appearance of drain current in the completed channel. Consequently, the charge-flow transistor functions as a transducer, converting a sheet resistance measurement into the measurement of a delay time.

An approximate theory of operation of the CFT formulated by Senturia modeled the polymer-oxide-substrate region as an RC transmission line. This theory and the calculations performed by Sechen are based on the following assumptions: (1) the polymer thickness is uniform across the gap, (2) the dielectric constant of the polymer is unity, (3) the contacts to the polymer are ohmic, (4) the substrate-oxide interface is an equi-potential and (5) conduction in the oxide is negligible. Although none of these assumptions is strictly correct, the theory is reasonably tractable and does yield immediate insight into observed CFT behavior.

With the above assumptions, a theoretical expression for the voltage as a function of time and of the distance from the gate electrode was ob-tained. The diffusion equation for the RC transmission line was solved

in the standard fashion outlined below. This solution was formulated for the case of steady-state excitation by a unipolar square wave of amplitude V_o and period 2T.

The diffusion equation is given by

$$\frac{\partial^2 v}{\partial x^2} = \frac{\rho\epsilon}{d_1 d_2} \frac{\partial v}{\partial t} \tag{3.1}$$

where equation (3.1) is written in terms of the voltage v, the polymer resistivity ρ, the polymer thickness d_1, the insulator thickness d_2, the distance x and the time t. This equation is solved by the technique of separation of variables. Because of the symmetry of the problem, the solution from x = 0 to x = W/2 is in fact identical to that from x = W to x = W/2. Hence, it is only required to solve equation (3.1) for the variance of x from 0 to W/2. The general form of the solution may thus be written as

$$v(x,t) = \sum_p A_p \cosh[p(W/2 - x)] + B_p \sinh[p(W/2 - x)] e^{\frac{d_1 d_2}{\rho\epsilon} p^2 t} . \tag{3.2}$$

Two boundary conditions are now applied. The first is simply that the solution must be periodic with period 2T. That is,

$$v(x,t + 2T) = v(x,t) . \tag{3.3}$$

This, in turn, implies that

$$e^{\frac{d_1 d_2}{\rho\epsilon} p^2 2T} = 1 \tag{3.4}$$

or

$$\frac{d_1 d_2}{\rho\varepsilon} p^2 \, 2T = \pm (2\pi i)n \tag{3.5}$$

where n is an integer. From equation (3.5) it clearly follows that

$$p = \pm \left(\frac{\rho\varepsilon\pi}{d_1 d_2 T}\right) \sqrt{n} \left(\frac{1 \pm i}{\sqrt{2}}\right) \quad . \tag{3.6}$$

Making the following four definitions,

$$\mu = \frac{1 + i}{\sqrt{2}} \tag{3.7}$$

$$\mu^* = \frac{1 - i}{\sqrt{2}} \tag{3.8}$$

$$L = \sqrt{\frac{d_1 d_2 T}{\rho\varepsilon\pi}} \tag{3.9}$$

$$\omega = \frac{\pi}{T} \tag{3.10}$$

equation (3.2) may now be written as

$$v(x,t) = A_o + \sum_{n=1}^{\infty} \left\{ \left[A_{1n} \cosh\left(\sqrt{n}\, \mu \frac{(W/2 - x)}{L}\right) + A_{2n} \sinh\left(\sqrt{n}\, \mu \frac{(W/2 - x)}{L}\right) \right] e^{in\omega t} \right.$$

$$\left. + \left[B_{1n} \cosh\left(\sqrt{n}\, \mu^* \frac{(W/2 - x)}{L}\right) + B_{2n} \sinh\left(\sqrt{n}\, \mu^* \frac{(W/2 - x)}{L}\right) \right] e^{-in\omega t} \right\} \tag{3.11}$$

The second boundary condition is that

$$\left.\frac{\partial v}{\partial x}\right|_{W/2} = 0 \tag{3.12}$$

for all t. Hence, from equation (3.11), it must be true that

$$\frac{\sqrt{n}\,\mu}{L} A_{2n}\, e^{in\omega t} + \frac{\sqrt{n}\,\mu^*}{L} B_{2n}\, e^{-in\omega t} = 0 \quad . \tag{3.13}$$

Expanding the exponentials then requires that

$$\frac{\sqrt{n}\,\mu}{L} A_{2n} + \frac{\sqrt{n}\,\mu^*}{L} B_{2n} = 0 \tag{3.14}$$

and

$$\frac{\sqrt{n}\,\mu}{L} A_{2n} - \frac{\sqrt{n}\,\mu^*}{L} B_{2n} = 0 \quad . \tag{3.15}$$

The implication of equations (3.14) and (3.15) is that

$$A_{2n} = B_{2n} = 0 \quad . \tag{3.16}$$

Consequently, the subscripts 1 and 2 may be dropped. This allows equation (3.11) to be simplified to

$$\begin{aligned} v(x,t) = A_o + \sum_{n=1}^{\infty} \Bigg\{ & A_n \cosh\left[\sqrt{n}\,\mu\left(\frac{W/2 - x}{L}\right)\right] e^{in\omega t} \\ & + B_n \cosh\left[\sqrt{n}\,\mu^*\left(\frac{W/2 - x}{L}\right)\right] e^{-in\omega t} \Bigg\} \quad . \end{aligned} \tag{3.17}$$

In addition, at x = 0, equation (3.17) reduces to

$$\begin{aligned} v(0,t) = A_o + \sum_{n=1}^{\infty} & A_n \cosh\left(\mu\frac{\sqrt{n}\,\mu W}{2L}\right) e^{in\omega t} \\ & + B_n \cosh\left(\frac{\sqrt{n}\,\mu^* W}{2L}\right) e^{-in\omega t} \quad . \end{aligned} \tag{3.18}$$

Of course, at x = 0, v(0,t) is simply a unipolar square wave of amplitude V_o and period 2T. This is easily decomposed into a square wave of amplitude $V_o/2$ and a dc voltage $V_o/2$. The Fourier series representation for the square-wave portion plus the dc term is given by

$$v(0,t) = V_o\left[\frac{1}{2} + \frac{2}{\pi}\sum_{(+)\text{odd } n}\frac{\sin n\omega t}{n}\right] \quad . \tag{3.19}$$

Upon comparing equations (3.18) and (3.19), it is immediately deduced that

$$A_n \cosh\frac{\sqrt{n}\,\mu W}{2L} + B_n \cosh\frac{\sqrt{n}\,\mu^* W}{2L} = 0 \tag{3.20}$$

$$i\left[A_n \cosh\frac{\sqrt{n}\,\mu W}{2L} - B_n \cosh\frac{\sqrt{n}\,\mu^* W}{2L}\right] = \frac{2V_o}{\pi n} \quad . \tag{3.21}$$

Solving these two equations for A_n and B_n yields the following results:

$$A_n = -\frac{iV_o}{\pi n \cosh\left(\frac{\sqrt{n}\,\mu W}{2L}\right)} \tag{3.22}$$

$$B_n = \frac{iV_o}{\pi n \cosh\left(\frac{\sqrt{n}\,\mu^* W}{2L}\right)} \quad . \tag{3.23}$$

Substitution of equations (3.22) and (3.23) into equation (3.17) renders the following:

$$v(x,t) = V_o\left\{\frac{1}{2} + \sum_{(+)\text{odd } n}\left(\frac{-i}{\pi n}\right)\left[\frac{\cosh\sqrt{n}\,\mu(W/2 - x)/L}{\cosh\sqrt{n}\,\mu W/2L}\,e^{in\omega t} - \frac{\cosh\sqrt{n}\,\mu^*(W/2 - x)/L}{\cosh\sqrt{n}\,\mu^* W/2L}\,e^{-in\omega t}\right]\right\} \quad . \tag{3.24}$$

Employing the identity

$$\cosh(x \pm iy) = \cosh x \cos y \pm i \sinh x \sin y \tag{3.25}$$

and performing algebraic manipulation, the following result is attained:

$$v(x,t) = V_o \left\{ \frac{1}{2} + \frac{2}{\pi} \sum_{(+)\text{odd } n} \frac{1}{n} \left[\frac{[-A_n(x)\, B_n(0) + B_n(x)\, A_n(0)]\cos \frac{n\pi t}{T}}{A_n^2(0) + B_n^2(0)} \right. \right.$$

$$\left. \left. \frac{+[A_n(x)\, A_n(0) + B_n(x)\, B_n(0)]\sin \frac{n\pi t}{T}}{A_n^2(0) + B_n^2(0)} \right] \right\} \tag{3.26}$$

where

$$A_n(x) = \cosh\left[\left(1 - \frac{2x}{W}\right) Z\sqrt{n}\right] \cos\left[\left(1 - \frac{2x}{W}\right) Z\sqrt{n}\right] \tag{3.27}$$

$$B_n(x) = \sinh\left[\left(1 - \frac{2x}{W}\right) Z\sqrt{n}\right] \sin\left[\left(1 - \frac{2x}{W}\right) Z\sqrt{n}\right] \tag{3.28}$$

and where

$$Z = \frac{W}{\sqrt{8}\, L} \quad . \tag{3.29}$$

Equation (3.26) was then evaluated by means of a digital computer. Figure 23 is a plot of equation (3.26) for a PSB-coated CFT for W = 1.0 mils, L = 0.11 mils and T = 20 seconds. An intriguing result is the fact that the minimum voltage in the gap does not necessarily reside at the midpoint of the gap for steady-state excitation. That is, to achieve a particular delay time (t_o), the unipolar square-wave amplitude (V_o) must be large enough such that the minimum voltage (wherever it may be in the gap) is

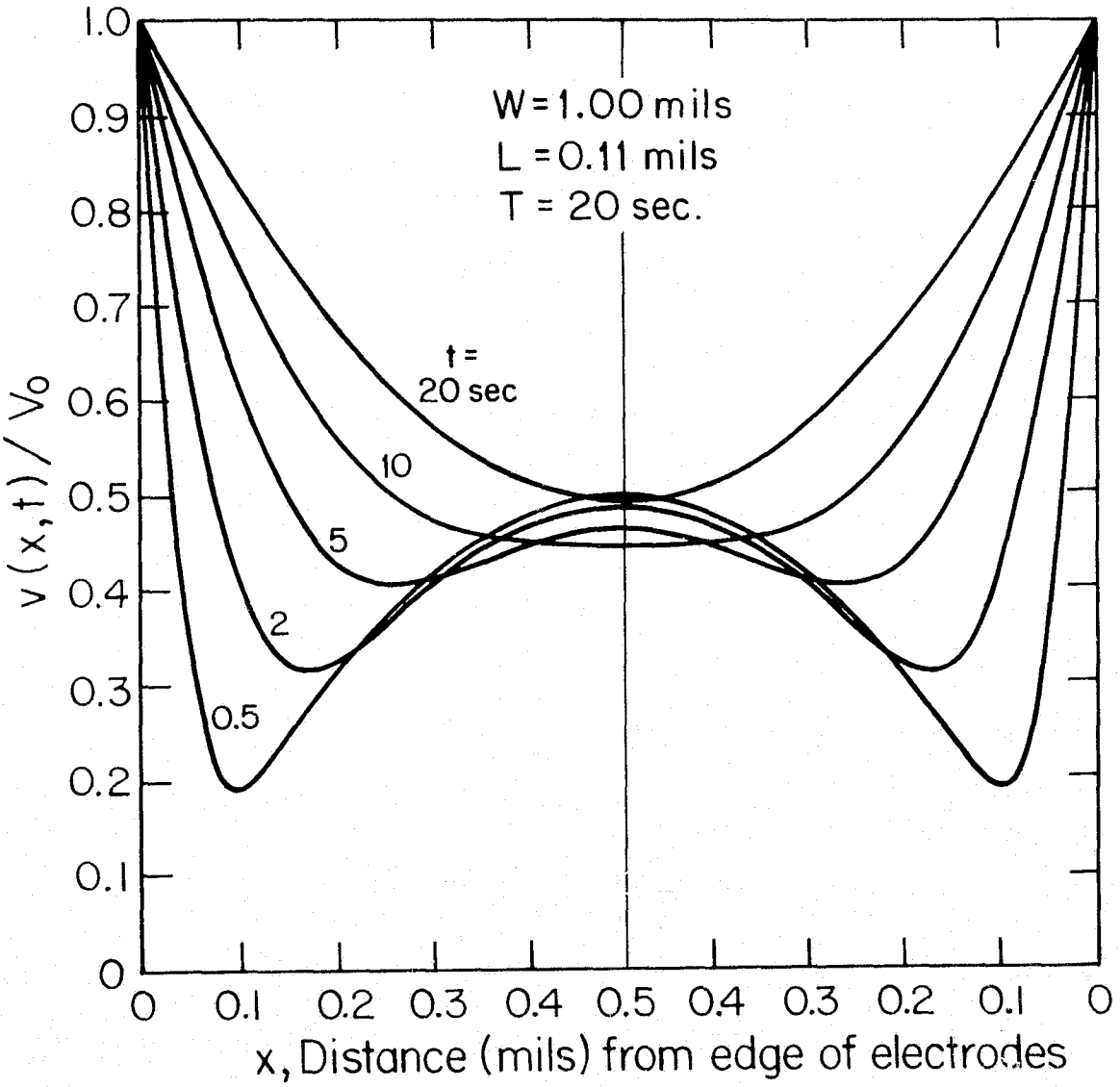

Figure 23

Theoretical CFT $v(x,t)/V_o$ characteristics

greater than the threshold voltage. In other words, the theoretical delay time is defined as the earliest time in the "ON" half-cycle ($0 \leq t \leq T$) for which $v(x,t)$ exceeds the FET threshold voltage for all x. Of course, for larger values of V_o, the delay time of the CFT will be shorter.

Theoretical t_o-versus-V_o characteristics of a CFT for various gap widths was obtained as follows. First, following equation (3.26), a time t is chosen. Then the minimum value of the ratio $v(x,t)$ divided by V_o is ascertained for the specific time t as x is varied. Thirdly, this minimum value is subsequently inverted [that is, it becomes V_o divided by $v(x,t)$] and multiplied by the threshold voltage (V_T). Consequently, what remains is the value of V_o required to turn-on the CFT in the time t. In this fashtion t_o (the delay time, which is in fact identical to the "t" mentioned above)-versus-V_o plots are generated. According to equations (3.27) - (3.29), the values of W and L must also be selected. Along these lines, Figs. 24-30 are plots of t_o versus V_o with the parameter being W. Each figure depicts the curves for a different value of L, thereby illustrating the effect of changing L.

While the t_o-versus-V_o curves will be examined later in relation to the experimental results, several characteristics are of interest at this point. Note the peculiar "kinks" in many of the curves. These are caused by the transition from a voltage minimum away from the midpoint of the gap to a minimum at the midpoint as the delay time t_o becomes longer. Moreover, as discerned from equations (3.9) and (3.11), L can be interpreted as a diffusion length for the charge flowing into the polymeric region. Note that L is proportional to the square root of the square-wave half-period T. That is, for larger values of T, the diffusion length is longer

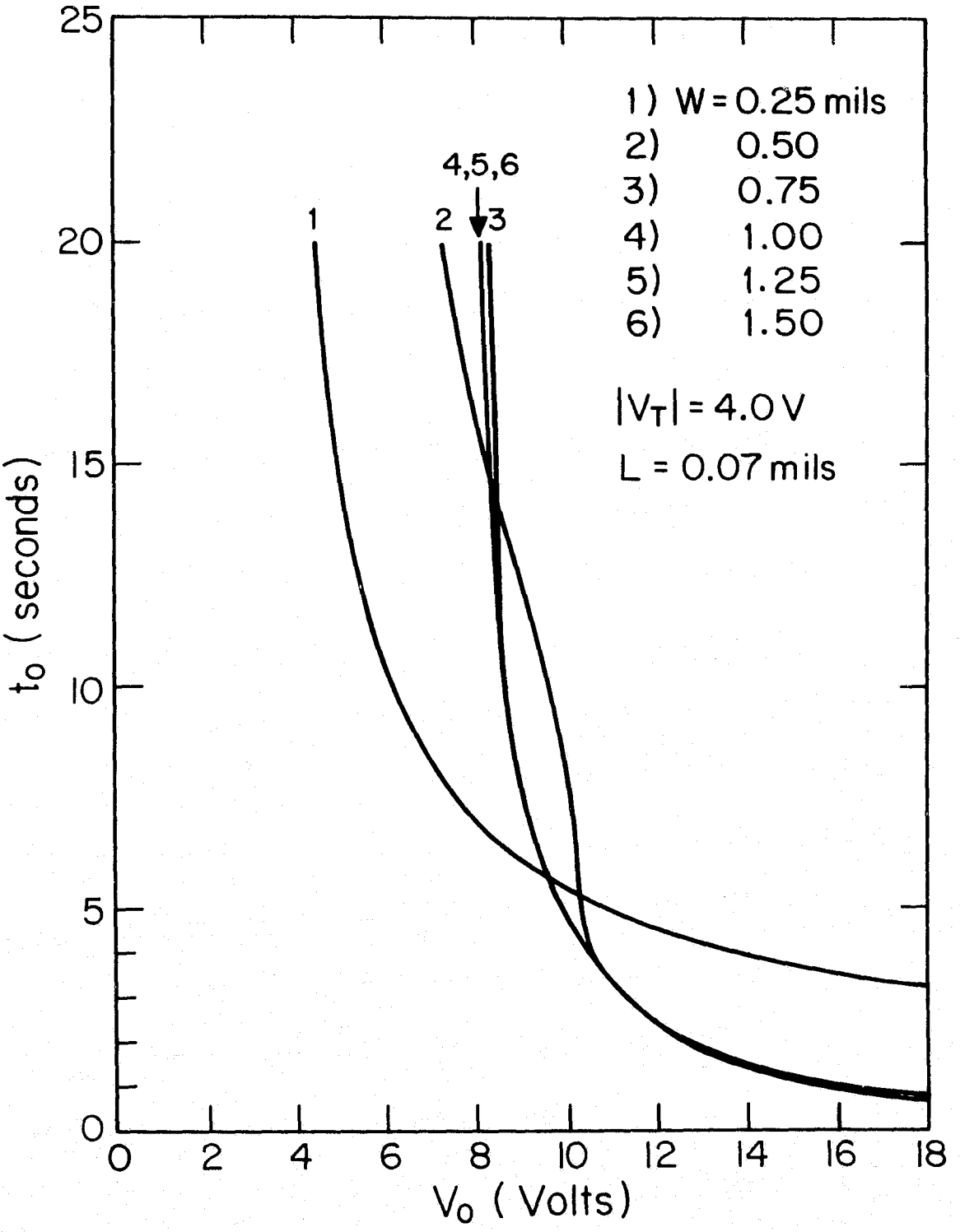

Figure 24

Theoretical t_o versus V_o

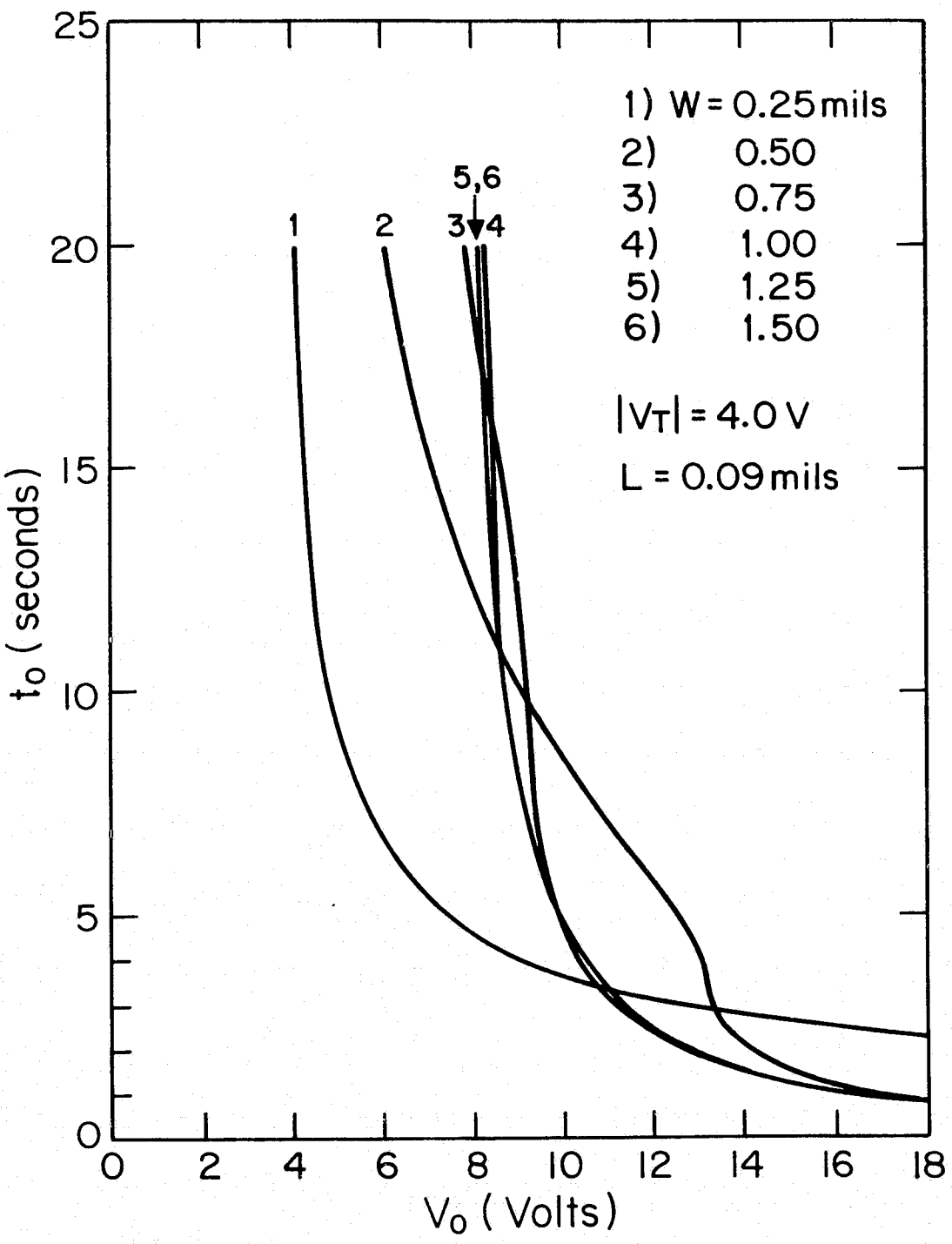

Figure 25

Theoretical t_o versus V_o

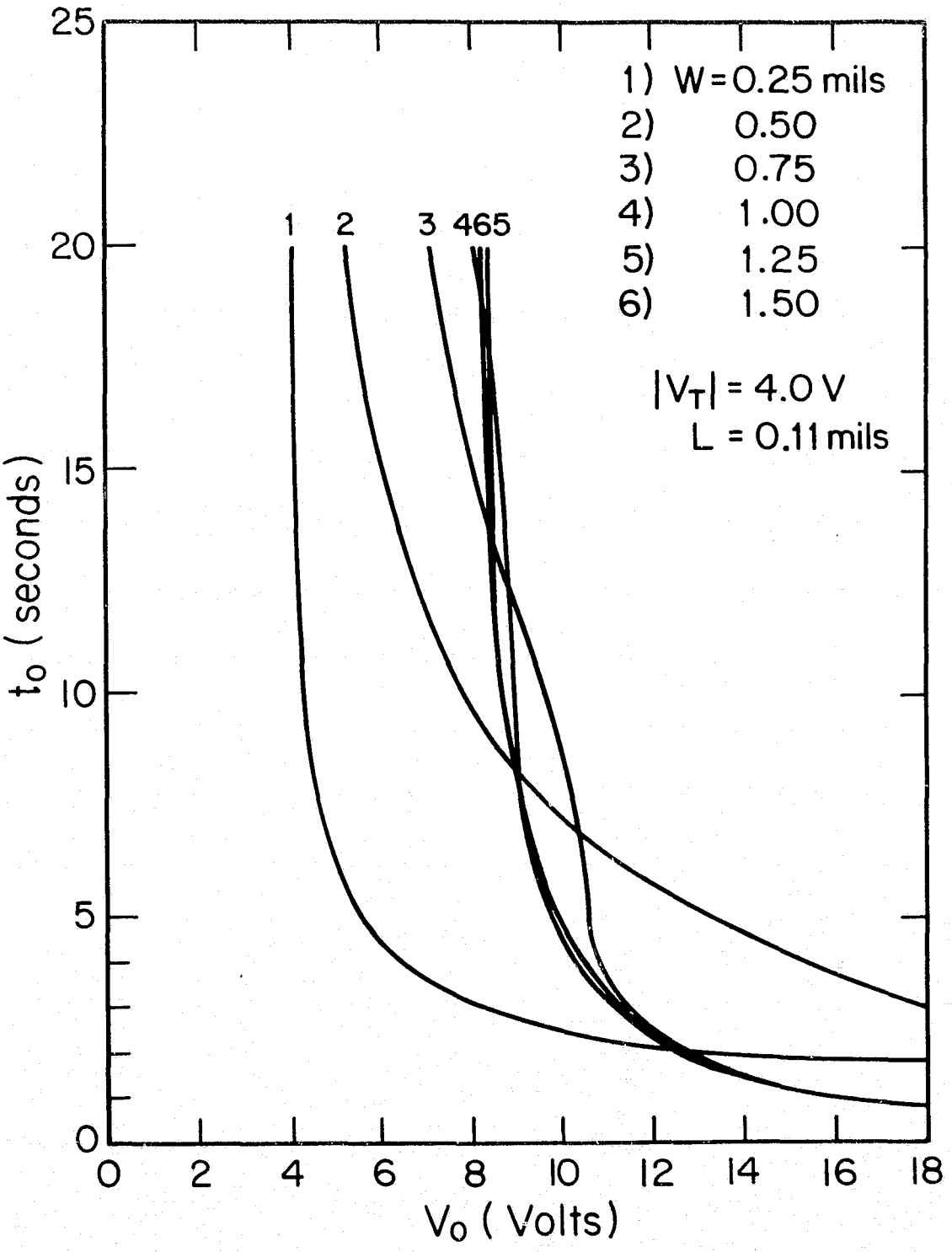

Figure 26

Theoretical t_o versus V_o

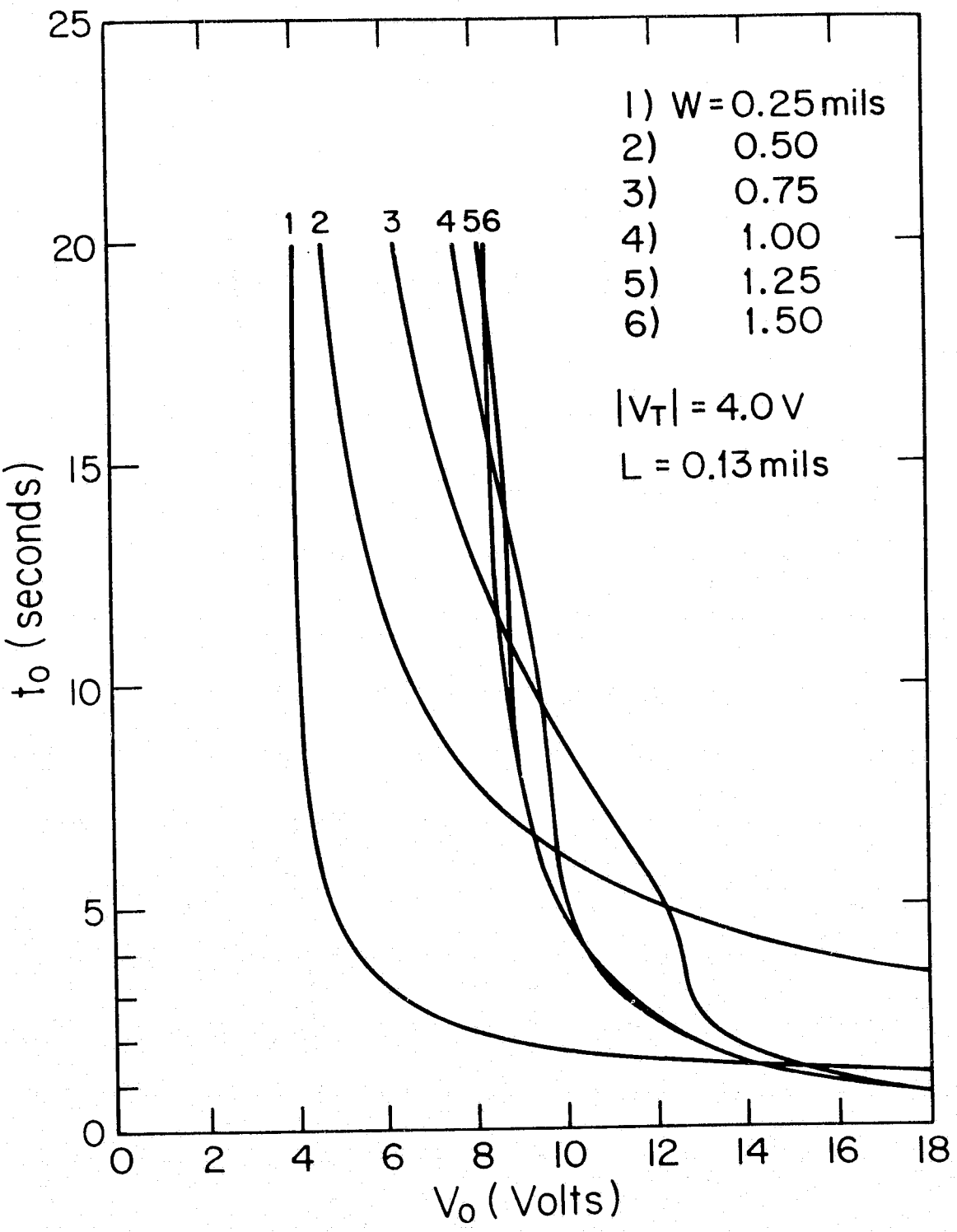

Figure 27

Theoretical t_o versus V_o

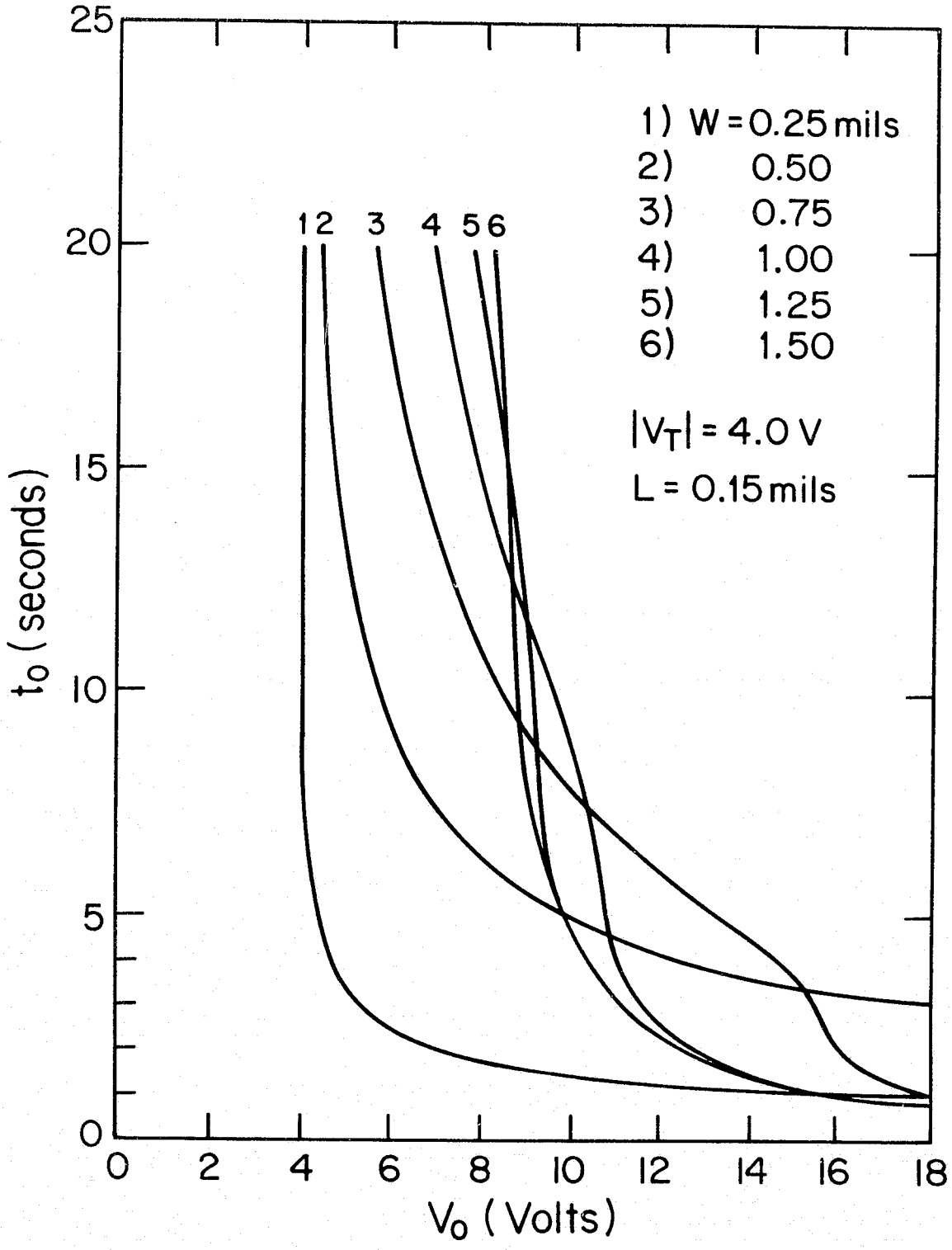

Figure 28

Theoretical t_o versus V_o

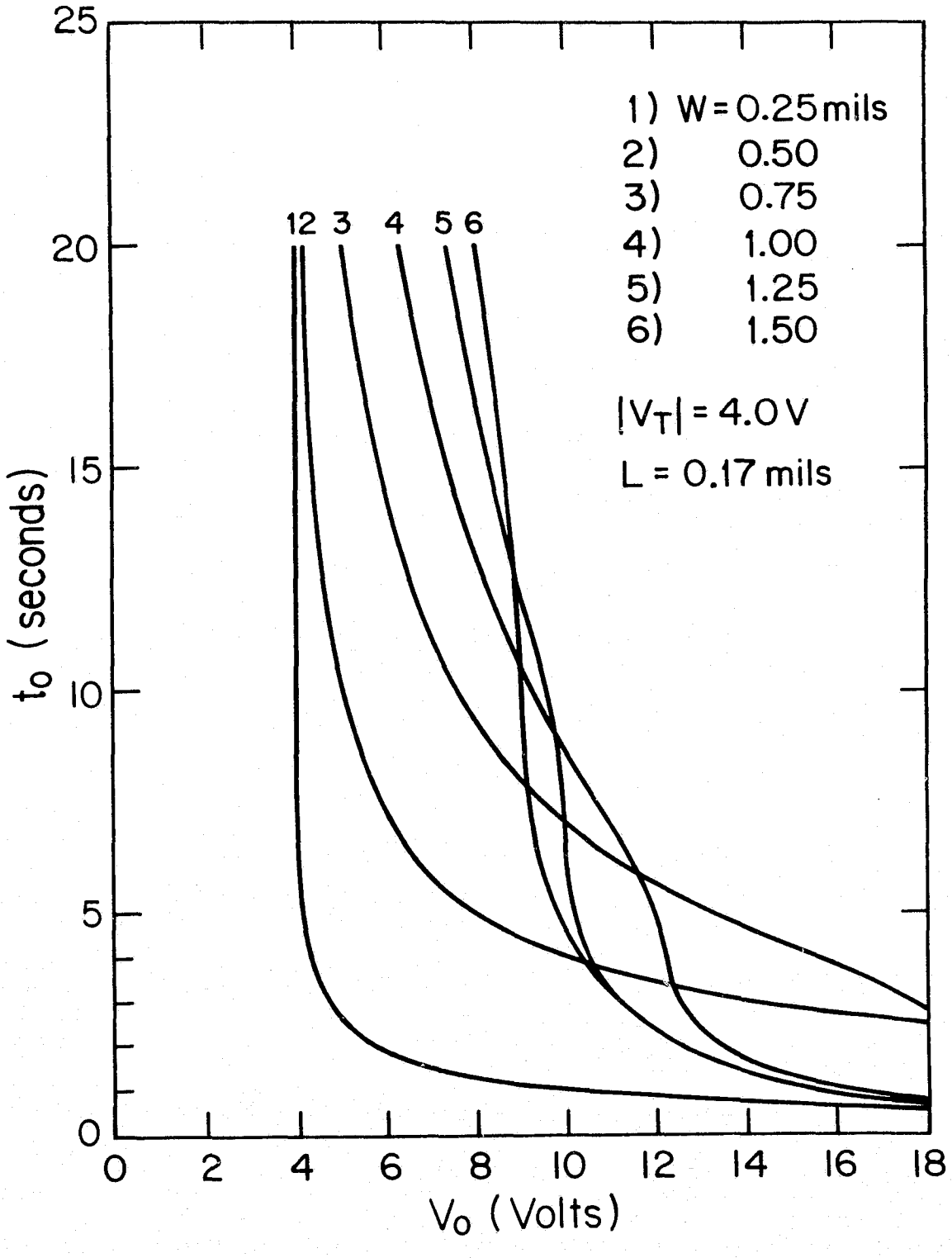

Figure 29

Theoretical t_o versus V_o

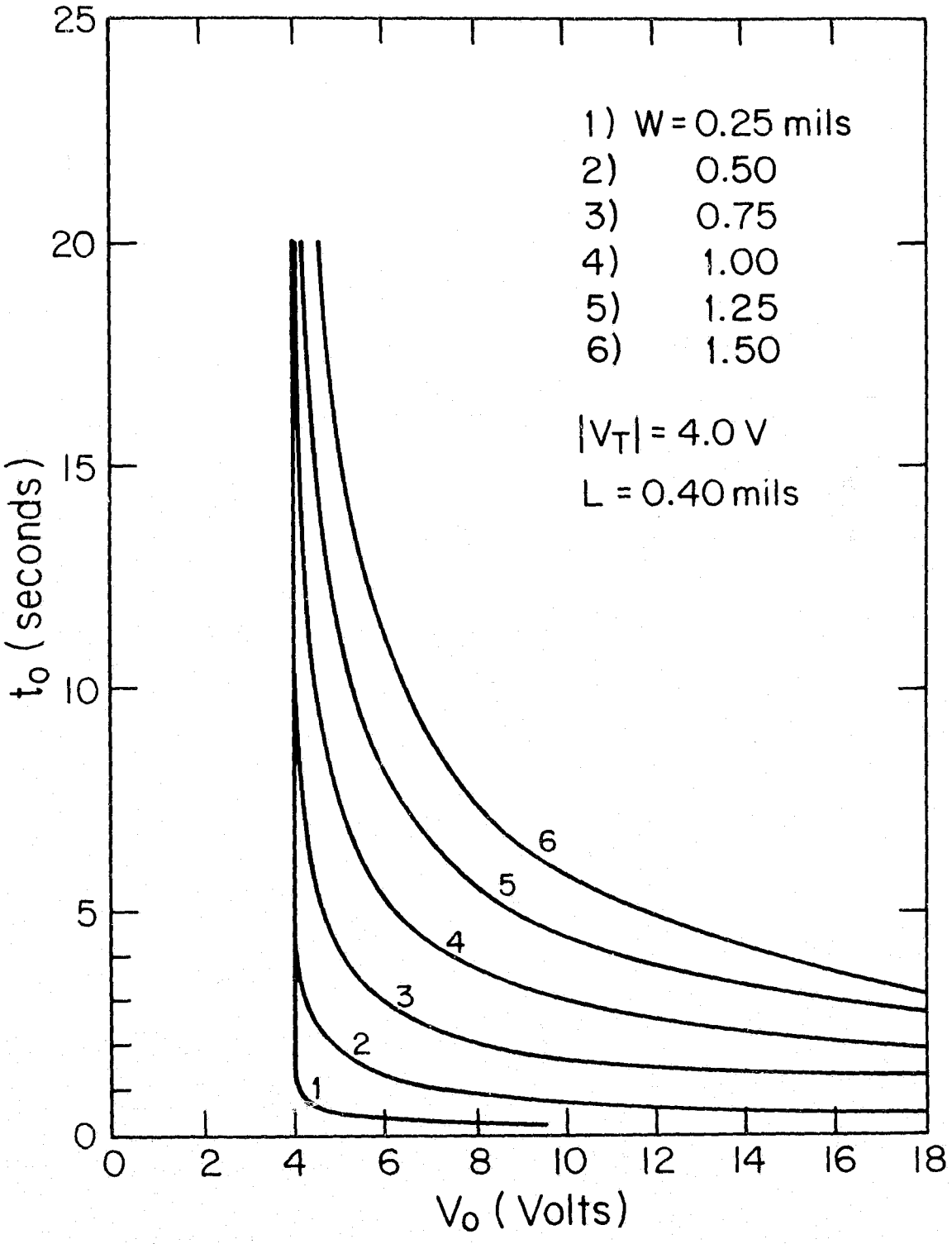

Figure 30

Theoretical t_o versus V_o

and thus the voltage minima at the end of each "ON" half-cycle reside nearer to the midpoint of the gap. Eventually T (and therefore L) becomes large enough such that the minimum resides at the midpoint and thus for all values of L larger than this critical value, the minimum remains at midgap. Clearly the value of T required to attain this critcial value is quite dependent on W. That is, the larger the value of W, the larger the value of T required to reach the critical value.

Observing Fig. 30, it is clearly seen that for a value of L very large relative to the gap widths, there are no "kinks" in the curves. This is because the voltage minima all exist at midgap for V_o less than 18 volts. On the other hand, Fig. 24 delineates a situation in which nearly the opposite is true. That is, as L approaches zero, all of the voltage minima (independent of W) are away from the midpoint of the gap. Consequently, the limit as L approaches zero, a single curve would represent the complete t_o-versus-V_o data for all values of W.

Of course, Figs. 24-29 illustrate cases somewhere between the two aforementioned extremes. Note that in every situation (for a given value of W) the "kinks" occur for larger values of t_o as L is decreased. In other words, as L is decreased for a given W, the voltage minima move away from the midpoint of the gap for larger values of the delay time t_o.

Another peculiarity is depicted by Figs. 24-26. Observe that in these instances, a charge-flow transistor with a wider gap (that is, larger W) actually turns-on sooner than a CFT with a smaller gap. This is particularly evident for the longer delay times. Once again, this interesting result is a consequence of the transmission-line properties of the CFT gate region. The charge-sloshing modes introduce the "kinks" as the

voltage minima begin to move away from the gap center. In fact, when the device is operated near this critical point, it is seen from Fig. 23 that the voltage profile is unusually flat (horizontally) for much of the gap region. This idiosyncrasy gives rise to a sooner-than-expected turn-on of the CFT. Furthermore, this also induces the anomalous crossings of the t_o-versus-V_o curves for incrementally increasing values of W.

One additional point of interest concerns the narrowest gap CFTs of Figs. 26-30. It can be surmised that the effective threshold voltage for a CFT can be extrapolated from the W = 0.25 mils curve. That is, for a delay time near the value of T (20 seconds for the figures of interest), the gap width W is so small (in relation to L) that only the FET threshold voltage need be applied to turn-on the CFT. This concept will be of particular importance when the experimental device properties are discussed in the next section.

The final theoretical consideration is based upon the fire-detection application. That is, the effect of a change in conductivity of the polymer region. From equation (3.9), it is seen that L is directly proportional to the square root of the conductivity of the polymer. Figure 31 portrays the effect of a change in L (for example, due to a change in the conductivity) on the t_o-versus-V_o characteristics of a CFT with W = 1.00 mil. Clearly, for a given V_o, the delay time change due to a change in L is quite dramatic. This is borne out in much more detail by Fig. 32 which depicts t_o versus V_o for a V_o of 8.0 volts. Supposing that the conductivity changed by a factor of 16 (Chapter 1 demonstrated the reasonableness of such a change), then L would change by a factor of 4. For example, assume L increased from 0.11 mils to 0.44 mils. The corresponding change in delay

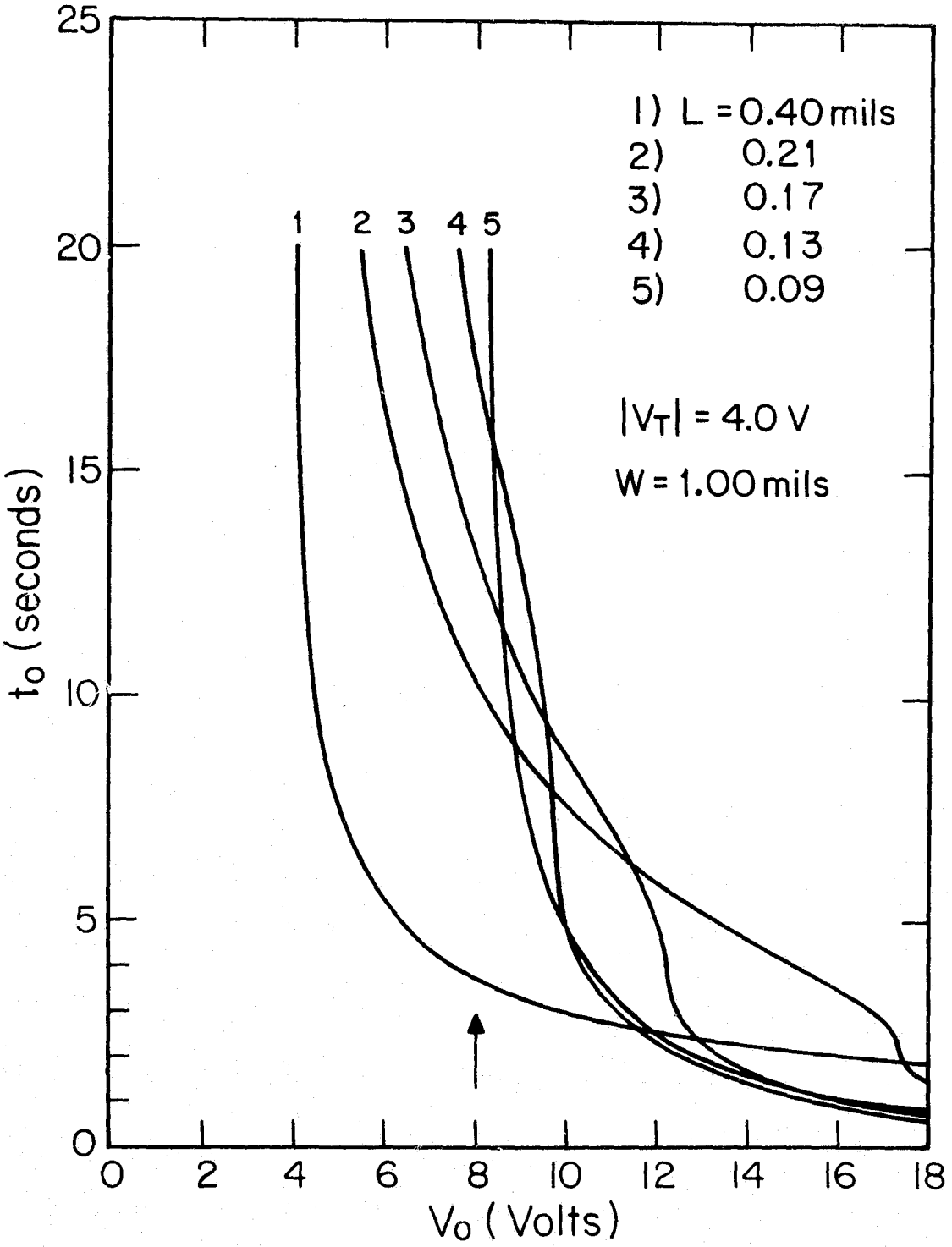

Figure 31

Theoretical t_o versus V_o

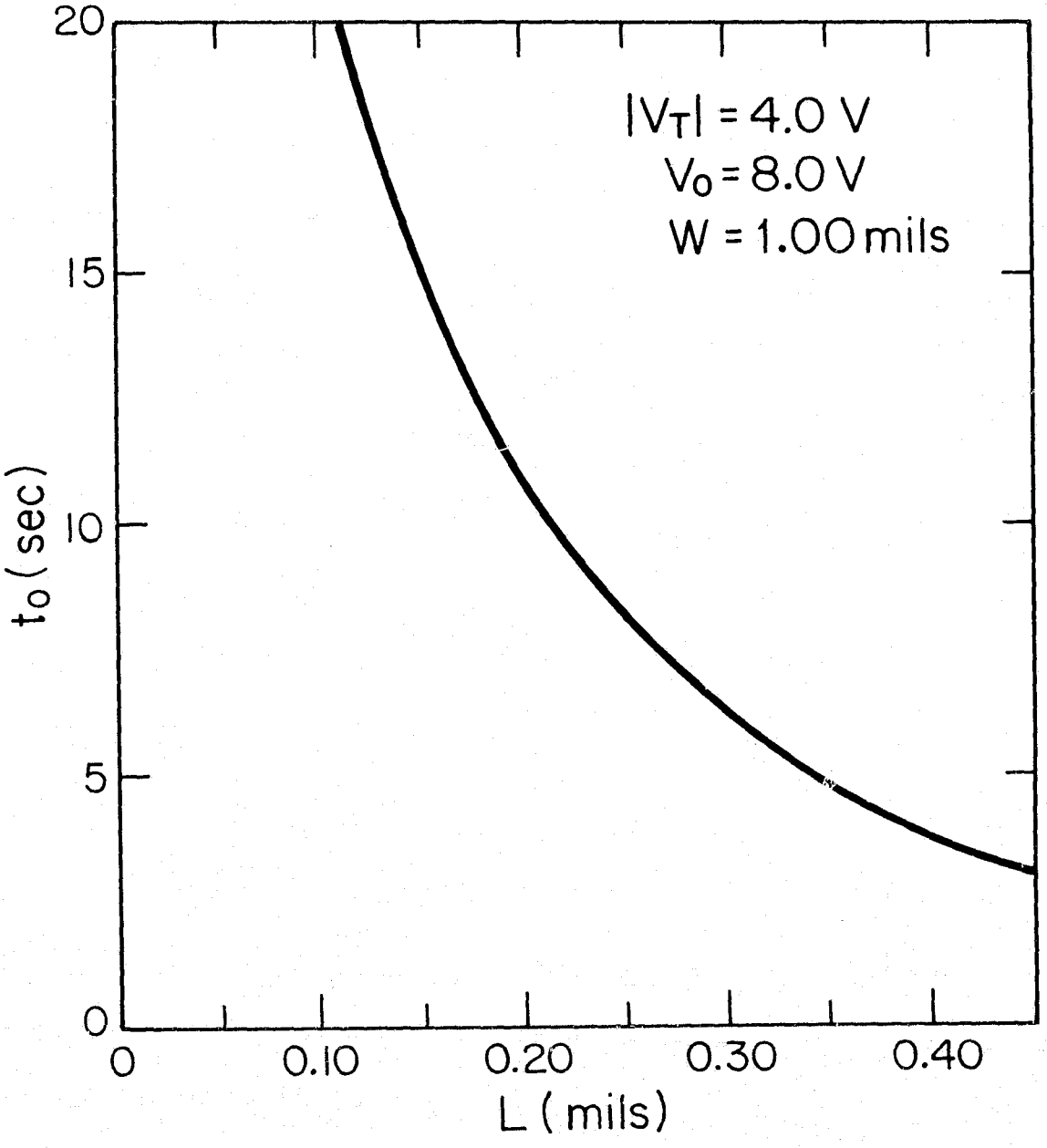

Figure 32

Theoretical t_o versus L

time is from 20.2 seconds to 3.1 seconds. Quite evidently, changes in the delay time of this magnitude are easily sufficient for fire-detection purposes. Hence, the feasibility of the CFT as an early-warning fire-alarm device has been vividly demonstrated on a theoretical basis.

3.4 DEVICE PROPERTIES

Measurements were performed to procure the experimental t_o-versus-V_o characteristics, with the gap width W being the parameter. These measurements utilized the standard MOSFET threshold-voltage definition as that gate-to-source voltage required to produce a drain current of 1 μA. Using the zero-gap devices which appear on the same chip as the CFTs, measured threshold voltages were 3.9 ± 0.1 volts. Drain current versus gate-to-source voltage profiles were obtained for several devices. Figure 33 illustrates a typical result in which the threshold voltage was 3.8 volts. The near-perfect square-law behavior of the test devices is particularly noteworthy.

The basic CFT measurement consisted of monitoring the steady-state drain current as a function of time for a unipolar square wave applied to the gate. A typical drain-current waveform is shown in Fig. 39. Note that the experimental delay time is that time between the beginning of the "ON" half cycle of the square wave and the point at which the drain current attains a value of 1 μA. Experimental delay-time data obtained in this fashion are plotted in Fig. 34. This figure portrays the variation of delay time with gap width and applied-voltage amplitude for PFT-coated devices for a unipolar square wave with the half-period T being 20 seconds. Notice the similarity of these experimental curves with the theoretical

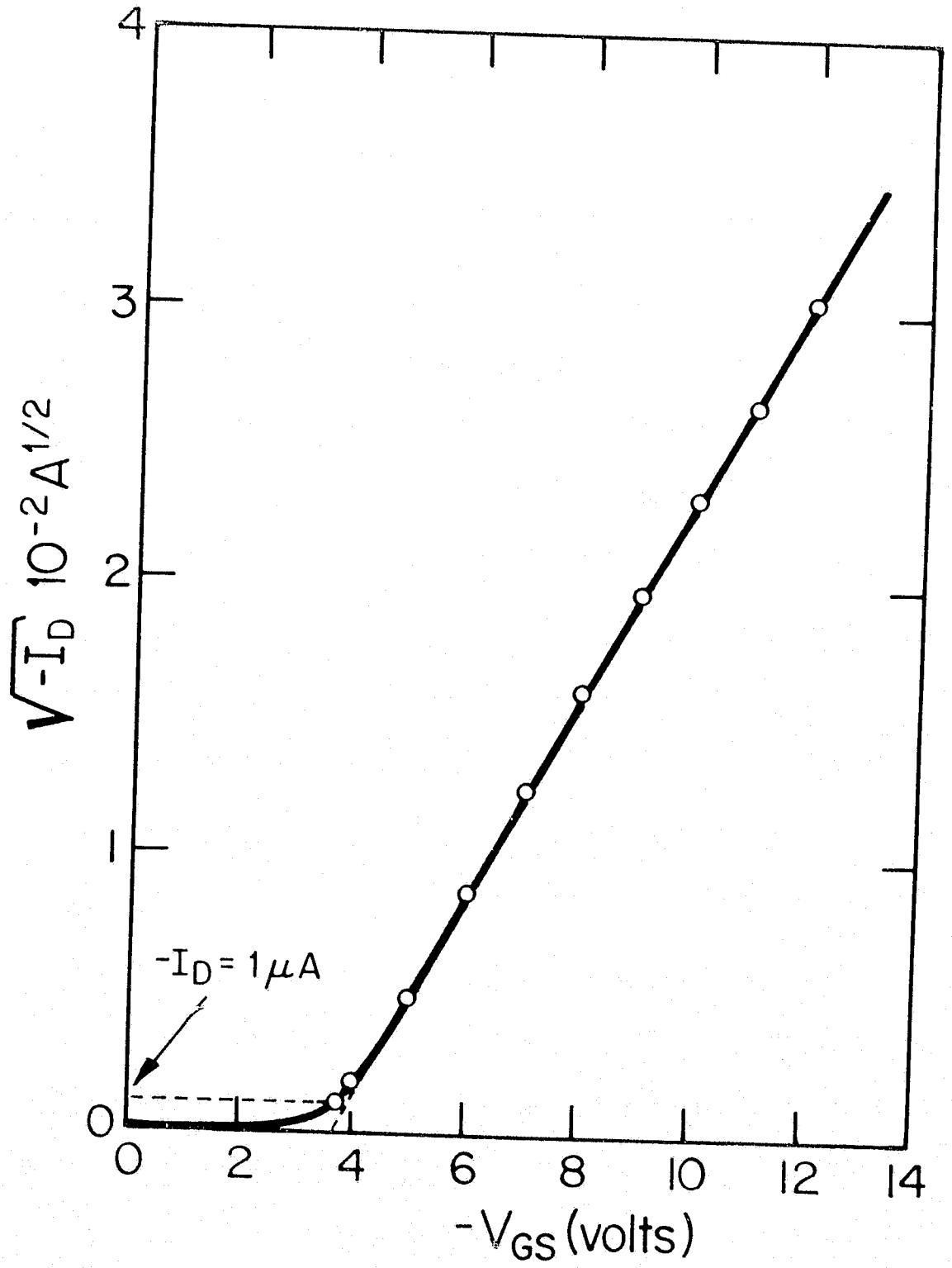

Figure 33

Square-law behavior of MOS test device

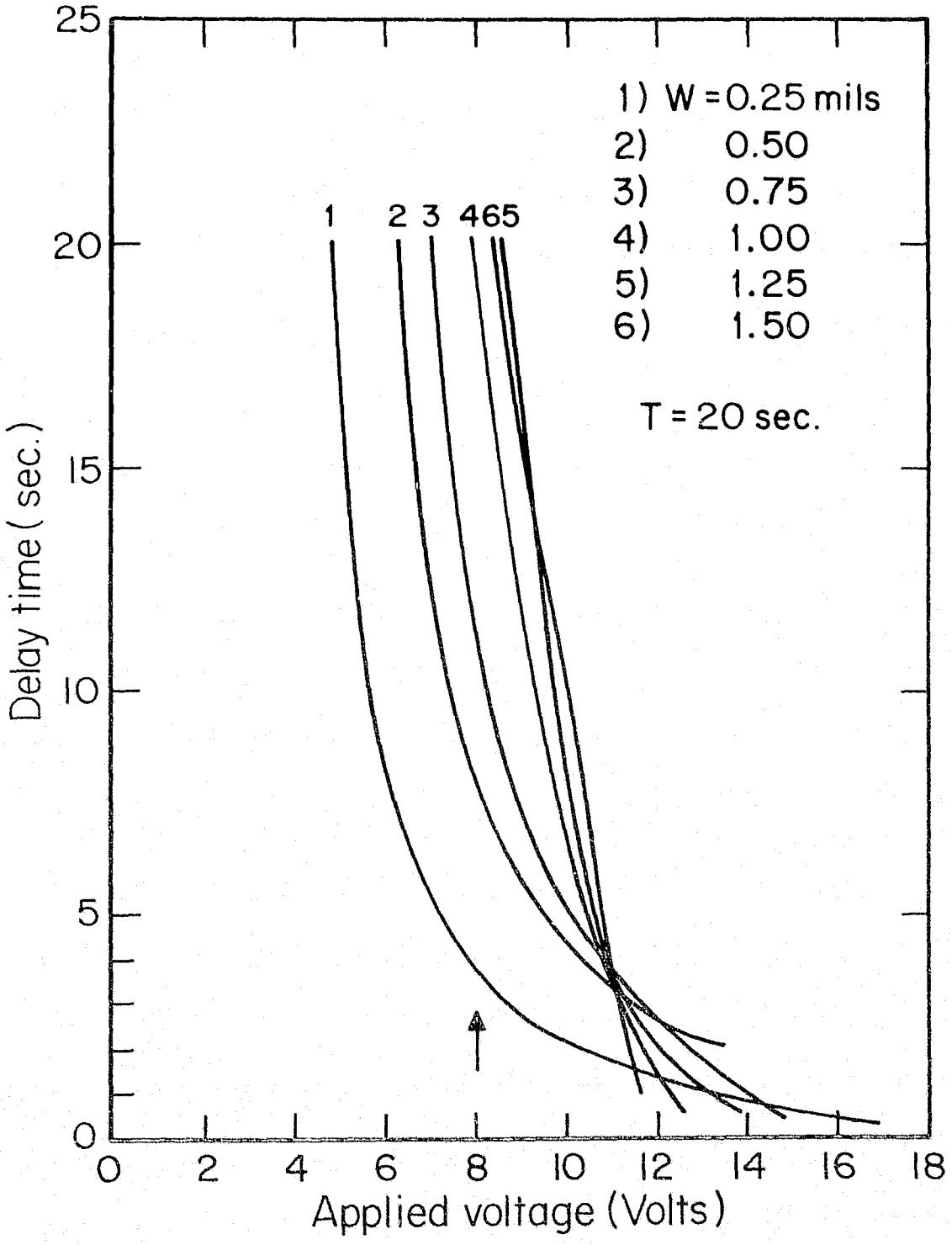

Figure 34

Experimental t_o versus V_o

curves of Figs. 24-30. The theoretical t_o-versus-V_o curves may be utilized to ascertain the value of L as follows. Referring to Fig. 26, where L is 0.11 mils, it is perceived that this family of curves has the largest L of the aforementioned figures in which the W = 1.50 mils curve has V_o smaller than the W = 1.25 mils curve for t_o = 20 seconds. However, there is just not enough discrimination between the curves having a gap width equal to 1.00, 1.25 or 1.50 mils to conclude that indeed this is the most probable value for L. Conversely, inspection of Fig. 28 reveals that this value of L (0.15 mils) is most likely too large. This was inferred for two reasons. First, the W = 1.50 mils curve lies considerably to the right of the W = 1.25 mils curve for t_o near 20 seconds. In addition, the separation of the curves for W = 0.25 mils and 0.50 mils appears to be insufficient.

Hence, it is deduced that of the seven figures, Fig. 27 most closely resembles the experimental curves. Here, where L is 0.13 mils, it is observed that the W = 1.50 mils curve lies predominately to the left of the W = 1.25 mils curve for large values of t_o. Furthermore, there is sufficient distinction between the curves for larger values of t_o, in accordance with the experimental data of Fig. 34.

Yet another argument for the correlation of the L = 0.13 mils data and the experimental results centers around the shapes of the curves for small values of t_o. Namely, observe that the first two curves (where W is 0.25 mils and 0.50 mils) do not intersect in either Fig. 26 or Fig. 34. Additionally, the W = 0.75 mils curve intersects the W = 0.50 mils curve for V_o about 12 volts in both figures. The two figures also indicate that the remaining three curves pass to the left of the W = 0.75 mils curve for

small values of t_o.

It should be recollected that the correlation between the experimental t_o-versus-V_o curves and the theoretical curves for L = 0.13 mils was, up to this point, deduced purely on the basis of the physical appearance of the whole set of curves. This correspondence can be examined further in the following fashion. Choosing V_o = 8.0 volts, it is observed from Fig. 34 that the measured delay times were 3.7, 7.8, 11.1 and 19.4 seconds for gap widths of 0.25, 0.50, 0.75, and 1.00 mils, respectively. On the other hand, Fig. 27 indicates that the corresponding theoretical delay times are 2.4, 8.3, 13.3 and 18.0 seconds. The relationship between the experimental and theoretical data is presented in Fig. 35. The good agreement of the two sets of results is particularly noteworthy.

The conclusion to be drawn is that L is, at the very least, fairly close to 0.13 mils. Utilizing this value of L, equation (3.9) was employed to obtain a value for the polymer resistivity. Using the values quoted in Section 3.2 for d_1, d_2 and T, and taking ε to be 3.9[5], the polymer resistivity ρ is 5.1×10^{10} Ω-cm. The value of the resistivity determined from the PFI lock-and-key device measurements was about 2×10^{10} Ω-cm. The small discrepancy is probably due to slightly different ambient conditions.

The single obvious discrepancy between Figs. 27 and 34 concerns the data for very small values of t_o. Note that the theoretical data indicates that the curves for W greater than or equal to 0.75 mils will be largely coincident for V_o greater than 13 volts. Meanwhile, the experimental data fails to exhibit this feature. This departure is probably due to the lack of reliability of the data for t_o less than 2 seconds. The data were acquired by means of a chart recorder, and the very short delay times

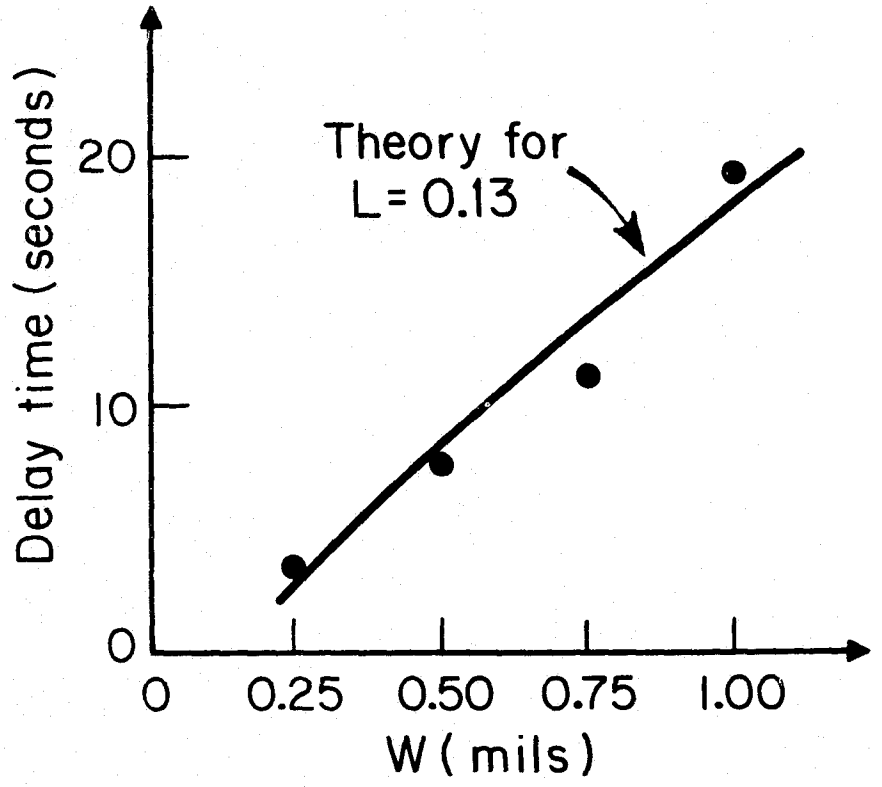

Delay Time vs W for V_o = 8 Volts

Figure 35

could not be accurately obtained by this method.

The final point of interest in this section pertains to the effective threshold voltage determination via the experimental t_o-versus-V_o curve for the narrowest-gap device. As was surmised in the previous section, when t_o = 20 seconds the value of V_o for the W = 0.25 mils device will be the effective threshold voltage of the CFT (assuming that the gap width W is small compared to L, so that only the FET threshold voltage need be applied to just turn on the CFT after 20 seconds has elapsed. Figure 27 clearly justifies this argument for the theoretical case). In Fig. 34, it is noted that the effective threshold voltage for the narrowest-gap device appears to be 4.85 volts. This is in disagreement with the expected value of 3.9 volts, and suggests that the polymer conduction mechanism on a time scale of seconds is primarily a surface rather than a bulk phenomenon, as explained below.

In Section 3.2, it was stated that the thickness of the polymer layer was 3000 Å. Hence, if the polymer conduction is at the surface, the actual dielectric thickness for the MOS capacitor is no longer 1000 Å, but rather 4000 Å. Figure 36 illustrates the fact that this would result in an increase in the FET threshold voltage. In the present case, since the substrate doping was $3.5 \times 10^{14} cm^{-3}$ (from Section 3.2), Fig. 36 shows a change in threshold voltage of about 0.75 volts as the dielectric thickness changes from 1000 Å to 4000 Å. In addition, it is recalled that the assumption was that W is very small compared to L. Should this be slightly violated, the expectation is that the value of the effective threshold voltage obtained from Fig. 34 would overestimate the actual CFT threshold voltage.

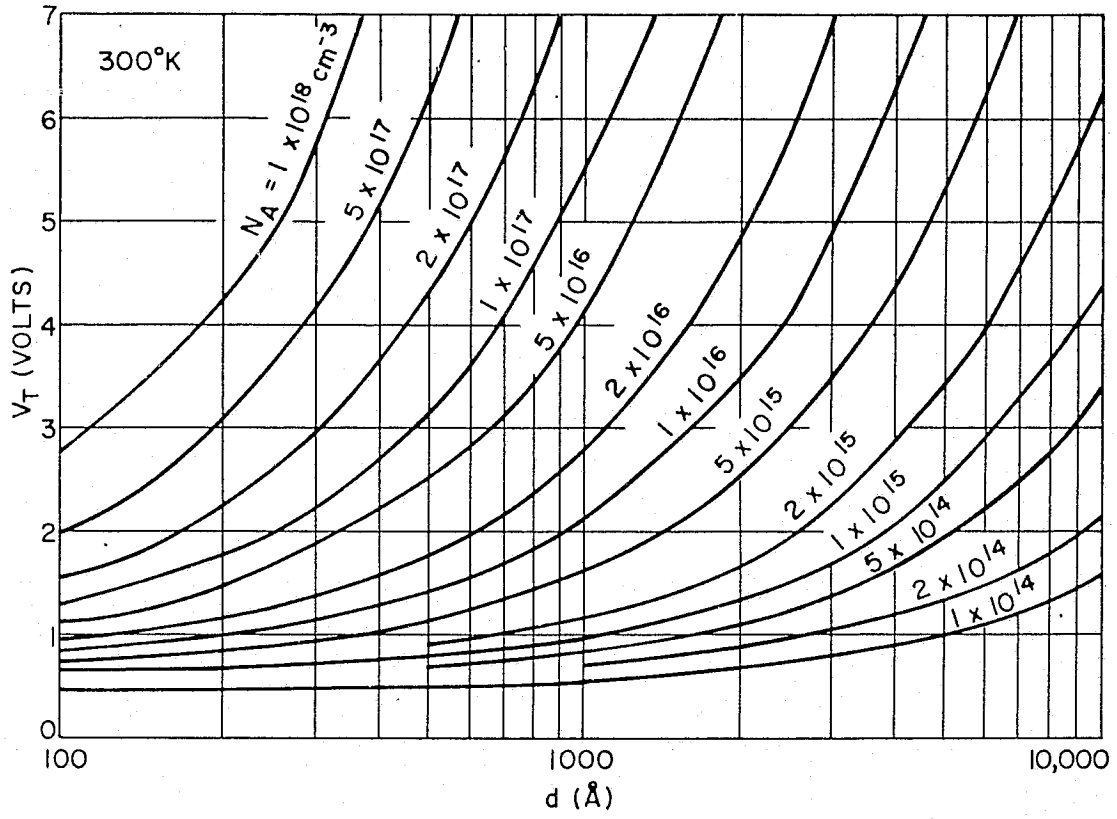

Figure 36

Threshold voltage versus silicon-dioxide-layer thickness for various Si substrate dopings (after Sze [9]).

By comparing Figs. 27 and 36, it is seen that the apparent change in the effective threshold voltage is 0.95 volts, in reasonable agreement with the size of the threshold shift expected from surface conduction. This and other related concepts will be discussed further in Section 3.6.

3.5 FIRE TESTS

Employing a PFI-coated charge-flow transistor with a 1.00 mil gap width, fire tests were performed in the same fashion as that described in Sections 1.5 and 2.3. Once again, a unipolar square wave of amplitude V_o and period $2T = 40$ seconds was applied as the gate-to-source voltage. The resulting drain current was then monitored by means of a chart recorder (which was connected to an electrometer).

Figure 37 depicts the results of a fire test in which 5.0 mg of polyurethane was burned. The value of the square-wave amplitude (V_o) was 5.61 volts. Observe that the initial delay time (i.e., prior to heater turn-on) was 18.25 seconds. When the emanations of the fire produced the maximum effect, the delay time reduced to a minimum of 6.5 seconds. This is almost a factor of 3 reduction in delay time.

Note that the maximum response (i.e. the shortest delay time) is attained about 160 seconds following heater turn-on. In addition, note that this maximum persists for a considerable period of time. Still further, a detectable response is observed even after just one cycle (40 seconds). Finally, it is noted that the delay time returned to its prefire value within eight cycles following heater turn-off. Comparing these results with earlier work, Fig. 11 revealed that the lock-and-key device response to polyurethane had the identical characteristic features. That is, a

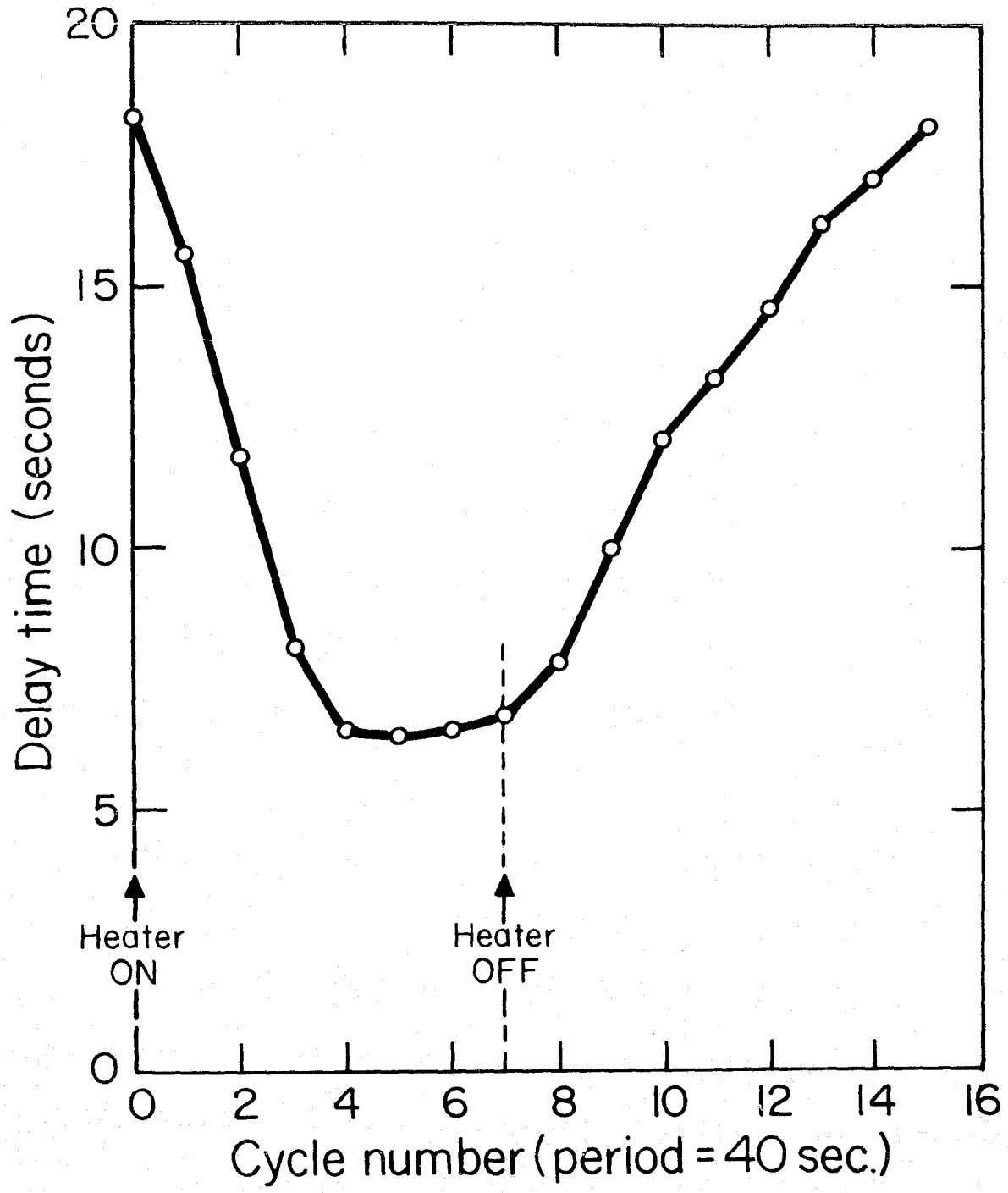

Figure 37

Charge-flow transistor (PFI with polyurethane)

significant response was detected within 40 seconds, the maximum occurred about 160 seconds after heater turn-on and then persisted for a considerable amount of time.

Figure 38 portrays the fire response of the same CFT in which 8.0 mg of acrylic was burned. This time the value of V_o was 7.23 volts and as in the previous example, T was 20 seconds. Note the very sharp-peaked response about 120 seconds after heater turn-on. The initial delay time was 17.25 seconds, and in contrast, the minimum delay time was only 5.6 seconds. Again, this is a factor of 3 reduction in delay time. Figure 9 shows that these same fire-response features were present in the lock-and-key device tests.

The magnitude of the delay-time reduction factor is of particular significance. Figs. 9 and 11 showed that for their respective amounts of material burned, the nominal lock-and-key device gain was about 10. Since the lock-and-key device response varies directly with the conductivity change, it can be inferred that the polymer conductivity increased by a factor of about 10. Meanwhile, equation (3.9) indicates that L is proportional to the square root of the conductivity. Hence, for the CFT fire tests, the value of L increases by a factor of $\sqrt{10}$, or about a factor of 3. Figure 32 indicates that for a prefire delay time of about 18 seconds, L is about 0.125 mils. For the case in which L increases by a factor of 3 (that is, L equal to 0.375 mils), Fig. 32 yields a corresponding delay time of about 4 seconds. While this delay time is slightly less than that observed experimentally, it is not surprising in that not all of the combustion products to which the CFT responds reach the device at the optimal time. That is, in order to achieve the minimum possible delay time, the

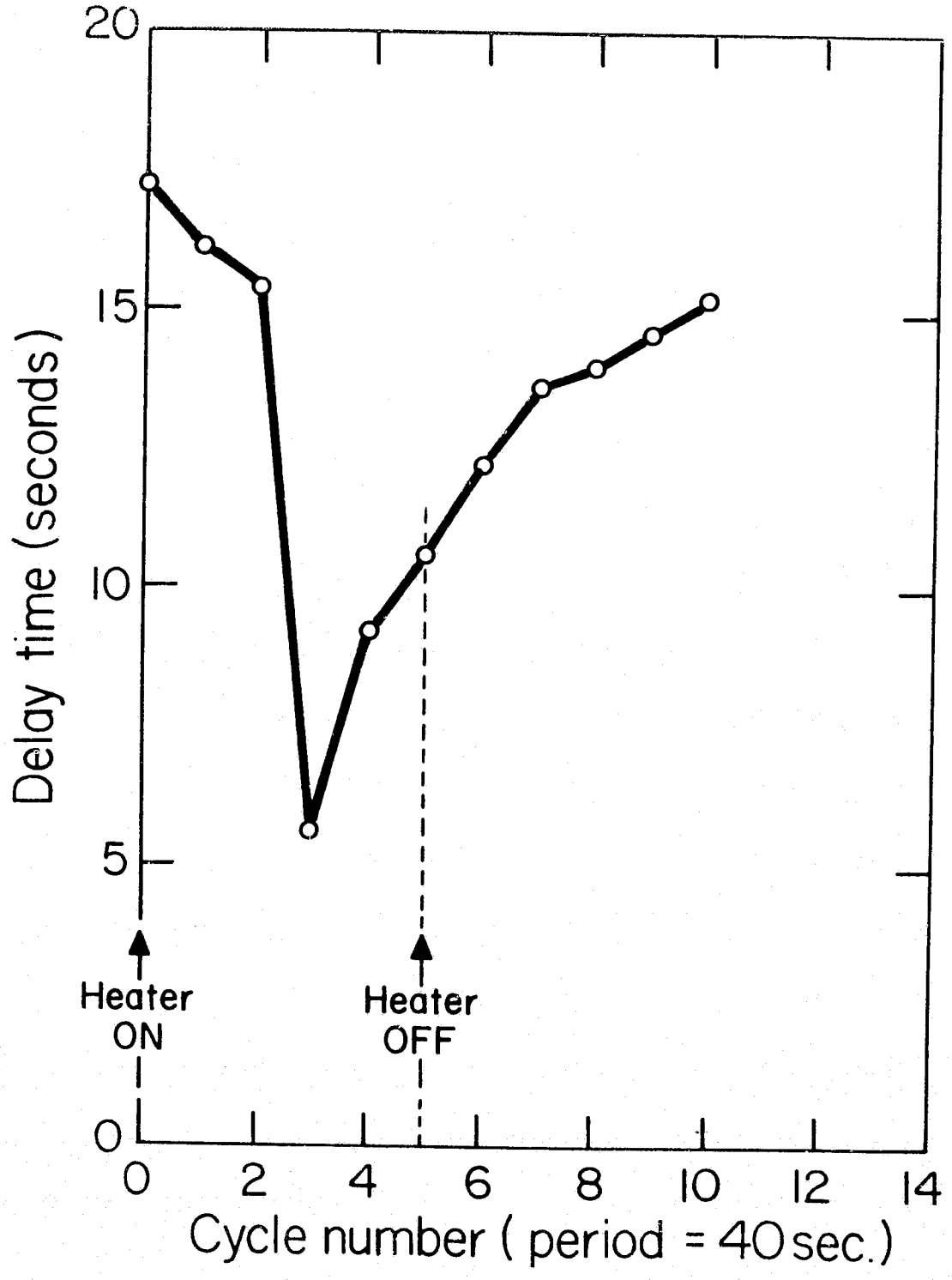

Figure 38

Charge-flow transistor (PFI with acrylic)

maximum release of combustion products to which the device responds must occur at precisely the time at which the gate voltage switches to its value in excess of the threshold voltage. Consequently, it is concluded that the experimental delay-time reduction for the fire tests agrees extremely well with that predicted by the theoretical model for CFT behavior. Thus, it is seen that the CFT easily has fire responses of sufficiently large magnitudes. While the lock-and-key devices and the charge-flow capacitors likewise responded very well, the CFT has drain currents in the microamp range as opposed to the previous two devices which have picoamp signal currents.

3.6 LONG-TERM EFFECTS

In Section 3.4 it was deduced that the conduction mechanism of the PFI polymer on a time scale of seconds was primarily a surface effect. In an effort to reinforce this conclusion, the CFT turn-on characteristics were examined on a time scale of days. That is, the unipolar square wave of amplitude V_o and half-period T = 20 seconds was applied as the gate-to-source voltage over a period of several days.

Figure 39 portrays the typical turn-on characteristics of a CFT with a gap width of 1.0 mil and a threshold voltage of 3.9 volts. Note that the delay time t_o is 17.5 seconds for V_o = 7.23 volts. This current-versus-time profile possesses the nominal shape for a CFT shortly after the application of the gate-to-source voltage. (In the fire tests reported in Section 3.5, the drain current-versus-time characteristics had a shape similar to that illustrated in Fig. 39.)

Application of the unipolar-square-wave gate-to-source voltage (with

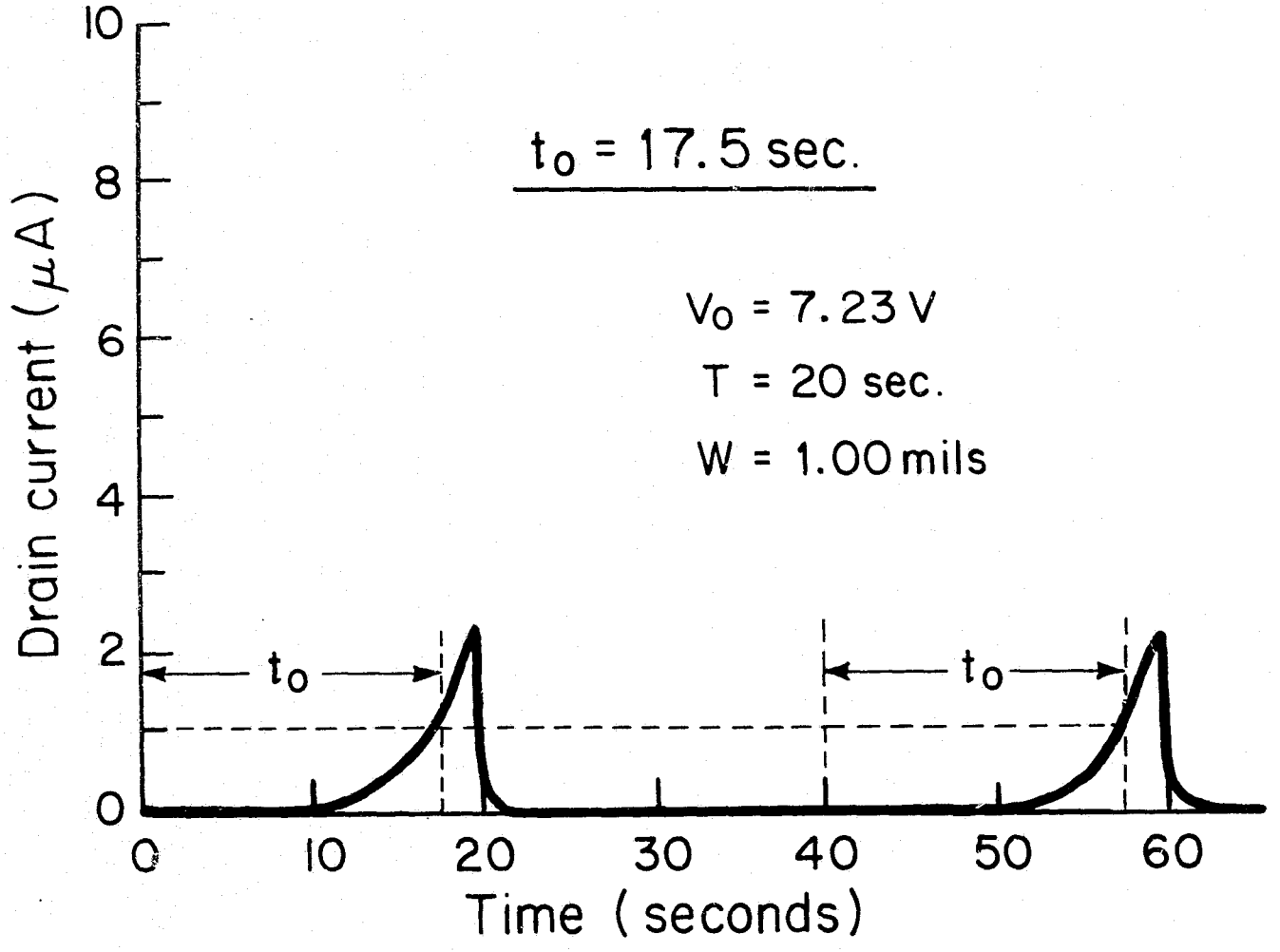

Figure 39

CFT turn-on characteristics

The ON half-cycles begin at t = 0 and t = 40 sec.

V_o equal to 7.23 volts and T = 20 seconds) was maintained for a period of about three days. Following this time period, the CFT turn-on characteristics were monitored. The delay time was observed to be virtually zero. Upon turning down the amplitude of the unipolar square wave to 4.98 volts, the turn-on characteristics shown in Fig. 40 were obtained. Despite the large decrease in V_o, the delay time was now only 12.5 seconds. Note that the change in shape of the turn-on profile was due to drain-current saturation. That is, for this value of V_o which is near the threshold voltage, the drain current saturates at approximately 10 μA.

The application of the unipolar-square-wave gate-to-source voltage with V_o = 7.23 volts and T = 20 seconds was maintained for an additional three days. Once again, upon monitoring the drain-current waveform, the turn-on was essentially instantaneous. After reducing the value of V_o to 4.88 volts, the delay time was observed to be only 5.0 seconds. Note that for this value of V_o the drain current saturates at roughly 5 μA.

A symmetrical bipolar square wave (zero average) of amplitude 7.23 volts (T = 20 seconds) was then applied to the same CFT for several days. Following this time period, the turn-on characteristics were monitored. Because no drain current was observed, the half-period T of the square wave was increased to 50 seconds. Still no drain current was detected. By increasing the value of V_o to 8.51 volts, a turn-on was finally noted. This profile appears in Fig. 42. The delay time was found to be 42.5 seconds.

The above experimental observations strongly suggest that the conduction mechanism of the PFI polymer consists of a surface component and a bulk component. Furthermore, the surface conductivity is much higher than

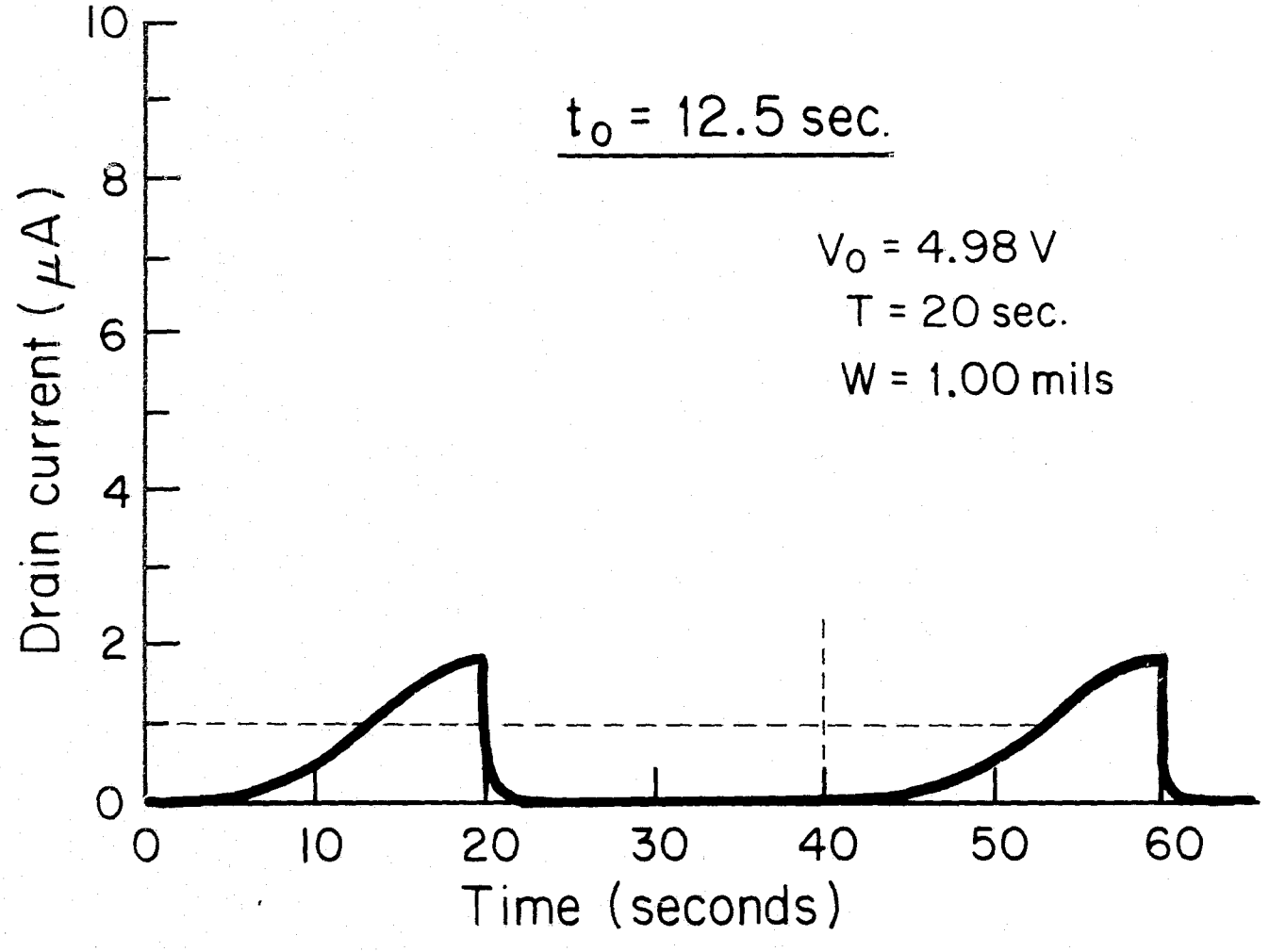

Figure 40

CFT turn-on characteristics

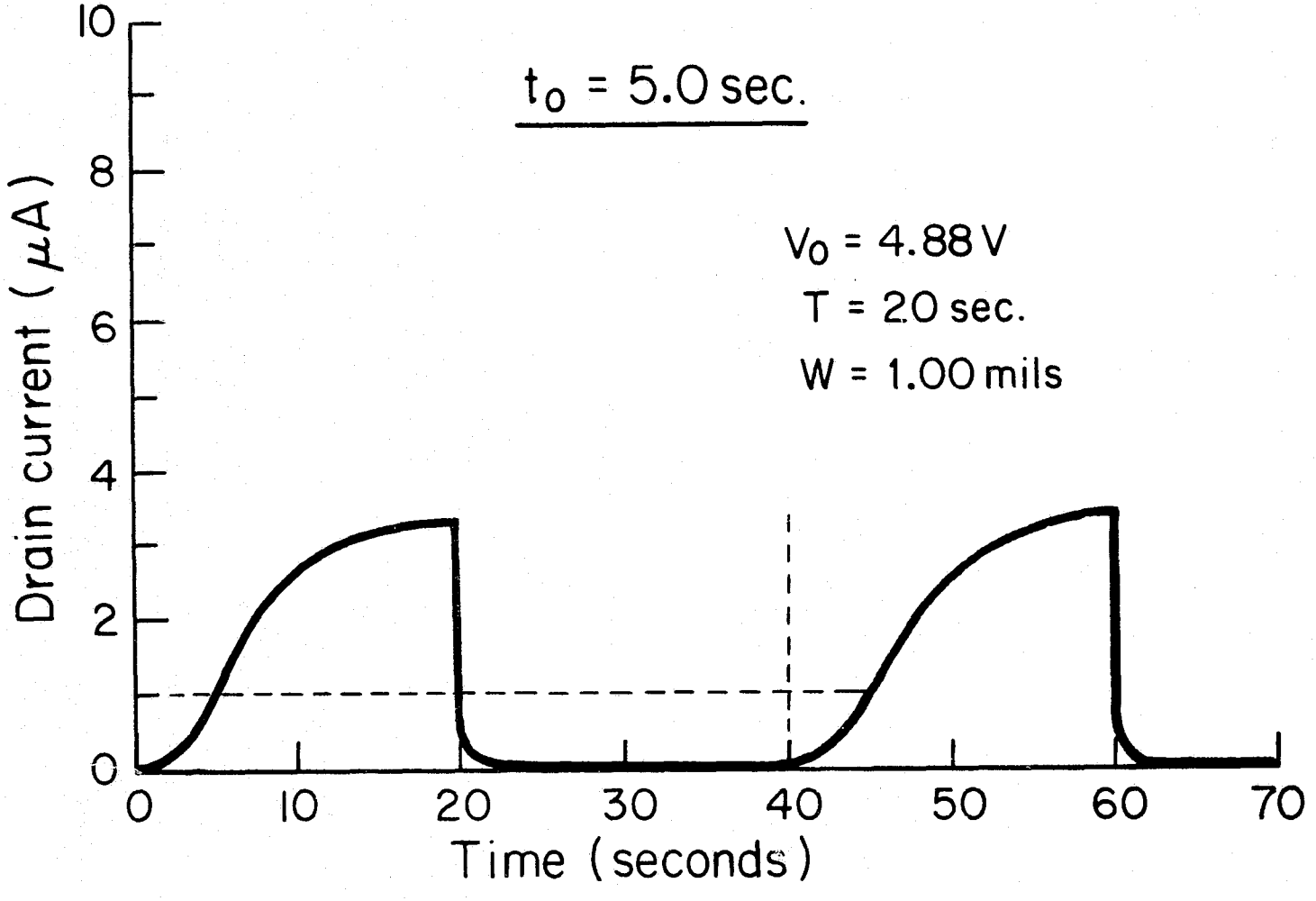

Figure 41

CFT turn-on characteristics

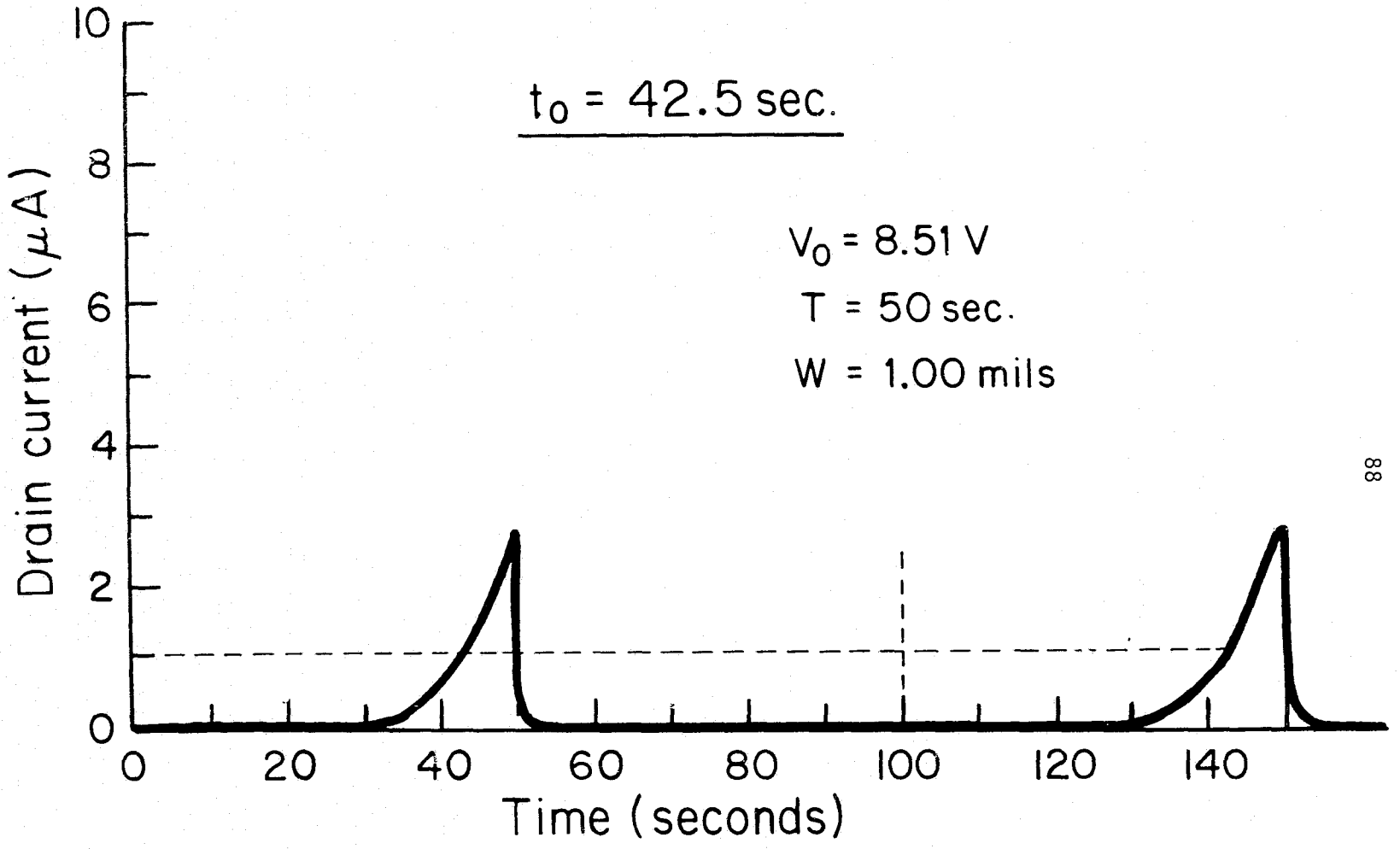

Figure 42

CFT turn-on characteristics

the bulk conductivity. The simultaneous existence of the two conduction modes can be elucidated with the aid of Fig. 43. Since the surface conductivity exceeds the bulk conductivity, when a gate voltage is applied to the CFT the accumulation of charges in the polymer will occur at the surface. If the gate-to-source voltage exceeds the zero-gap threshold voltage by a finite amount (the dielectric thickness is now substantially greater requiring a higher effective threshold voltage), the CFT will turn-on when sufficient charge has accumulated at the surface such that the electric field is large enough to invert the entire channel. For the PFI polymer, this phenomenon takes place on a time scale of seconds.

Because of the bulk component of the polymer conduction mechanism, the charges at the surface drift toward the polymer-oxide interface. This is depicted in Fig. 43c. For the PFI polymer, because of the much larger value of the bulk resistivity, this process occurs on a time scale of days. When the polymer-oxide interface becomes fully charged (Fig. 43d), the effective threshold voltage reduces to the zero-gap value since the dielectric thickness is now just the oxide-layer thickness.

When a bipolar square wave (zero average) with a period on the time scale of minutes is applied to the gate of a PFI-coated CFT, essentially only the surface component of the conduction mechanism is exploited. This yields delay times on a time scale of minutes as seen in Fig. 42. However, if a unipolar square wave is applied to the gate, this nonzero average voltage stores charge in the polymer. Furthermore, this charge begins to migrate toward the polymer-oxide interface on a time scale of days. As a result, the electric field at the oxide-substrate interface increases, thereby reducing the time required to invert the channel (the delay time

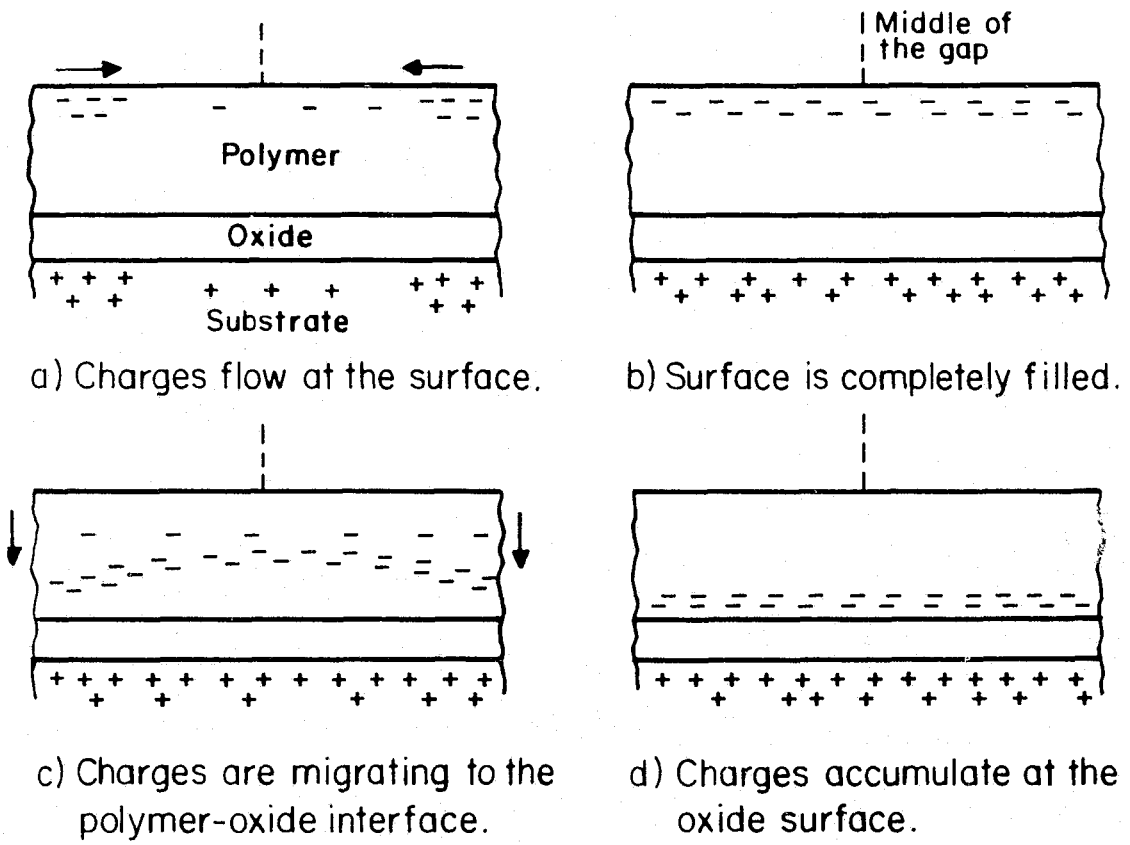

Figure 43

Charge-flow model in which surface conduction is predominant

t_o). This also implies that the amplitude of the unipolar square wave (V_o) required to yield a given delay time is reduced as time increases. It is precisely this effect which results in the delay-time reduction (even for smaller values of V_o) illustrated in Figs. 39-41.

An important observation here is that charge accumulated at the polymer-oxide interface can also be removed. That is, by subsequently applying a bipolar square wave, the charges originally at the polymer-oxide interface will migrate back up toward the polymer surface. This results in a higher effective threshold voltage and substantially longer delay times, as depicted in Fig. 42.

The fact that the effective threshold voltage is somewhat higher than the zero-gap threshold voltage upon the application of a bipolar square wave yields conclusive evidence that the dominant polymer conduction mode is the surface component. Furthermore, although uncoated silicon dioxide has a higher surface conductance than the PFI polymer, when the polymer is deposited upon the oxide, the dominance of polymer-surface conduction in the device characteristics shows that the oxide-polymer interface has much lower surface conductance than the uncoated oxide. This substantiates the earlier assumption that the conduction properties of the lock-and-key device and the charge-flow capacitor are due to the conductivity of the polymer, and are not dependent on substrate conduction.

CHAPTER 4: DISCUSSION

4.1 SUMMARY

The properties of the polymer-coated lock-and-key devices were examined first. Two polymers, PFI and PSB, were found to be particularly suitable for fire detection since they had good fire responses and very small humidity responses. One polymer, PAPA, was found to be promising as a relative-humidity sensor. The major drawback of the lock-and-key device was the picoampere current levels.

The charge-flow capacitor was examined next. Its behavior was successfully modelled as an RC transmission line. Because the current levels were also in the picoampere regime, the major utility of the charge-flow capacitor was its incorporation into the gate structure of an MOS transistor.

Lastly, the charge-flow transistor was investigated. For a unipolar-square-wave voltage applied to the gate, an RC-transmission-line model was successfully developed which yielded theoretical delay time-versus-unipolar square-wave amplitude characteristics which agreed well with the experimental results. Extensive fire tests performed with a PFI-coated CFT indicated very good sensitivity with microamp current levels. It was also discovered that by noting the effective threshold voltage of the CFT, the dominant conduction component (surface or bulk) of the thin film could be ascertained. For the case of PFI, the surface conductivity was substantially larger than the bulk conductivity.

4.2 FUTURE CONSIDERATIONS

General areas for future investigation of the charge-flow transistor include:

(1) sensing applications, (2) utility in the determination of the dominant conduction mechanism of a thin film and (3) improvement of the CFT theoretical model.

Sensing applications include fire detection, which was the common denominator of this thesis. The CFT may also be used as a relative-humidity sensor. Section 1.4 clearly indicated that the conductivity of the PAPA polymer was very much dependent upon the ambient relative humidity. Consequently, by incorporating the PAPA polymer into the gate structure of a CFT, the delay time would be a function of the relative humidity. Specifically, a higher relative humidity would result in a shorter delay time. This property may be employed in the construction of a relative-humidity transducer. In addition, the relative-humidity-sensing CFT could be used to compensate another CFT incorporating a different polymer whose humidity response is undesirable. For example, this would be particularly appealing for the case whereby a polymer has a good fire response but which is masked by a humidity response.

Furthermore, the CFT may be used as a photosensing device. The delay time of a CFT incorporating the PFI polymer was found to be photosensitive. Specifically, when a fluorescent light was turned on in the vicinity of the device, the delay time was observed to be somewhat shorter than when the light was off. Thus, by employing appropriate thin films whose conductivity is photosensitive, CFTs may be utilized in a variety of detection schemes.

One caution is that because the CFT sensor cannot be fully encapsulated, it will be more susceptible to long-term contamination than encapsulated MOS devices. Hence, deposition of suitable passivation layers

over the gate oxide and/or over the entire chip may be required. Thus far, threshold-voltage drift has not been observed on a time scale of months with the devices operated in normal ambients at room temperature.

Even if passivation layers are added to the device, the application of the sensing film is the final processing step. The polymer films were spun-on from solution but the CFT could also be made with evaporated, sputtered or even sprayed-on films. Thus, MOS-compatible and MOS-integrable sensing devices can be made with materials which previously could only be used in discrete-device form.

An application of particular promise is the ability to ascertain whether a given thin film has its conduction properties dominated by surface or bulk components. This effect can be exploited as follows. After ascertaining the zero-gap threshold voltage, a CFT with a very small gap width (for example, 0.25 mil) would then have its t_o-versus-V_o characteristics recorded. As t_o is increased, V_o will asymptotically approach the effective threshold voltage. If this value is approximately equal to the zero-gap threshold voltage, then it is concluded that the conduction mechanism of the thin film is largely a bulk effect. Alternatively, if the effective threshold voltage is somewhat greater than the zero-gap value, the conclusion is that the surface conduction predominates for the particular thin film. Hence, the CFT may be utilized to resolve the surface-versus-bulk conduction question for a thin film.

Future work can also be directed toward improving the theoretical model of the CFT. The model presented here is strictly valid only for the case in which the thin-film conduction is a bulk phenomenon. For cases in which the surface conduction is dominant, a net charge will accumulate at

the polymer-oxide interface upon the application of a unipolar-square-wave gate voltage. That is, application of a unipolar square wave with a nonzero average permits manipulation of the delay time-versus-unipolar-square-wave amplitude characteristics (Section 3.6). A more complete theoretical model of the CFT could be developed which accommodates the predominance of surface conduction for excitation by a nonzero-average gate voltage.

REFERENCES

1. N.R. Byrd, "Space Cabin Atmosphere Contaminant Detection Techniques", McDonnell Douglas Report SM 48446-F, July 1968.

2. N.R. Byrd and M.B. Sheratte, "Synthesis and Evaluation of Polymers for use in Early Warning Fire Alarm Devices", NASA CR-134693, 1975.

3. S.D. Senturia, "Fabrication and Evaluation of Polymeric Early-Warning Fire-Alarm Devices", NASA CR-134764, 1975.

4. J.A. Wishneusky, "Device Structures for Microelectronic Gas Sensors", S.M. and E.E. Thesis, M.I.T., Sept. 1974.

5. S.D. Senturia, op. cit., p. 41.

6. S.D. Senturia, ibid., p. 70.

7. S.D. Senturia, ibid., p. 61.

8. Therese M. Luse, "Electrical Properties of Poly (p-aminophenylacetylene)", S.B. Thesis, M.I.T., May 1975, p. 20.

9. S.M. Sze, Physics of Semiconductor Devices, Wiley, 1969, p. 521.

10. S.D. Senturia, C.M. Sechen and J.A. Wishneusky, "The Charge-Flow Transistor: A New MOS Device", Applied Physics Letter, 30 106 (1977).

11. S.D. Senturia, C.M. Sechen and J.A. Wishneusky, "The Charge-Flow Transistor", paper 12.8 in Technical Digest 1976, IEEE IEDM (Washington, D.C., Dec. 6-8, 1976).

12. S.D. Senturia and C.M. Sechen, "The Use of the Charge-Flow Transistor to Distinguish Surface and Bulk Components of Thin-Film Sheet Resistance", paper 3 of Session IV in Technical Digest of 1977 Device Research Conference, Cornell University, June 27-29, 1977.